

3-11-2018

Effect of Pipe Rotation on Casing Pressure Within MPD Applications

Zahrah Ahmed Al Marhoon

Louisiana State University and Agricultural and Mechanical College

Follow this and additional works at: https://digitalcommons.lsu.edu/gradschool_theses



Part of the [Petroleum Engineering Commons](#)

Recommended Citation

Al Marhoon, Zahrah Ahmed, "Effect of Pipe Rotation on Casing Pressure Within MPD Applications" (2018).
LSU Master's Theses. 4630.

https://digitalcommons.lsu.edu/gradschool_theses/4630

This Thesis is brought to you for free and open access by the Graduate School at LSU Digital Commons. It has been accepted for inclusion in LSU Master's Theses by an authorized graduate school editor of LSU Digital Commons. For more information, please contact gradetd@lsu.edu.

EFFECT OF PIPE ROTATION ON CASING PRESSURE WITHIN MPD APPLICATIONS

A Thesis

Submitted to the Graduate Faculty of the
Louisiana State University and
Agricultural and Mechanical College
in partial fulfillment of the
requirements for the degree of
Master of Science

in

The Department of Petroleum Engineering

by
Zahrah Ahmed Al Marhoon
B.S., Texas A&M University, 2012
May 2018

This work is dedicated to my family and friends. Especially my husband who's without his support, this would not have been possible.

This is for you *Hussain*

This is for you *Rihana*.

Acknowledgments

First, I would like to extend my deepest gratitude to my committee chair, Dr. Babak Akbari, for his continuous support throughout the making of this work. I appreciate his readiness to answer all questions quickly and for being considerate and accommodating to my personal circumstances.

I would also like to acknowledge my committee members: Dr. Tyagi, Dr. Almeida and Mr. Erge. I am gratefully indebted to them for their valued comments on this thesis.

Finally, I would like to express my profound thankfulness to my parents, husband, family and friends for their faith in me and their non-stop support throughout this and all other journeys.

TABLE OF CONTENTS

ACKNOWLEDGMENTS	iii
NOMENCLATURE	vi
ABSTRACT	viii
CHAPTER 1: INTRODUCTION AND LITERATURE REVIEW.....	1
1.1 Introduction to Managed Pressure Drilling.....	1
1.2 Well Control Methods and MPD Well Control.....	4
1.3 Pipe Rotation and Eccentricity Effect on Frictional Pressure Loss	16
1.4 Two Phase Flow in Wellbore with Gas Kick	17
CHAPTER 2: STATEMENT OF PROBLEM AND APPROACH.....	21
2.1 Statement of Problem.....	21
2.2 Approach	22
2.3 Real Scale Experiments in LSU#2 Well	24
2.4 Pipe Rotation Frictional Pressure Loss Effect Correlations.....	27
CHAPTER 3: ANALYSIS OF FRICTIONAL PRESSURE CHANGES ON CASING PRESSURE CAUSED BY PIPE ROTATION IN OIL BASED MUDS USING DISSOLVED GAS MODEL.....	39
3.1 Overview	39
3.2 Dissolved Gas Model for Oil Based Muds.....	40
3.3 Example of Full-Scale Data Output (OBM).....	41
3.4 Pipe Rotation Effect on Casing Pressure in OBM Using Dissolved Gas Model	42
3.5 Validity of the Dissolved Gas Model in OBM.....	47
3.6 Summary of the Results and Conclusion of Dissolved Gas Model for OBM.....	48
CHAPTER 4: ANALYSIS OF FRICTIONAL PRESSURE CHANGES ON CASING PRESSURE CAUSED BY PIPE ROTATION IN WATER BASED MUDS USING SINGLE BUBBLE MODEL	50
4.1 Overview	50
4.2 Single Bubble Model for Water Based Muds.....	51
4.3 Example of Full Scale Data Output (WBM)	54
4.4 Pipe Rotation Effect on Casing Pressure in WBM Using Single Bubble Model.....	55
4.5 Summary of the Results and Conclusion of Single Bubble Model for WBM	60

CHAPTER 5: VALIDITY OF SINGLE BUBBLE MODEL AND GAS DISTRIBUTION	62
5.1 Overview	62
5.2 Gas Kick Distribution in Wellbore	63
5.3 Pipe Rotation Effect on Gas Distribution.....	66
5.4 Conclusion on Validity of the Single Bubble Model.....	74
CHAPTER 6: ANALYSIS OF CASING PRESSURE CHANGES CAUSED BY GAS BUBBLE BREAKAGE USING DISPERSED BUBBLE MODEL	76
6.1 Overview	76
6.2 Dispersed Bubble Model for WBM.....	76
6.3 Conclusion of Dispersed Bubble Model	83
CHAPTER 7: SUMMARY, APPLICATIONS, AND RECOMMENDATIONS FOR FUTURE RESEARCH.....	85
7.1 Summary	85
7.2 Application	88
7.3 Recommendations for Future Research	91
BIBLIOGRAPHY	93
APPENDIX A: REAL SCALE EXPERIMENTS DATA OUTPUT.....	96
APPENDIX B: COPYRIGHT MATERIAL.....	98
APPENDIX C: FRICTIONAL PRESSURE CALCULATION EXAMPLE	99
VITA	102

NOMENCLATURE

A_{ann}	Area of the Annulus	OBM	Oil Based Mud
BHP	Bottom Hole Pressure	P	Pressure
BOP	Blowout Preventer	CP_{RPM}	Casing pressure with Rotation
CBHP	Constant Bottom Hole Pressure	C_{STATIC}	Casing pressure without rotation
DC	Drill Collar	FP	Frictional pressure loss including pipe rotation effect
D_g	Location of gas at a certain time step	P_t	Pressure of gas at the top of the well
DFD	Dynflodrigill	PV	Plastic Viscosity
D_i	Inner Diameter of Annulus	PWD	Pressure While Drilling
D_o	Outer Diameter of Annulus	R	Universal Gas Constant
DP	Drill pipe	R_i	Radius of Inner Pipe, $D_i/2$
ECD	Equivalent Circulating Density	R_o	Radius of Outer Pipe, $D_o/2$
HP	Hydrostatic Pressure	RPM	Rotation Per Minute
K	Consistency index of mud	SG	Specific Gravity of gas
L_g	Length of the gas section	T	Absolut Temperature
L_1	length of the mud section below the gas with pump rate	t	the time step
L_3	length of the mud section above the gas with the increased mud rate	t_0	Time at which the gas exited the well
m	Flow behavior index	Ta	Taylor number, Dimensionless
MM	Molecular Mass of air	TD	Total Depth
MPD	Managed Pressure Drilling	v	Axial Velocity, m/s
MW	Mud Weight (Density)	v_{peak}	peak velocity of the mud taken from OBM velocities
N	Generalized flow behavior Index	v	Velocity

V	Volume	τ_y	yield stress of mud
V _b	Volume of kick at the bottom of the well	γ_z	Axial Shear rate , s ⁻¹
v _e	The extra velocity of gas added to peak velocity of liquid	γ_θ	Radial Shear rate, s ⁻¹
V _t	Volume of gas at the top of the well.	ρ_g	Gas density $\frac{SG \times MM \times P}{RT}$
WBM	Water Based Mud	ρ_{mix}	Density of the mixture in the dispersed gas model
WCM	Well Control Matrix	ρ_{mud}	Mud density
YP	Yield Point	λ_{mud}	Void fraction of mud in the dispersed gas model
ω	Rotational Speed	μ_{app}	Apparent Viscosity
β	Void fraction of gas of annulus		

ABSTRACT

Well control is one of the most crucial sectors in drilling engineering. Human lives and safety depend on the correct execution of the engineering design. Managed Pressure Drilling (MPD) is a new technology that has recently emerged in the oil and gas industry. It has special well control abilities supported by the RCD to continue drilling or carry operations that involve pipe rotation, while circulating out a gas kick. This thesis examines the effect of pipe rotation on casing pressure profiles within MPD kick circulation application. The analysis was carried on real scale kick experiments. These experiments were carried in a controlled environment that mimicked downhole conditions with a gas influx entering the wellbore. Both water based mud and oil based mud were evaluated. Then, the real scale tests analysis was coupled with the effect of pipe rotation through the application of correlations. The correlations estimate the change in frictional pressure loss in the annuls for non-Newtonian fluids with pipe rotation. A study of the effect of a larger size gas bubble breakage into smaller size bubbles on the maximum anticipated casing pressure is also included in this research.

The thesis was divided into three models: (1) dissolved gas model in OBM. (2) single bubble model in WBM. (3) dispersed bubble model in WBM. The first two models studied the effect of frictional pressure changes on the anticipated casing pressure. The dispersed bubble model studies the effect of breaking the gas bubble into many very small bubbles. The practical outcome is to further the precision of the estimation of downhole pressure limits since MPD address narrow fracture-pore pressure window and to find if casing pressure changes would have any effect on the RCD rating selection and if the rotation can be safely conducted.

CHAPTER 1: INTRODUCTION AND LITERATURE REVIEW

1.1 Introduction to Managed Pressure Drilling

Drilling Engineers deal with several challenges with each well they plan. New technologies have emerged in the oil and gas industry to address these challenges. These technologies allow drilling engineers to carefully design and efficiently carry the operation. One of these new technologies is managed pressure drilling (MPD).

1.1.1 Definition of managed pressure drilling

The IADC defines MPD as “an adaptive drilling process used to precisely control the annular pressure profile throughout the wellbore. The objectives are to ascertain the downhole pressure environment limits and to manage the annular hydraulic pressure profile accordingly.”

The term MPD was used for the first time in Amsterdam Drilling Conference in 2004. MPD is especially important for the application of narrow operational window between pore pressure and fracture pressure. MPD introduced for a long time as a method to overcome some industry challenge to make drilling in more difficult environment visible such as pressure profile uncertainty, ballooning and loss circulation. Casing string failure of reaching to total depth due to pressure regime and low ROP are just examples of the well challenges that MPD could help in

1.1.2 Importance of MPD

MPD has had a growing demand in the industry for many reasons. 70% of the hydrocarbon resource available offshore are not economically drillable using conventional methods (Ian 2004). MPD allowed to drill in a well that could not be drilled otherwise. In a survey done for more than 600 SPE members worldwide, the results showed 25% of the wells that were not able

to be drilled with the old technology (Fig 1.1), and that MPD technology opens the possibility of drilling those wells safely (Jacobs and Donnelly 2011). In the Gulf of Mexico, MPD implementation decreased the drilling cost by \$25-40 per foot (Rehm et al. 2008).

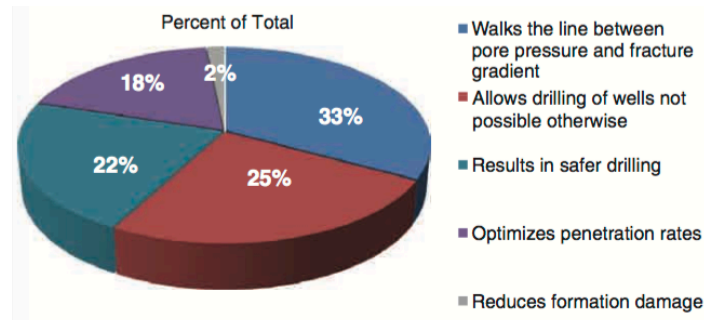


Figure 1. 1: Importance of MPD survey (Jacobs and Donnelly 2011)¹

1.1.3 Types of MPD Operations and Equipment

There are various types of operation for MPD:

- 1) Constant Bottom Hole Pressure (CBHP) that allow to reduce the NPT by enabling fewer and deeper casing string especially where the pore pressure and fracture pressure window is narrow. In this method RCD is implemented to control the bottom hole pressure by applying backpressure to the annulus even while circulating.
- 2) Pressurized Mud Cap Drilling (PMCD) allow more drilling through increasing rate of penetration and decrease in flat time in drilling in a loss circulation environment.
- 3) Dual Gradient (DG) enable drilling to target depth with the desired hole size, especially in deep water drilling (“Introduction to Managed Pressure Drilling with MicroFlux™ Control” 2012).

¹ Copyright permission included in appendix B

Rotating control device

RCD is commonly used in all MPD implementation. The RCD, specifically in some onshore fixed platforms, is installed on the BOP to allow for rotation during connection and tripping and it can hold the pressure. To control and reduce the temperature circulated oil is used to lubricate the bearing while rotating. It consists of two main parts. The rotating control head and the bearing assembly as in Fig.1.2. The first introduction of the rotating head was in 1937 in Shaffer tool company catalog.

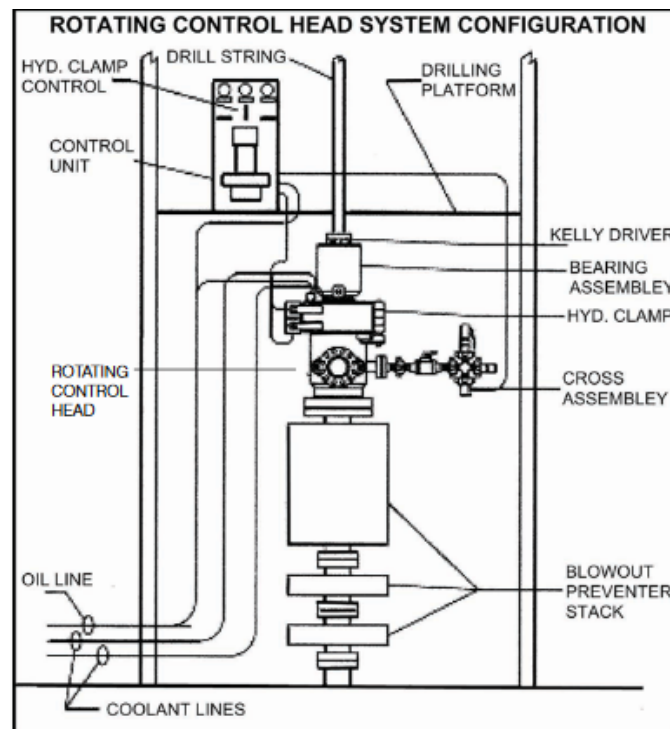


Figure 1. 2: Rotating Control Device system configuration (Rehm et al. 2008).

Choke

The RCD lines are then connected to a separate onshore MPD manifold. It is very similar to well control manifold but is used more frequently in the purposes of applying more back pressure.

1.2 Well Control Methods and MPD Well Control

1.2.1 Conventional well control methods

To prevent any kicks or influxes, the well needs to be filled with mud during all operations with a density that is able to overbalance formation pressure. There are several reasons as to why a kick may enter the well. These reasons include: mud density lower than needed to keep pore pressure, losing some of the mud to the formation (lost circulation), failure to keep the well filled while moving the drill pipe in and out of the wellbore which is also known as tripping.

There are a number of signs that may suggest a well kick. Change in pump pressure caused by the changes in hydrostatic pressure, increase in flow rate triggered by formation fluid entering the well, changes in the rate of penetration (drilling break) caused by facing a porous formation are among many other warning signs. When any of these warning signs are encountered, the conventional well control methods require a shut in procedure. Most procedures include ceasing drilling, elevating the drill pipe to bottom, stopping the pump and using the blowout preventer whether by closing the pipe rams or the annular preventer. Then, the kick needs to be displaced out of the well. During the shut-in period, a continuous record of the drill pipe's shut in pressure, annulus pressure, and pit gain is crucial to control the kick. Two famous kick displacement methods are described next, drillers method and weight and wait (Engineer's)(Grace et al. 1960).

Driller's method

This method requires less calculations than the engineer's method mentioned in the next section. A measurement for the frictional pressure loss while the pump is at low flow rate is needed throughout different stages of the drilling operation as a preparation for the required procedure of

both methods. The disadvantages of this method is that it requires more than one circulation to complete the killing operation. The steps are as follows:

- 1) Record shut in drill pipe pressure and casing pressure
- 2) Reduce pump flow rate is set to a low flow rate known as kill flow rate.
- 3) Circulate out the kick to surface while keeping drill pipe pressure is kept constant. After the kick has been displaced out of the well, the casing pressure should be equal to the drill pipe shut in pressure. If it was not equal another circulation is needed to ensure the kick is completely displaced.
- 4) Calculate new mud kill density by Eq. 1.1

$$MW_{kill} = \frac{MW_{original} D + SIDPP}{.052 D} \quad \text{Eq 1. 1}$$

Where MW_{kill} is the new mud density to be pumped (ppg), $MW_{original}$ is the original mud weight in wellbore while the kick was taken (ppg), D is the total depth of the well in (ft) and $SIDPP$ is the final shut in drill pipe pressure in psi

- 5) Change the mud density to the new calculated kill mud weight
- 6) Fill the drill pipe with kill mud while keeping the casing pressure constant
- 7) Fill the annulus with kill mud while keeping the drill pipe constant
- 8) Check shut in pressures for both drill pipe and casing pressure to be zero and the well is not flowing (Grace et al. 1960).

As it can be seen in Fig 1.3, the first circulation holds the drill pipe pressure constant to keep. When the kill mud entering the well, the pump pressure starts to decrease in the second circulation

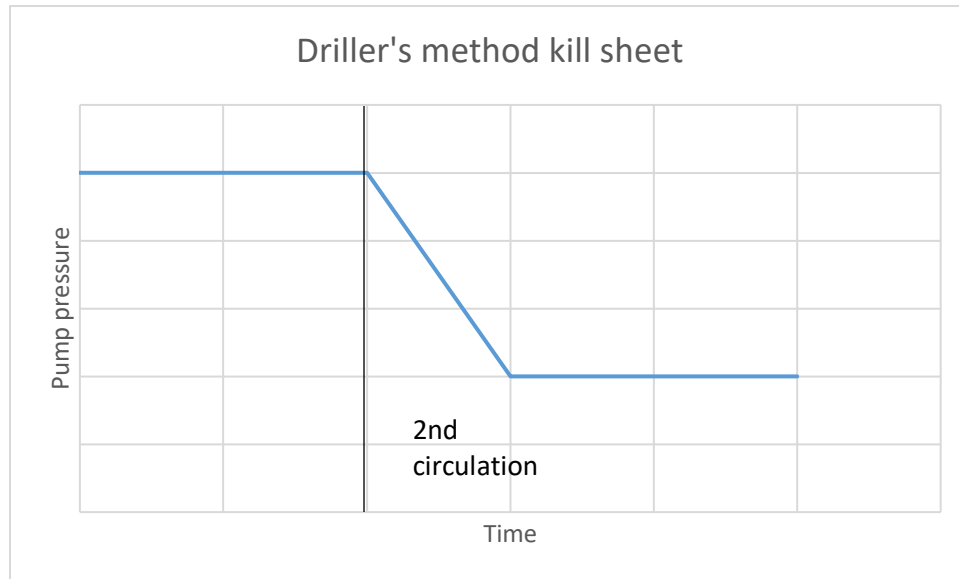


Figure 1. 3: Pump pressure changes using the driller's method

Wait and Weight method

Unlike the drill's method, the kill mud density is changed and pumped into the well while the kick is circulated out. This makes it possible for the kick to be circulated out in one circulation instead to the two needed for driller's method which is one of the advantages of this method. The disadvantage of this method is that it requires more calculation from the crew before the start of the killing operation. The steps recommend is as follows.

- 1) Recoded the shut in drill pipe pressure and casing pressure.
- 2) Calculate mud kill density using the same equation as in Eq. 1.1.
- 3) Calculate initial drill pipe circulation pressure and final drill pipe circulation pressure using Eq. 1.2 and 1.3

$$ICP = SIDPP + SPP$$

Eq 1. 2

Where ICP is the initial Circulating pressure in psi, SIDPP is the shut-in Drill pipe pressure in psi, and SPP is the slow pump pressure in psi which refers to the frictional pressure loss at a low flow rate

$$FCP = SPP \times \frac{MW_{kill}}{MW_{original}} \quad \text{Eq 1. 3}$$

FCP is the final circulating pressure in psi and MW are the mud weights in ppg for both kill and original muds.

- 4) Plan the pumping schedule using a graph of the pump pressure vs volume of mud being pumped (known as kill sheet) from the start of the kill operation till the kill mud fills up the drill pipe Fig. 1.4. The pump pressure starts from initial circulating pressure and end with final circulating pressure when the kill mud fills up the drill pipe. The steps are decided based on the difference between ICP and FCP divided by the volume of mud required to fill up the drill pipe.
- 5) Change the mud density to the new calculated kill mud weight
- 6) Fill the drill pipe with kill mud while following the pump schedule as in step 4
- 7) Fill the annulus with kill mud while keeping the drill pipe constant
- 8) Check shut in pressures for both drill pipe and casing pressure to be zero and the well is not flowing (Grace et al. 1960).

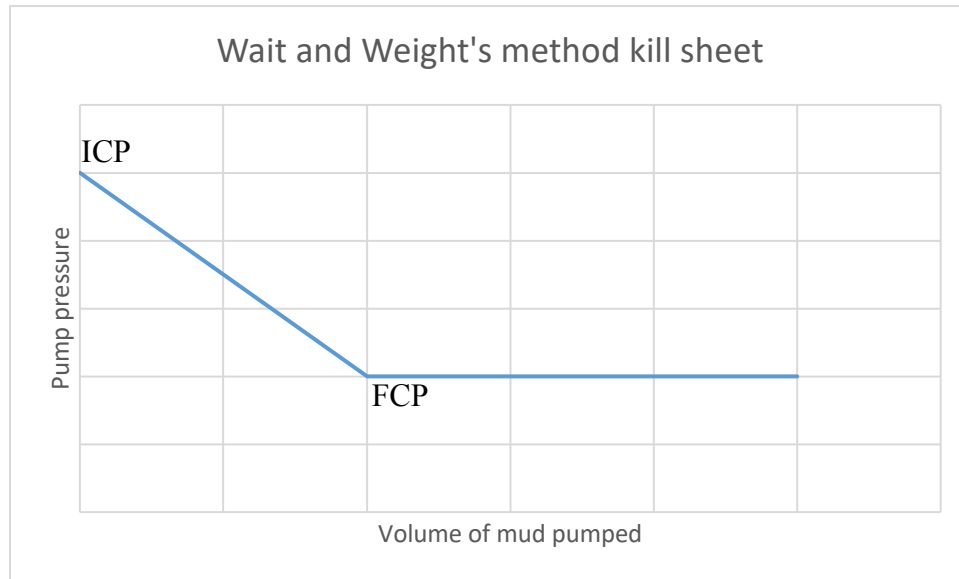


Figure 1. 4: Pump pressure changes using the wait and weight method

1.2.2 Well control with in Managed pressure drilling

Special well control capabilities of MPD systems

The strategy for well control when a kick is taken differs when Managed Pressure Drilling is being applied. It involves collection of tools to control the backpressure, so it is reactive and proactive for the kick tolerance in the well. The system is reactive when the well is drilled conventionally and the RCD tool is existing for added safety on any unexpected downhole problem. While the system is proactive when it designed during the drilling plan to employ the MPD technology for more precise wellbore profile pressure (Hannegan and Fisher 2005). The first reaction to an influx is not necessarily an immediate shut in of the BOP. Some small size kicks can be handled with only choke pressure applied. When the kick is of a bigger size and cannot be controlled by the MPD equipment, conventional well control procedures are applied. The main procedure of managed pressure drilling is to make the circulation system as a closed loop where the pressure on the annulus is controlled by the MPD choke manifold to keep bottom

hole at the desired pressure. The primary use of constant bottom hole pressure is when the window between pore pressure and fracture pressure is narrow and an exact value of BHP needs to be applied and varied depending on the operation.

Dynamic well control

Dynamic well control is defined in this context as continuing mud circulation even if the gas kick has entered the well without shutting in the well. There are many benefits to this procedure:

- 1) With continued circulation, frictional pressure added to ECD is still in effect. This prevents any additional influx from entering the well from loss of pressure exerted on bottomhole.
- 2) The ability to rotate the pipe further helps in solving a stuck pipe issue.
- 3) Quicker overall process for full circulations to get rid of the gas in the wellbore.
- 4) Less pressure is exerted on the shoe since the surface applied pressure needed is lower due to the frictional pressure loss from circulation (Rajabi, Hannegan, and Moore 2014).

Drilling while circulating influx case history

There are many instances where “flow drilling” was applied successfully. Flow drilling is continuing drilling without shutting in when the well is flowing and hydrocarbon influxes enter the well. Both regular rate circulation and pipe rotation are taking place even with a kick in the wellbore. The influx, whether it was gas or liquid, is separated out in the surface from the mud (Rajabi, Hannegan, and Moore 2014).

Among these successful examples is an example in the Austin chalk. A drilling challenge was encountered in a fractured carbonate formation with high pressure and high temperature

environment. A combination of UBD and MPD was used to complete the well successfully. The MPD was used to evaluate the limits of downhole pressure operations which helped in easing the handling limits of UBD. Underbalanced drilling was utilized by allowing the influx to enter the well. Drilling is continued until the influx cannot be handled by MPD. When that happens, well control relays on the traditional BOP shut in. The equivalent mud weight was small as 0.5 ppg between pore pressure and fracture pressure. The case was successful due to the use of PWD. PWD has helped in monitoring ECD and allowing continuing drilling while circulating out influx. The strategy involved taking several kicks. In this case study, repeated well control situations caused damage to the annular preventer and variable bore rams especially with the varying properties of mud and the kick fluid plus the high temperature (Elmore, Medley, and Goodwin 2014).

Micro flux Detection of kicks in OBM

Santos have analyzed real scale data which has also been utilized in this thesis. The main purpose of the tests was to see the capability of the micro flux system to detect a kick in OBM which has been known to be difficult due to the solubility of gas in oil. The tests were done in a 11 ppg oil mud with 70% volume diesel. The results showed a positive response detecting kick in OBM as accurate as WBM. The main rationale that was proposed for this was the accuracy of the flow meter deployed in the choke manifold. It is able to detect kicks as small as 0.5 bbl in contrast to basic metering systems deployed in rigs with 5 bbl detection volume (Santos et al. 2007). As can be seen in Figure 1.5, a simulation for diffract gas kicks volumes in both WBM as well as OBM. It shows the expected results of pit gain for OBM was smaller than that of WBM. Another phenomena that was worth noting here is that at lower gas kick volumes, the pit gain for

both mud types were virtually the same. Within the capabilities of micro flux system this detection can be easily made.

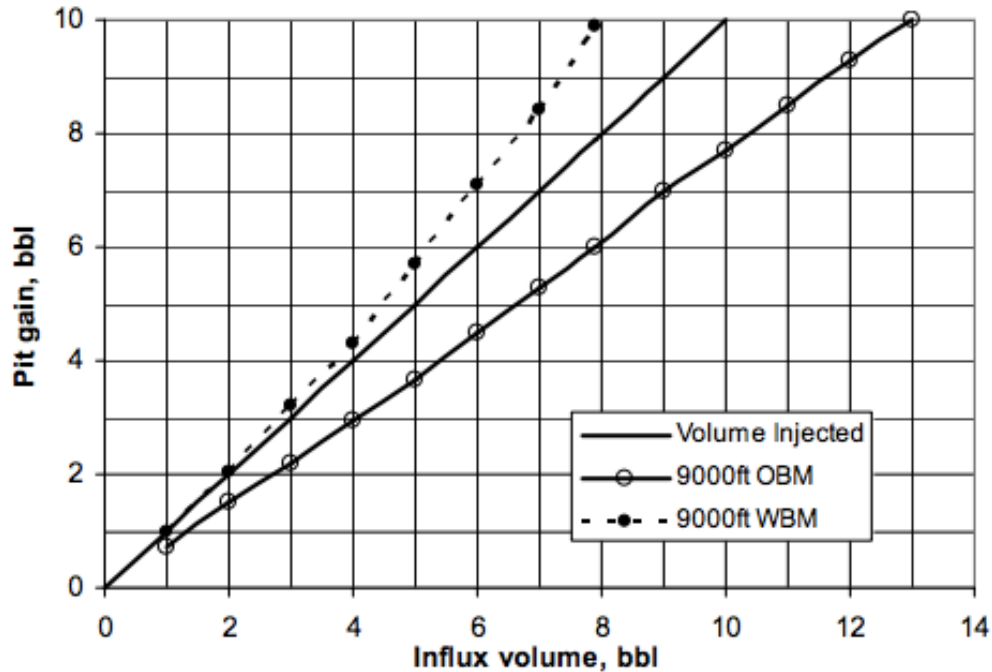


Figure 1. 5: Pit gain comparison for OBM and WBM

Well Control Matrix

The well control matrix is a guide to both the drilling crew and the MPD personnel. It clearly states at which point the responsibility of the kick mitigation shifts from MPD personnel to the drilling crew. The MPD system can process small size kicks without interrupting the drilling process. The threshold for the size of the kick depends on the following factors: rotating control device rating, formation fracture pressure, gas handling capacity, and liquid handling capacity of the rig. WCM is to be built and discussed before drilling starts (Rajabi, Hannegan, and Moore 2014).

Literature review of simulation studies on initial responses to gas influx during MPD operations

Several theses have been published with regards to well control in MPD operation (Davoudi 2009; J. E. Chirinos 2010; Guner 2009; Piccolo 2013; Das 2007). Specifically, CBHP application in MPD.

Das

Back in 2008, Das thesis was to simulate different well control initial responses within MPD constant bottom hole pressure application to evaluate the benefits and the drawbacks of each response. The simulated initial responses included shutting in the well, increasing back pressure through choke, increasing flow rate and collectively apply both back pressure and increase in flow rate. The kick fluid types studied were both gas and oil. The simulation was carried in a software called Ubits.

The outcome of Das's simulation study showed that the best initial response depends on the availability of certain equipment, geometry of the well, and the main objective while carrying out well control (reducing maximum casing pressure, keeping weak formation intact, staying within RCD rating). One sole best initial response was not identified as each initial response had advantageous and disadvantageous. All simulations were based of a WBM drilling fluid type. In MPD application, each well is a standalone well that needs to be thoroughly studied to find its own best initial response in case of well control. In this study, no real scale experiments were carried out for validation (Das 2007).

Davoudi

Davoudi also evaluated nine different initial responses to an MPD well control incidents. He used same industry well configuration of simulated examples as Das did. However, the software used was Drillbench (DynfloDrill) which serves as a multiphase transient flow system. The case simulated was a kick produced by a higher formation pressure than planned. Guner and Das studied an addition of instability of bottom hole pressure and shallower formation of higher pressure cases (Davoudi 2009).

The focus of Davoudi's study was a weak zone above the high-pressure zone that had loss circulation when traditional well control procedures was applied. The criteria that was used to detect the presence of a kick is a 2-bbl. gain with accurate flowrate measurement and 20 bbl. for inaccurate measurement. To validate the data historical real-life experiments carried out in 1986 in LSU #2 was used to compare results of dynflodrill (DFD).

When the data was validated for the use of Dynflodrill, the steady state case showed less than 6% error for Robertson-stiff rheology model and Dodge_Metzner friction factor model showed the least error.

The outcome of the evaluation of the nine-different circulating and non-circulating responses showed that when there is an accurate flow meter, the best response was a rapid increase of casing pressure, while if flow meter was not accurate an immediate shut in was recommend. As in the flow chart Fig 1.6 (Davoudi 2009).

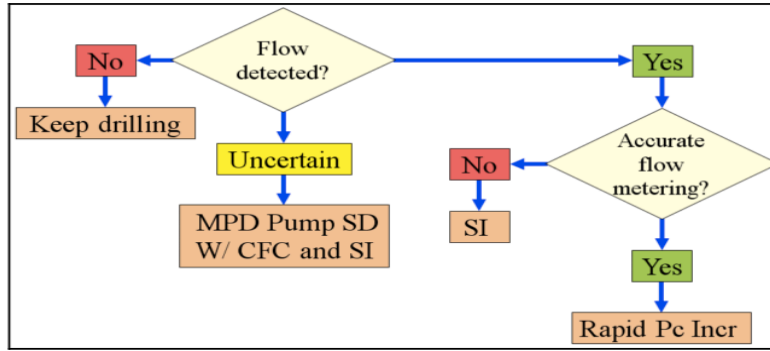


Figure 1. 6: Best initial response results(Davoudi 2009).

Chirinos

Chirinos thesis has three main methods: 1) Increasing the pump pressure gradually to minimize BHP irregularities while circulating out any gas influx. 2) Approximating Formation zone pressure while taking a kick in CBHP operations in MPD 3) Estimating maximum casing pressure to be planned for in drilling programs by a simple method of triangular gas shape. All if the three methods utilized both simulation data and real life experiments done in PERTT lab in 1986 for DEA project 7 as well as some experiments done in 2009 by the LSU MPD consortium (J. E. Chirinos 2010).

In Chirinos work, the full-scale test was done after the gas influx has entered and the process of circulating out the kick to obtain an approximate Constant BHP. Both Simulations using DFD and real life experiments showed around the same BHP with no significant fluctuations in Downhole pressure (J. E. Chirinos 2010). The actual BHP changes that happens during a pump start up happens due to different factors. One of which is the crew's ability to respond fast, the presence of an automated system, and the geometry of the well. The slimmer the well the more fluctuations there is in the BHP. This is primary caused by the BHP being affected by the size occupied by the gas with in the annulus weather around DC or regular DP. However, the LSU #2

experiments showed a reliable steady BHP within ± 25 psi when compared to the acceptable overbalance.

Maximum Casing Pressure Studies: one of the most important parameters to be estimated before spudding the well is the maximum casing pressure. This pressure is important to design the casing type, BOP rating and RCD rating in the case of MPD. Chirinos applied a simple method using Ohara's triangular gas distribution was applied. There are few assumptions that are necessary to be addressed to use this method. Single bubble gas with no slippage or dissolution is assumed. The method uses real gas law and the frictional pressure is negligible. The main idea of the Ohara method is to treat the gas as triangle with each vertex having different velocities. These velocities depend on gas bubble depth and inputting that variable into an empirical correlation made by Ohara (J. Chirinos, Smith, and Bourgoyne 2011; J. E. Chirinos 2010).

Chirinos focused on the circulating stage of well control during CBHP in MPD. DEA project 7 data were used to validate water based mud (circulating cases) simulations. As can be seen in Figure 1.7, 4 different formulae were applied to estimate maximum casing pressure. The best match was the Ohara method with only 25 psi difference than the actual. This shows that, at least for this LSU #2 geometry, range size of kick, and mud rates ranges, well control maximum casing is properly estimated by Ohara. However, it is worth noting that this geometry is the same used by Ohara and that could induce bias in the results (J. E. Chirinos 2010).

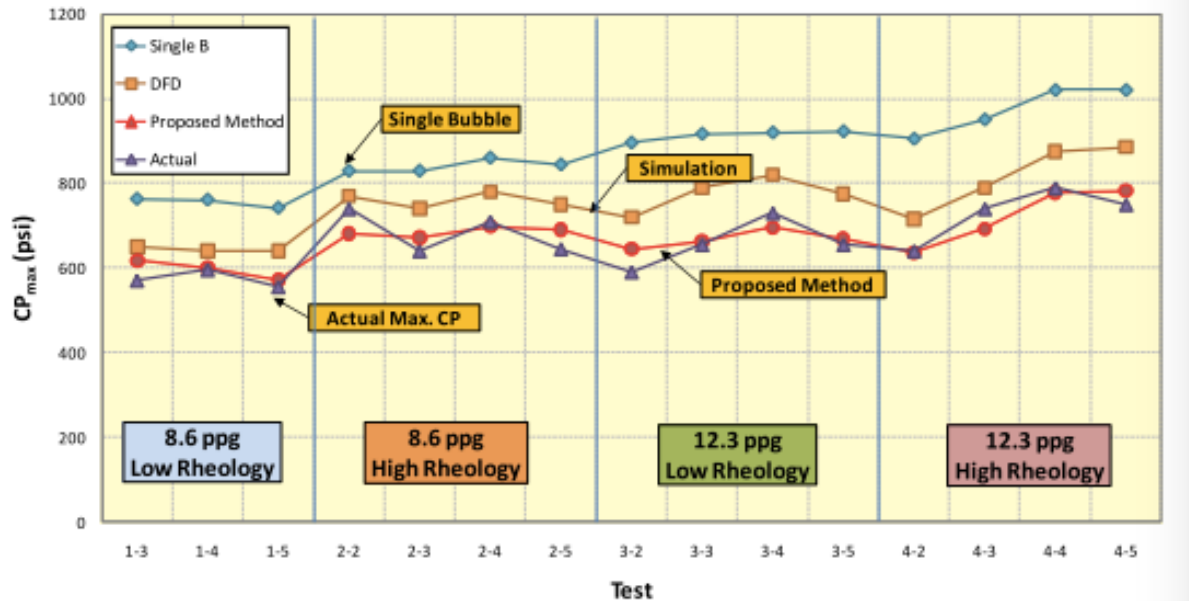


Figure 1.7: Maximum casing pressure using different formulas (Chirinos 2010)

1.3 Pipe Rotation and Eccentricity Effect on Frictional Pressure Loss

The effect of pipe rotation has been studied and a number of experiments have been conducted to analyze the effect of the rotation in the pressure losses. Different literature and models estimated the flow in the annuli using the Yield Power Law(YPL). In 1979 a numerical solution was given by Hank for laminar flow in concentric annuli. Also, in 1995 inner pipe rotation in both Newtonian and Non Newtonian fluid was studied by Escudier and Gouldson. In, 2006 Ozbayoglu and Omurla used the Computational Fluid Dynamics (CFD) to understand the frictional loss in the annuli especially for eccentric drill string. Erge studied the effect both numerically and experimentally. Yield Power Law (YPL) model was used in his experiment as a Non-Newtonian fluid. The effect of eccentricity was found to be significant, a decrease of 44% in the pressure losses for the range of properties of the tests conducted. The effect of the rotation was investigation in concentric scenarios and found that as the rotation increased, the pressure loss increased (Erge et al. 2015).

Eccentricity has a direct effect on the pressure loss by reducing the annular frictional pressure. YPL is used because of the existing of three variables that fit most of the drilling fluid. The problem with the YPL is the complexity of finding the pressure losses, Reynolds number and velocity profile (Erge, et al., 2015).

1.4 Two Phase Flow in Wellbore with Gas Kick

1.4.1 Initial Black Box Models.

The study of two phase flow in pipes is a complex process. It involves many variables. These variables consist of the properties of each phase, the flow mechanism and velocity for these phases, and in addition, the interaction between these two phases. Early studies of two phase flow needed some major assumptions to conclude a reasonable approximation of the flow.

“Black box” models early studies did not involve the details of flow patterns (Shoham 2005).

Homogenous No-Slip Model

One of the “black box” models treats the system as a single-phase model. It assumes a homogenous phase that has the average properties of the two phases. This model also averages the velocity of the two phases. This means that the two phases are undistinguishable. These approximations assume that there is no slip between the phases (Shoham 2005).

The assumptions of this model are: steady state flow, one average phase that represents the two phases, no slippage takes place between phases, compressible fluid of each phase, the area of the cross section may vary and mass could transfer between the two phases. The first few assumptions provides, especially the no slippage assumption, a limitation to the accuracy and applicability if the model.

Separated Model

The other extreme approach for representing two phase flow is treating each phase separately. In contrast to the homogenous model, it assumes no interaction between the two phases. The liquid phase and the gas phase are analyzed separately as a single-phase flow with applying the hydraulic diameter method. The hydraulic diameter is the equivalent diameter that each phase occupies in the cross-sectional area of the pipe. Each of these phases is then independently evaluated and treated for frictional factors and heat transfer for instance (Shoham 2005).

1.4.2 Recent Modeling.

Recent models are more rigorous in representing the two phase flow behavior. The modeling method could range from experimental to exact solution. It also includes intermediate methods such as numerical simulation and a combination of the empirical results and a simple physical model. The two phase studies include many variables such as volumetric flow rate, in-situ liquid hold up, no slip liquid hold up, superficial velocity, actual velocity, and slip velocity among many other variables (Shoham 2005) .

In situ liquid hold up (H_L) is defined as the “element in two phase flow field occupied by the liquid phase”. When the system has no slippage which is only accurate in few cases, the no slip liquid hold up (λ_L) is equal to the in situ liquid hold up. When there is no slippage in between the two phases (velocity of liquid is equal to velocity of gas) λ_L is calculated as the following equation

$$\lambda_L = \frac{Q_L}{Q_L + Q_g}$$

Where Q_L is liquid flow rate, Q_g is gas flow rater and λ_L is the in situ liquid hold up.

Superficial velocity is defined as the velocity of each phase if only that phase was present in the pipe such that for liquid superficial velocity $v_{sl} = \frac{Q_L}{A}$ where A is the cross sectional areal of the pipe. The actual velocity however is the velocity of each phase divided by the fraction of the volume occupied by that phase. The difference between the two velocities is known as the slip velocity.

To further examine two phase flow compared to single phase flow, a critical difference is studied which is the two phase flow patterns. The pattern is defined as the geometrical configuration of each phase on the pipe. The pattern depends on the flow rate of the gas, the geometry of the system (diameter and angle of inclination) as well as fluid properties of each phase (density, viscosity and surface tension). Fig 1.8 shows the different patterns that were recently commonly agreed on by researchers(Shoham 2005).

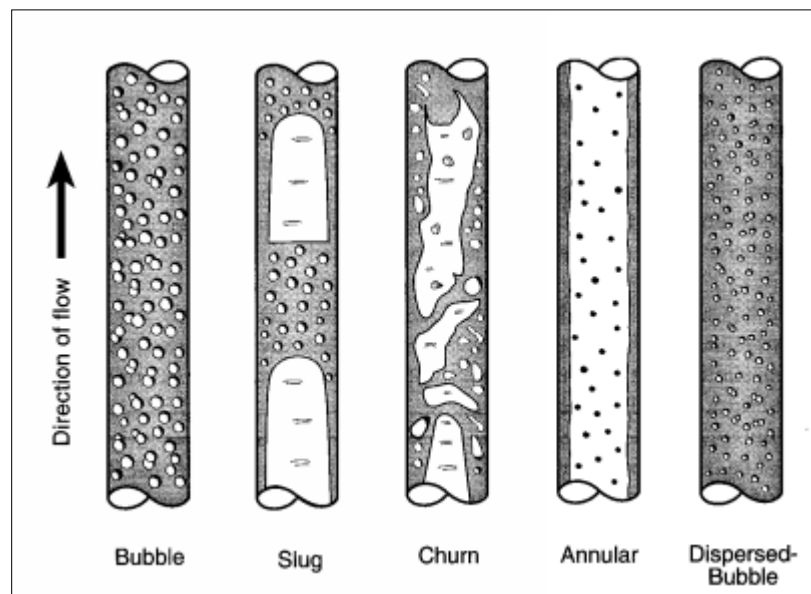


Figure 1.8: Flow patterns of two phase flow in vertical wells(Shoham 2005).

The main two flow patterns that are considered for this research is the slug flow as well as the dispersed bubble flow. *Slug flow*: The slug flow represents the flow of large bubble with a bullet shape known as the “Taylor-bubble”. The bubble occupies most of the cross-sectional area of the location it is in. This pattern is used in this research with only one bubble of gas coming up the well in the cases considered and referred to in later chapters as single bubble model. In contrast, *dispersed bubble flow*: This flow occurs at high liquid rates. The gas bubbles are small in such a way that the gas and liquid has the same velocity which supports the no slip homogenous case. Which was briefly examined for the model of dispersed bubble flow in water based mud (Shoham 2005).

CHAPTER 2: STATEMENT OF PROBLEM AND APPROACH

2.1 Statement of Problem

MPD system of well control allows for circulating out a certain volume of gas using the MPD choke without the need to revert back to conventional shut-in methods. This reduces unproductive time within drilling operation. In some cases, the operation being carried can proceed uninterrupted including drilling. This is made possible, partially, by the use of the rotating control device (sec 1.1.3) that provide the needed pressure control while allowing for the drill pipe to be rotated.

The possibility of rotating the drill pipe while the gas is being displaced out of the well raises the question of the effect of that rotation on integrity of the operation including the RCD required rating. The maximum anticipated casing pressure can alter by rotation due to two physical phenomena. First, the introduction of pipe rotation can change the annular frictional pressure loss calculated for the system. Second, the rotation of the pipe can allow for breakage of the gas bubble into smaller scattered bubbles throughout the wellbore instead of one single body of gas.

These physical phenomena work differently depending on the mud type, mud properties and operational variations. For example, in an OBM system, the gas can dissolve in the mud whereas the solubility of gas in WBM is small. In addition, the gas distribution throughout the well is expected to behave differently with well inclination, flow rate, mud properties and possibly pipe rotation. Mud type, mud properties and gas behavior in the wellbore have been taken into account to evaluate the effect of pipe rotation on the casing pressure while circulating out an influx on an MPD choke and simultaneously rotating the pipe whether for drilling or any other related operation.

2.2 Approach

2.2.1 Overview

The approach of addressing the problem was carried by, *first*, analyzing real scale kick circulation tests. These tests were carried in a controlled environment that mimicked downhole conditions with a gas influx entering the wellbore. These tests included a variation of mud properties, mud kill rates and mud types (OBM and WBM). The casing pressure profiles were gathered from these tests. However, these tests lack the effect of the pipe rotation as configuration is fixed in the tested well. *Second*, correlations were applied to estimate the effect of frictional pressure loss. These changes in frictional pressure loss is caused by pipe rotation and as a result changes the casing pressure values. These correlations are by Erge (Erge et al. 2014) and Ozbayoglu and Sorgun (Ozbayoglu and Sorgun 2010). The study was separated into three different models and cases: dissolved gas in OBM, single bubble in WBM and dispersed bubble in WBM.

Dissolved gas in OBM

The oil based mud cases were simplified by assuming that all gas was dissolved in the mud and the correlations were carried with the approximations of liquid only in the wellbore. Although this assumption is not truthful for all real operational cases, the test procedure for the real scale experiments were carried in a manner that ensures the dissolution of the gas in the mud prior to circulating out the influx.

Water based mud

Single bubble model

For the case of water based mud, the assumption of gas dissolution in mud is no longer valid.

The volume of gas and its expandability need to be taken into account. The approach to address WBM cases were first carried by the use of the common, however unrealistic, single bubble model. This model assumes that the entire volume of gas in the wellbore stays as a single body of gas and does not break down nor distributes throughout the wellbore. The well was divided into three different sections for each time step; two liquid regions and one gaseous phase region. The gas volume at each time step was calculated using the ideal gas law and the location of gas was evaluated using a correlation of gas velocity from the same real scale data set analyzed in this work. The model is explained in detail in Chapter 4.

To further investigate the validity of the single bubble model, extensive analysis and review of the gas bubble breakage and distribution is discussed in Chapter 5.

Dispersed bubble model

The study of the validity of the single bubble model suggested that the gas is more likely to be distributed throughout the well and the bubble does not stay in one gaseous phase. A study of the effect of a larger size gas bubble breakage into smaller size bubbles on the maximum anticipated casing pressure was conducted. This model assumes the other extreme of the spectrum, compared to the single bubble model. It assumes that the gas bubble is broken down into very small bubbles either caused by high rotational speed, different operational variations, and/or well inclination. The assumption entails that these gas bubbles were very small that no

slip velocity is present between the two phases and the dispersed bubble pattern equations are used. Further details are discussed in Chapter 6.

2.3 Real Scale Experiments in LSU#2 Well

In 1986, a consortium of professional companies along with Louisiana State University personnel conducted real-life scale field analysis of well control. The PERTT lab setup in LSU allows for a full size well control experiments. In these tests, approximately 10 bbl of gas is injected into a point close to the bottom of the well. These experiments are the closest to a real life kick in an actual well. The test was repeated over 20 times for both WBM systems as well as OBM systems. When the well was filled with WBM, nitrogen was injected except for few natural gas cases. For wells with OBM, natural gas was injected in all cases. Different mud weights, mud rheology, mud rates, gas rates have been tested in combination to result in a comprehensive study for both mud types. Shown in Table 1.1 is for water based muds and Table 1.2 is for oil based muds (“DEA Project 7” 1986).

2.3.1 Real scale well schematic

The tests were completed in LSU #2 well in the PERTT lab. As Fig 2.1 illustrates, The well is 5884’ deep with 9 5/8’’ casing to bottom. The well has a 3 1/2’’ tubing that reaches 5822’ that was used to circulate the mud. Another 1 1/4’’ pipe is located inside the 3 1/2’’ tubing used to inject gas at the depth of 5852’.

Eccentricity of LSU#2

The eccentricity of the LSU#2 well is not certain. For that reason, multiple scenarios of eccentricity were studied throughout the analysis of the tests.

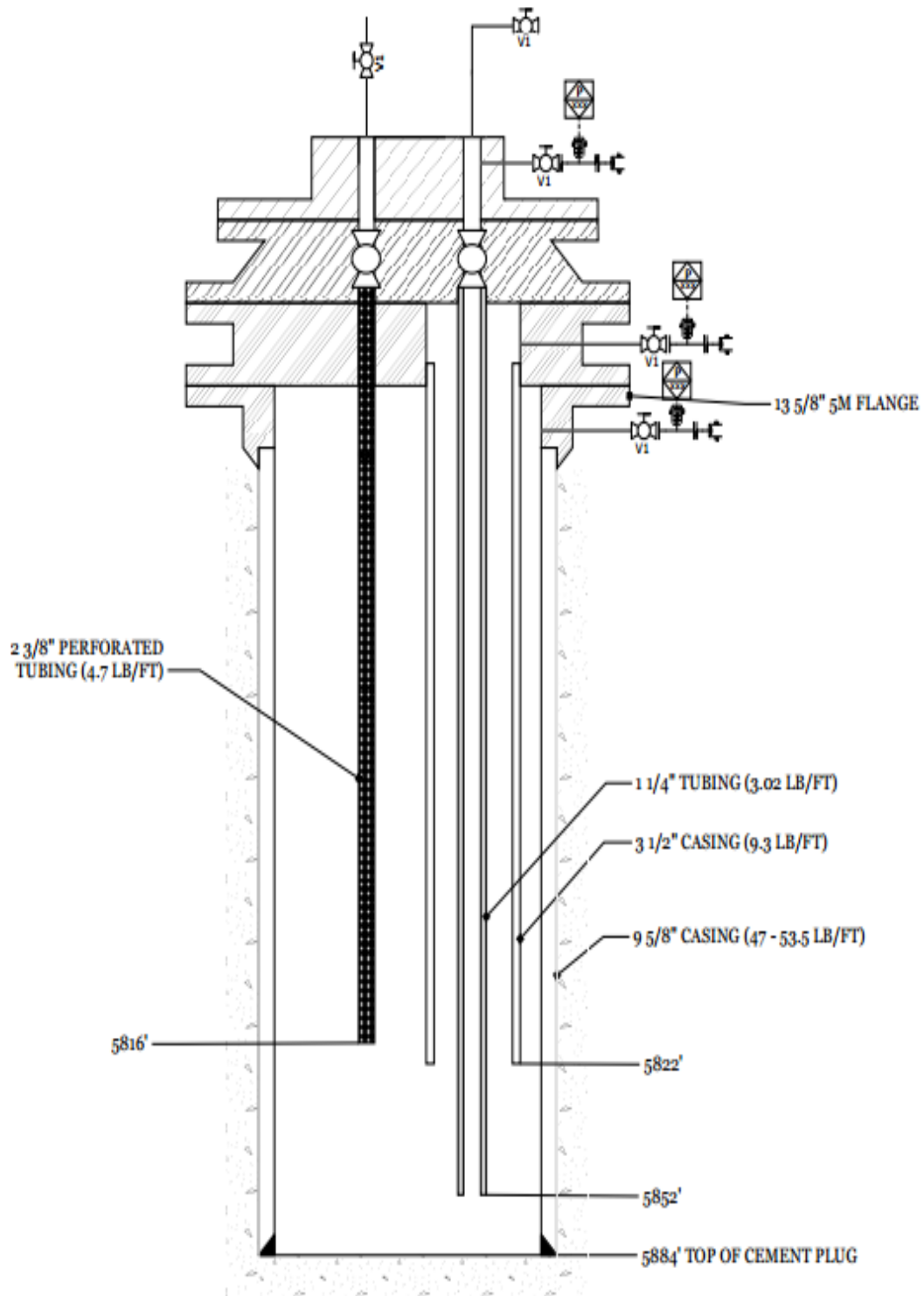


Figure 2.1: LSU #2 Well Schematic ("PERTT Lab Features" 2017).

2.3.2 Mud properties of real scale experiments

Multiple tests with gas injection were conducted. Various mud properties for each test were used.

As in Table 2.1 and Table 2.2, each test number was repeated 4 to 5 times with different kill rates and mud circulation rates.

Table 2.1: Water based mud properties for each test

Test #	Mud wt., ppg	PV	YV	10 sec gel	10 min gel
1	8.6	7.8	1.8	3.8	3.8
2	8.7	24.2	20.6	21.8	16.6
3	12.4	21.0	4.0	8.8	6.0
4	12.4	28.4	14.0	19.0	12.4

Table 2.2: Oil based mud properties for each test

Test #	Mud wt., ppg	PV	YV	10 sec gel	10 min gel
1	7.92	13.00	3.60	8.60	6.00
2	7.98	20.00	6.40	12.40	6.60
3	12.92	33.60	7.60	20.40	15.80
4	12.80	39.80	16.20	27.80	21.20

2.3.3 Real scale experiments data output

While each test was conducted, the data recorded summarized in Table 2.3.

Table 2.3: Real scale experiment recorded data.

Data	unit	notes
Drill pipe surface pressure	psi	The gauge was placed in the choke manifold. The pressure needs to be adjusted to friction
Surface casing pressure	psi	
Circulated out mud choke in pressure	psi	
Circulated out mud choke out pressure	psi	
Gas wellhead pressure	psi	
Gas wellhead flow rate	scf/hr	Needs to be used with caution due to flow meter calibration issues
Mud flow rate	gpm	
Mud tanks volume	bbls	
Mud gain/loss		Affected by changes in mud flow rate or leaking valves
Mud density in and out	ppg	using micromotion

2.3.4 Test procedures

The gas injecting procedure starts with the correct manifold valve positions. It ensures a flow from gas storage wells into the 1 ¼” gas injection lines into LSU#2. After the initiation of the gas injection, the PERTT lab staff monitor pit gain. The gas will displace mud in the 1 ¼” tubing. When the pit gain reaches 9 to 10 bbl., the injection process stops (“DEA Project 7” 1986).

After 9-10 bbl. of gas has been injected, a pump is turned on to displace the gas volume in the 1 ¼” pipeline. There are separate manifold lines for each mud type (WBM and OBM). The Schlumberger gradiometer representative monitors the gas going into the 3 ½” -9 5/8” annulus. Once all gas has passed the gradiometer position, the PERTT lab staff turns off the pump (If the test required the gas to be circulated out after injection. The pump stays on operating position, mud is only injected between 1 ¼” tubing and 3 ½” tubing). In all these tests, bottom hole pressure was kept constant. This is accomplished by applying surface pressure on the 1 ¼” tubular. The gradiometer is relocated closer to the surface line. The gradiometer records the arrival of the gas bubble to its location. *OBM test* take a different route to determine the gas being displaced into annulus. The gas goes directly into solution in OBM annulus choke on the annulus is closed. Once choke pressure on the 1 ¼” pipe stabilizes, it the sing that the gas went into solution.

2.4 Pipe Rotation Frictional Pressure Loss Effect Correlations

The rotation of the pipe effect on pressure drop is to be applied based on the work done by both (Erge et al. 2015) and (Ozbayoglu and Sorgun 2010). Field measurements using PWD showed an increase in ECD when RPM is increased (Erge et al. 2015). However, the literature varies on the

effect of rotation on the frictional pressure as has been discussed previously. In YPL mud model when $m \leq 1$, the fluid is shear thinning which means the higher the velocity or shear rate, the lesser the apparent viscosity (slope of shear stress vs shear rate at a certain shear rate). The basic model is in Eq 2.1.

$$\tau = \tau_y + K\gamma^m \quad \text{Eq 2. 1}$$

Where τ_y is the yield point shear stress in (Pa) , K is the consistency index of fluid in (Pa.s^m) and m is the flow behavior index (no unit).

When the shear thinning behavior of fluid takes place, higher liquid velocity is expected to result in a decrease in frictional pressure loss because of the lower apparent viscosity. Nevertheless, the inertial forces could act against viscous forces and increase the frictional pressure. For that reason, Erge conducted a study on a 90 ft horizontal pipe with a rotating inner pipe to measure the annulus pressure loss. The researchers have developed a correlation to best estimate the frictional pressure loss depending on the flow regime with pipe rotation. The eccentricity of the drill pipe was also included in the correlation (Erge et al. 2015).

Erge Correlation

The proposed formula first starts with finding the wall shear rate from the rheology model as in Eq 2.2:

$$Q = \frac{wh^2}{2 \cdot K^{1/m} \cdot \tau_w^2} \left(\frac{m}{1+m} \right) (\tau_w - \tau_y)^{\frac{1+m}{m}} \left(\tau_w + \frac{m}{1+m} \tau_y \right) \quad \text{Eq 2. 2}$$

Where $h = \frac{D_o - D_i}{2}$ and $w = \frac{\pi}{2} (D_o + D_i)$, D_o is the outer diameter, D_i is the inner diameter of the annulus in (m). τ_w is the shear rate at the wall in (Pa), and Q is the flow rate in (m³/s).

Eq 2.2 is applied to the mud specific rheological model. The shear stress is found using mud specific shear stress vs shear rate graph.

Then the approximation of the generalized flow behavior index is found using (Ahmed and Miska 2008) equation as in Eq 2.3.:

$$\frac{3N}{1+2N} = \frac{3m}{1+2m} \left[1 - \left(\frac{1}{1+m} \right) x - \left(\frac{m}{1+m} \right) x^2 \right] \quad \text{Eq 2. 3}$$

Where $x = \frac{\tau_y}{\tau_w}$, N is the generalized flow behavior index. In the mud properties of LSU #2 case, m was 1 as in Bingham plastic rheological model. Also, generally, whenever t_y is zero, as in the regular power law, the N would be equal to m.

The Reynolds number is then used for YPL.

$$Re_{YPL} = \frac{12\rho v^2}{t_w} \quad \text{Eq 2. 4}$$

Where ρ is the density of the liquid (or mud) in (Kg/m³) and v is velocity of liquid in (m/s) Re_{YPL} is calculated to check the flow regime. Flow regimes defined in Erge's work are laminar, transitional, and turbulent. The criteria for flow regimes is provided in Eq 2.5 and 2.6. If the $Re_{YPL} < Re_1$, the flow was laminar. If $Re_1 < Re_{YPL} < Re_2$, the flow is transitional and if $Re_{YPL} > Re_2$, the flow was turbulent.

$$Re_1 = 2100 \cdot [N^{0.331}(1 + 1.402\kappa - 0.977\kappa^2) - 0.019eN^{-0.868}\kappa] \quad \text{Eq 2.5}$$

$$Re_2 = 2900 \cdot [N^{-0.039Re_1^{0.307}}] \quad \text{Eq 2.6}$$

Where $\kappa = \frac{D_i}{D_o}$, $e(\text{eccentricity}) = \frac{2E}{D_o - D_i}$, E is the distance of the drill pipe from the center of the annulus in (m).

In most of the cases of the real scale experiments, the flow is laminar. For laminar flow, the frictional factor is found using Eq 2.7

$$f_{lam,con} = \frac{24}{Re_{YPL}} \quad \text{Eq 2.7}$$

The above equation is for the frictional pressure not accounting for pipe rotation. To add the pipe rotation factor $f_{lam,con}$ is multiplied by c (Eq 2.8- Eq 2.11)

$$c_{lam} = 0.2287 \cdot N - 0.0580 \cdot F_d + 0.1237 \cdot w_d + 0.4289 \quad \text{Eq 2.8}$$

$$c_{trans} = -1.0267 \cdot N - 0.0096 \cdot F_d + 0.0390 \cdot w_d + 1.2422 \quad \text{Eq 2.9}$$

$$F_d = \frac{\text{Axial Compression Force}}{\text{Force required to buckle pipe sinusoidally}} \quad \text{Eq 2.10}$$

$$\omega_d = \frac{\omega(\frac{rev}{min})}{500 \frac{rev}{min}} \quad \text{Eq 2.11}$$

N is the generalize flow behavior index found by Eq 2.3, F_d is the dimensionless force defined in Eq. 2.10 (it was set to zero for LSU #2 data as the drillpipe is in tension) and ω_d is the dimensionless speed of rotation and ω is the rotational speed in RPM. Then to find the frictional pressure loss (FP) Eq 2.12 used, where f (frictional factor) is modified using Eq 2..8 or 2.9

$$FP_{Erge} = \frac{2fpv^2}{D_o - D_i} \times L \quad \text{Eq 2.12}$$

L is the length of drillpipe that frictional pressure loss was subjected to in (m).

The units from this correlation are metric. Then, units were converted from metric to field units for parameters of the LSU#2 case and mud properties. The experimental tests that Erge based his correlation on were done for a range of eccentricities. The range of flow rate is 0-120 gpm and rotational speed is 0-120 RPM. The mud properties were done on a power law rheological model that falls around the rheological model of the real scale experiments' mud (Erge et al. 2015).

Ozbayoglu and Sorgun Correlation

To apply this correlation, effective axial viscosity (μ_{e_a}) and radial viscosity (μ_{e_r}) are defined as follows in Eq 2.13 and 2.14

$$\mu_{e_a} = \left(\frac{K(D_o - D_i)^{1-m}}{144 v^{1-m}} \right) \left(\frac{2 + \frac{1}{m}}{0.0208} \right)^m \quad \text{Eq 2.13}$$

$$\mu_{e_r} = K \left(\frac{1}{m} \right)^m \epsilon \left(\frac{1}{\omega} \right)^{1-m} \quad \text{Eq 2.14}$$

$$\epsilon = \left(\frac{D_o^2 - D_i^2}{D_o^2} \right) \left(\frac{15}{\pi} \right)^{1-m} \left(1 - \left(\frac{D_o}{D_i} \right)^{2/m} \right)^{-m} \quad \text{Eq 2.15}$$

D_o and D_i are outer and inner diameter of the pipe, respectively in (ft), K is the consistency index in (lbf/100ft²s^m), m is the flow behavior index which is dimensionless, v is the axial flow velocity in (ft/s) and ω is the rotational speed of drillpipe in RPM

Then, these viscosities are inserted in a Reynolds number equations for separately defined axial Reynolds number (Re_a) and radial Reynolds number (Re_r) (Eq 2.16 and Eq 2.17, respectively) and the frictional factor depends on Total Reynolds number (Re_T) as follows:

$$Re_a = \frac{757 \rho v (D_o - D_i)}{\mu_{e_a}} \quad \text{Eq 2.16}$$

$$Re_r = \frac{2.025 \rho \omega (D_o - D_i) D_i}{\mu_{e_r}} \quad \text{Eq 2.17}$$

The frictional pressure factor is then decided on the following constraints and limits,

If $(Re_T) < 3000$

$$f = 8.274 Re_a^{-0.9075} + 0.00003 Re_r$$

If $3000 < (Re_T) < 7000$

$$f = 0.0729 Re_a^{-0.3017} + 0.00011 Re_r$$

If $7000 < (Re_T) < 10000$

$$f = 0.006764 Re_a^{-0.0286} + 0.0001 Re_r$$

If $10000 < (Re_T) < 25000$

$$f = 8.28 Re_a^{-0.7258} + 0.00001 Re_r$$

If $25000 < (Re_T) < 40000$

$$f = 0.006764 Re_a^{-0.2262}$$

If $(Re_T) > 40000$

$$f = 0.03039 Re_a^{-0.1542}$$

These frictional factors are then inserted into Eq. 2.18 to find the frictional pressure loss of the entire length of section of concern:

$$FP_{Ozb} = \frac{f \rho v^2}{21.1(D_o - D_i)} \times L \quad \text{Eq 2.18}$$

Where L is the length of the section that the flow rate and inner pipe rotation is subjected to in(ft) and FP is the frictional pressure loss in (psi)

The experimental tests that Ozbayoglu and Sorgun based their correlation on were only done for an eccentric well. The range of flow rate is 0-150 gpm and rotational speed is 0-120 RPM. The mud properties were based on a power law rheological model that falls around the rheological model of the real scale experiments mud (Ozbayoglu and Sorgun 2010).

Sensitivity Analysis of Erge's Correlation Parameters:

A sensitivity analysis on Erge's correlation model was conducted. The effect of various parameters such as pipe rotational speed, mud rheology model, and surface applied force on drill pipe, generalized flow behavior index, flow rate and eccentricity were studied. The range of parameters that were studied are within the values of the PERTT lab test data. The outcome of those results only applies to inputs that are of similar values for those in the test mentioned in the mud properties summary table (Sec 2.3.2) while applying a Bingham plastic modification where $m=1$.

The most important parameter studied here is the speed of pipe rotation. Fig 2.2 shows a general trend of increase of pressure loss with the increase of pipe rotation speed. The rheology model of

the mud plays a slight role in the rate of increase. As it can be seen for lower rheology as in (WBM1), the increase rate is lower than for that in higher mud rheology (OBM2). More importantly, the expected concentric non-rotating case frictional pressure loss is actually higher than that of a rotating case. This behavior is not the most common, however, for the set of flow rate and mud rheology being tested shows a decrease in frictional pressure loss from non-rotation to rotation case.

Since the geometry of the wellbore being tested is constant ($D_o = 8.62''$ & $D_i = 3.5''$), the stability criteria depends on mud properties. For this case (flow rate = 300 gpm, Concentric Annulus $E=0$, $f_d=0$) in Fig 2.2, WBM1 follows the transitional flow criterion (Eq 2.9), whereas OBM2 and OBM3 are under laminar flow (Eq 2.8). This is evident in the bigger effect that pipe rotation has in laminar flow since its coefficient in the “c” parameter is larger than that of transitional flow as illustrated in Equation 2.8 and 2.9. When applying this correlation, the increase in rotational speed does not play a role in defining the flow regime.

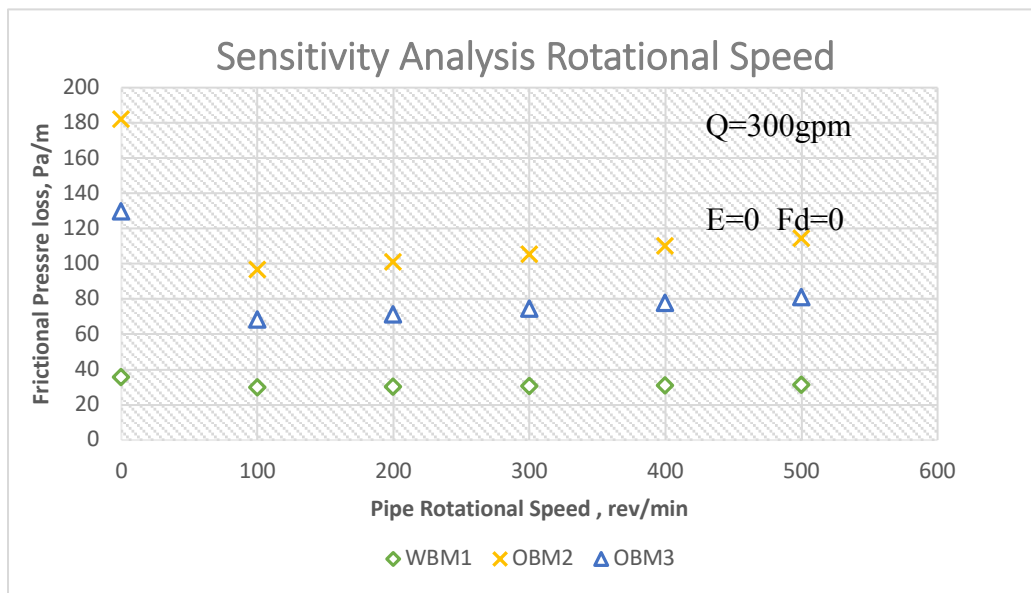


Figure 2. 2: Sensitivity analysis on the change of rotational speed

One of the assumptions to apply Erge's correlation is that the value of N , generalized behavior index, must be between 0.15 and 0.4 which are illustrated in Fig 2.3 by the red lines. N is a parameter that is formulated to combine the effect of flow behavior index ($m=1$ in Bingham plastic), shear stress at the wall and yield shear stress at a particular flow rate to account for the profile change in shear stress profile throughout yield power law flow in pipe (Eq 2.3). An increase in the value of N shows a steady increase in frictional pressure loss in annulus as in Fig 2.3. This is also the result of flow rate increase as in Fig 2.4. For this case, other parameters were held constant ($\omega=0.3$, $F_d=0$, Concentric Annulus $e=0$)

It is important to note the slope change in the Fig 2.3 and Fig 2.4 for OBM3 and WBM1 are due to the change in flow regime from Laminar flow to transition flow. The onset transition for WBM1 and OBM2 are illustrated in Fig 2.4

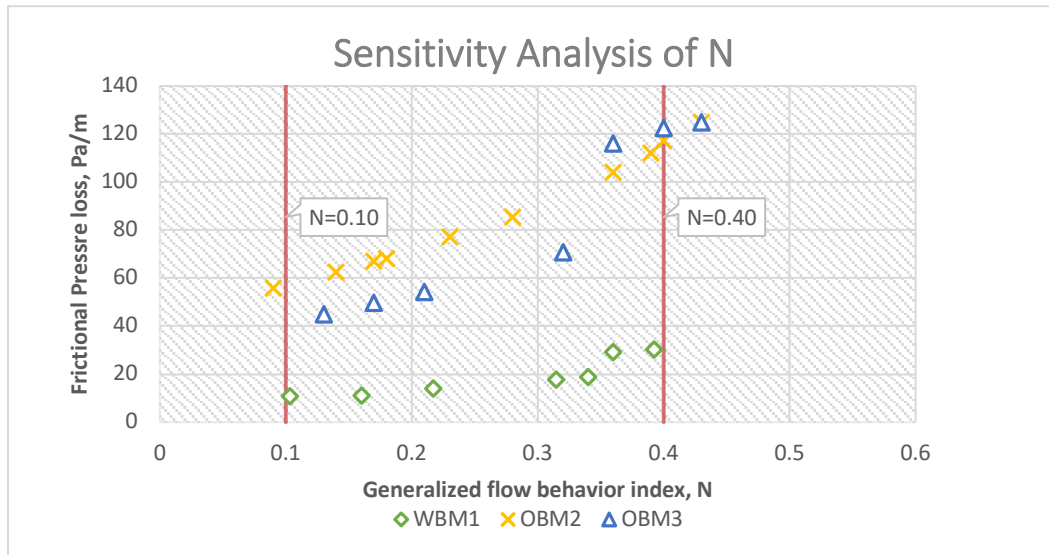


Figure 2. 3: Sensitivity analysis flow behavior index

Effect of Eccentricity

The effect of eccentricity for Erge correlation shows that the higher the eccentricity, the lower the frictional pressure loss. The velocity of fluid in an eccentric well is lower than a concentric well because of the spread flow is on the larger area. The main change of varying eccentricity is

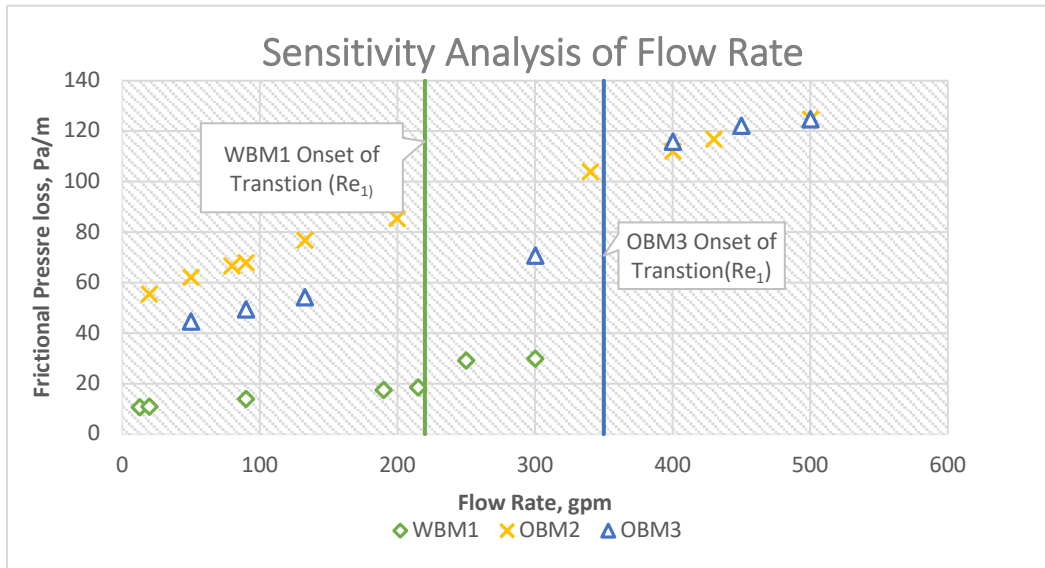


Figure 2. 4: Sensitivity analysis of Flow Rate

the non-rotation case compared to the rotating case. This dictates whether or not the overall frictional pressure loss is going to increase or decrease when applying pipe rotation. The accuracy of this observation is crucial for the baseline measurements of the casing pressure from the real scale experiments. Fig 2.5 shows the effect of changing eccentricity of on the estimated frictional pressure loss. As the eccentricity (e) increases, the frictional pressure loss decreases.

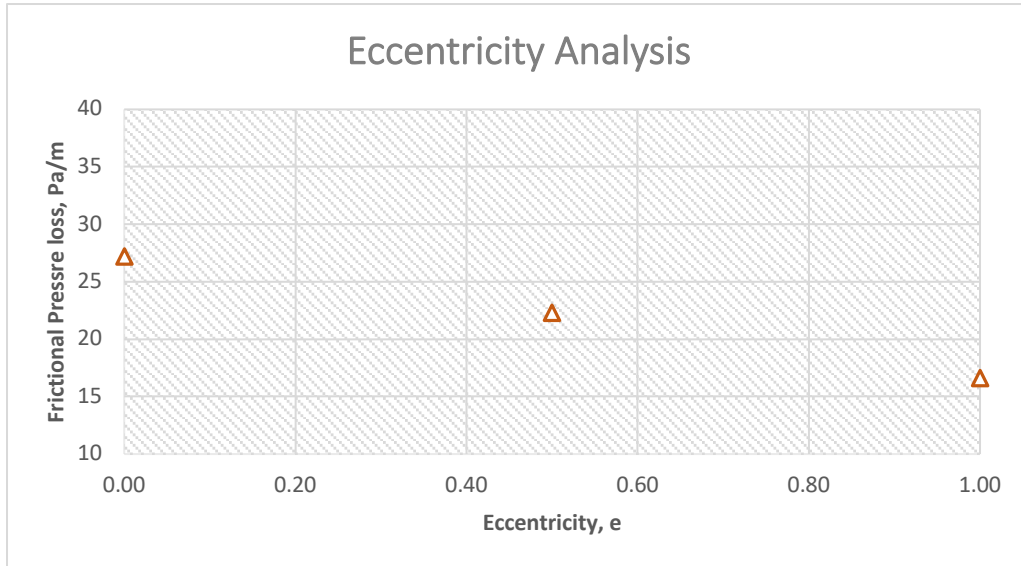


Figure 2.5: General sensitivity analysis for eccentricity

The frictional pressure loss with rotation is not affected by the eccentricity as can be seen in Fig 2.6. The main effect happens when the drill pipe is not rotating (i.e. $\omega=0$).

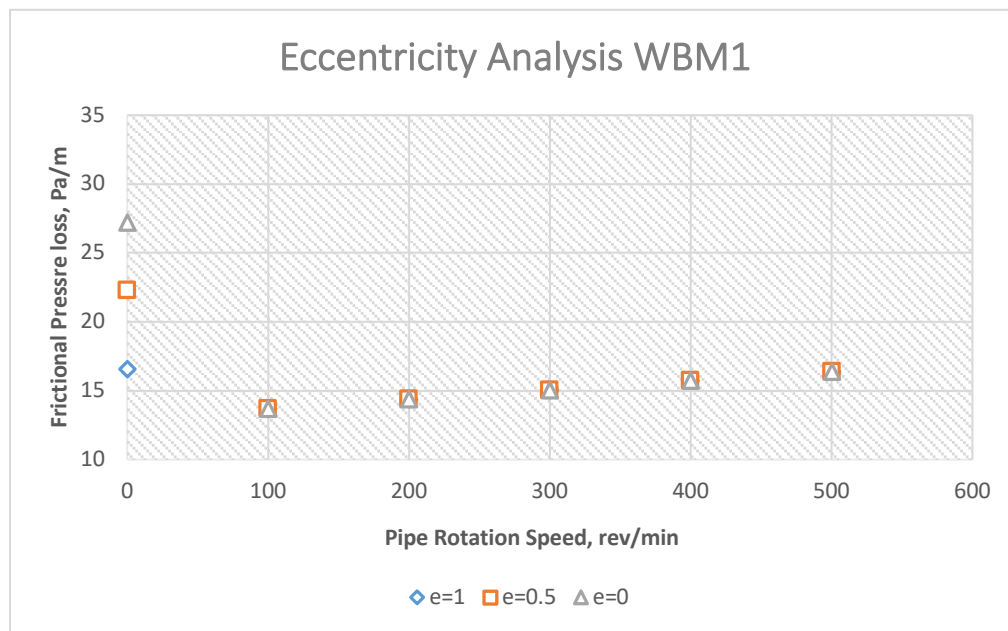


Figure 2.6: General sensitivity analysis for eccentricity

Comparison between the correlations

A comparison between the results of the two correlations for the same mud properties, flow rate, and well schematic (including only eccentric case limited by Ozbayoglu and Sorgun correlation) is shown in Fig 2.7 and 2.8. For a flow rate of 90 gpm and the mud properties for WBM1, the frictional pressure loss for Erge's model was higher than that for Ozbayoglu and Sorgun correlation. The increase in speed of rotation in both correlations showed an increase in frictional pressure loss. Non-rotation case of Erge model showed a higher pressure loss than the case with rotation.

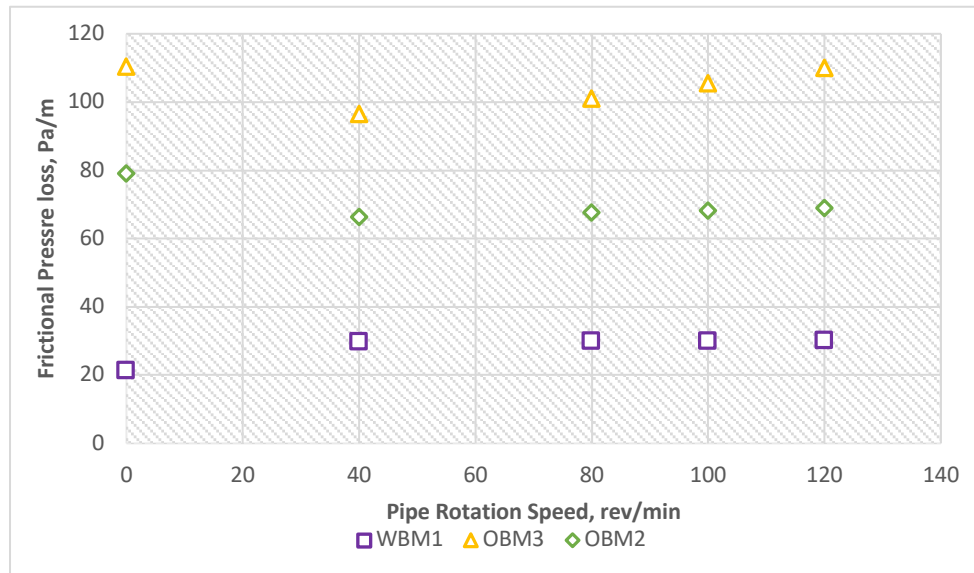


Figure 2.7: Effect of rotation on frictional pressure loss using Erge correlation example

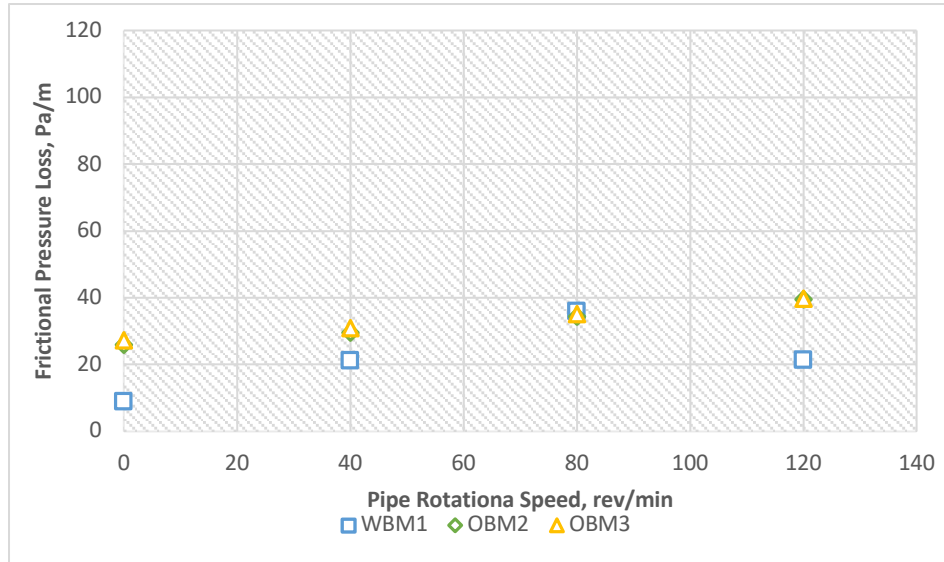


Figure 2.8: Effect of rotation on frictional pressure loss using Ozbayoglu correlation example

2.4.1 Gas bubble breakage effect

The single bubble model of well control has been the most commonly used model in the case of gas influx. It can be described as the worst case scenario in terms of maximizing the casing pressure when the kick reaches the surface. However, this model is not the most accurate as many physical variations to the operation and mud properties can break the gas bubble into multiple smaller bubbles. Kill rate, mud type, mud rheology, choice of time for well shut in and pipe rotation are among those physical variations that can play a role in breaking the gas bubble. The gas bubble breakage and distribution is discussed in detail in Chapter 5.

CHAPTER 3: ANALYSIS OF FRICTIONAL PRESSURE CHANGES ON CASING PRESSURE CAUSED BY PIPE ROTATION IN OIL BASED MUDS USING DISSOLVED GAS MODEL

3.1 Overview

The aim of this study is to calculate the changes in casing pressure caused by the pipe rotation in OBM while a kick is circulated out of the well. As it has been mentioned earlier, the setup of MPD systems allow for gas kicks to be circulated out while continuing drilling or other related operations that involve pipe rotation. The main factor that alters the casing pressure, considered for this section, is the change in annular frictional pressure loss when the pipe is being rotated. This is accomplished by the analysis of the OBM real scale experiments. These experiments were then coupled with the pipe rotation correlations (sec 2.4) to calculate the frictional pressure loss of each test.

Four different tests were analyzed for the effect of pipe rotation on OBM casing pressure operations while displacing the gas to surface. Each test had a distinct set of operational variations, mud rheology, and mud weight. The procedure for all these tests is similar. This process ensures that the gas goes into solution in the oil based mud. Then, the kick is circulated out of the well. The data for the casing pressure profile, mud flow rates, is collected throughout the procedure. Then, the effect of frictional pressure changes is applied. That change in casing pressure is analyzed to see if it has any practical changes for the RCD rating for choice.

The general concept of the model for OBM used in this chapter is that the well, with gas completely dissolved in mud, only contains liquid. Therefore, the correlations of pipe rotation were applied with assuming only liquid flow in the annulus. This assumption is valid in certain cases. The study of a gas kick in OBM is significantly affected by the gas solubility in the mud.,

especially when the process takes place in a high pressure environment such as downhole wellbore conditions. A brief study of that effect on the validity of the liquid approximation model to estimate the frictional pressure loss is included in this chapter.

3.2 Dissolved Gas Model for Oil Based Muds

This model is a simplified model to address frictional pressure changes in OBM systems with gas kicks. The gas was assumed to be completely dissolved in the mud at bottom hole pressure. Therefore, when applying the pipe rotation approximation, only liquid is assumed to be in the wellbore. This assumption is supported by the procedure that was carried for the real scale tests in oil based mud. The procedure ensures that gas goes into solution before starting the kick circulation out process as illustrated in Fig 3.1. After approximately 10 bbl. of gas is injected into the wellbore (step 1), the pump is turned off and the annulus choke is closed to maintain enough pressure to dissolve the gas into the mud (step 2). When the pressure of the 1 1/4" drill pipe stabilizes (refer to 2.3.1), the gas was decided to be completely in solution. Once this was established, the circulating out process starts (step 3). The casing pressure changes is approximated using Eq. 3.1

$$CP_{RPM} = CP_{static} - FP \quad \text{Eq 3. 1}$$

Where CP_{RPM} is the casing pressure with rotation, CP_{static} is the casing pressure for non-rotational case (real scale test data) and FP is the frictional pressure increase calculated from each correlation (Erge and Ozbayoglu)using only liquid flow in the well bore. The units are all in (psi).

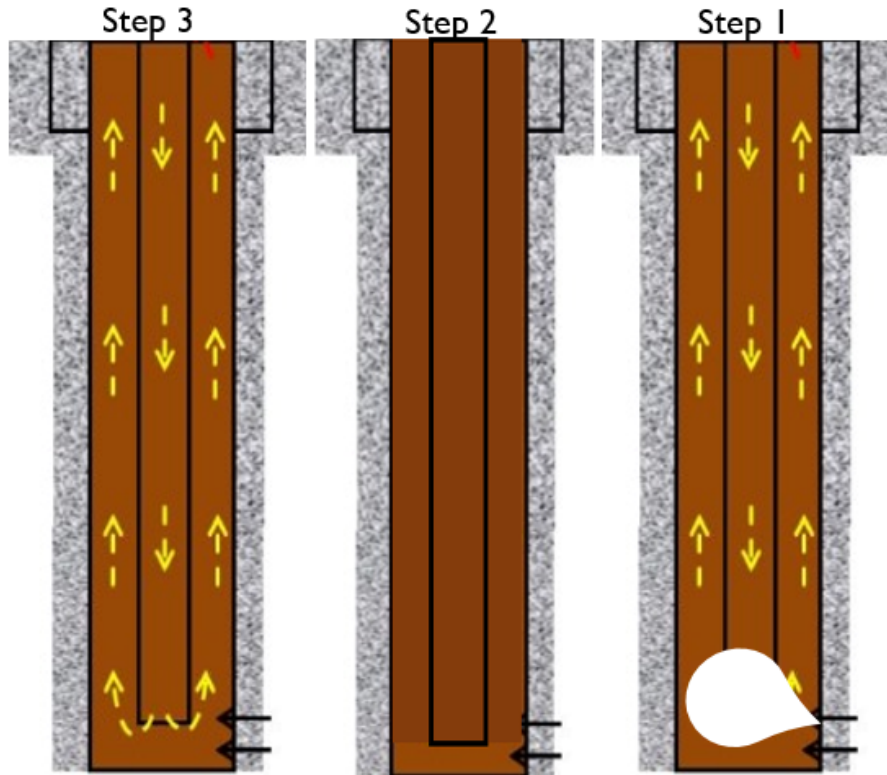


Figure 3. 1: OBM real scale procedure illustration

3.3 Example of Full-Scale Data Output (OBM)

An example of one of the OBM tests of the real scale experiments data output and measurements are shown in Fig 3.2. The casing pressure data with time was the main curve that analysis was run on. Measurements such as the flow rate and mud properties (rheology and density) were included in the calculation of the frictional pressure loss caused by pipe rotation.

Fig 3.2 also illustrates some of the procedure steps. The kill rate for this test was 90 gpm.

Around min 50, after the gas was injected, the pump was turned off and the annulus choke was closed to dissolve the 10 bbl of gas is in the mud. At this point, the volume of the mud pit did not go back to its original value; this is mainly caused by the volume of the dissolved gas added to

the circulation system. Once this gas dissolution was established, circulation was restarted around 110 min mark.

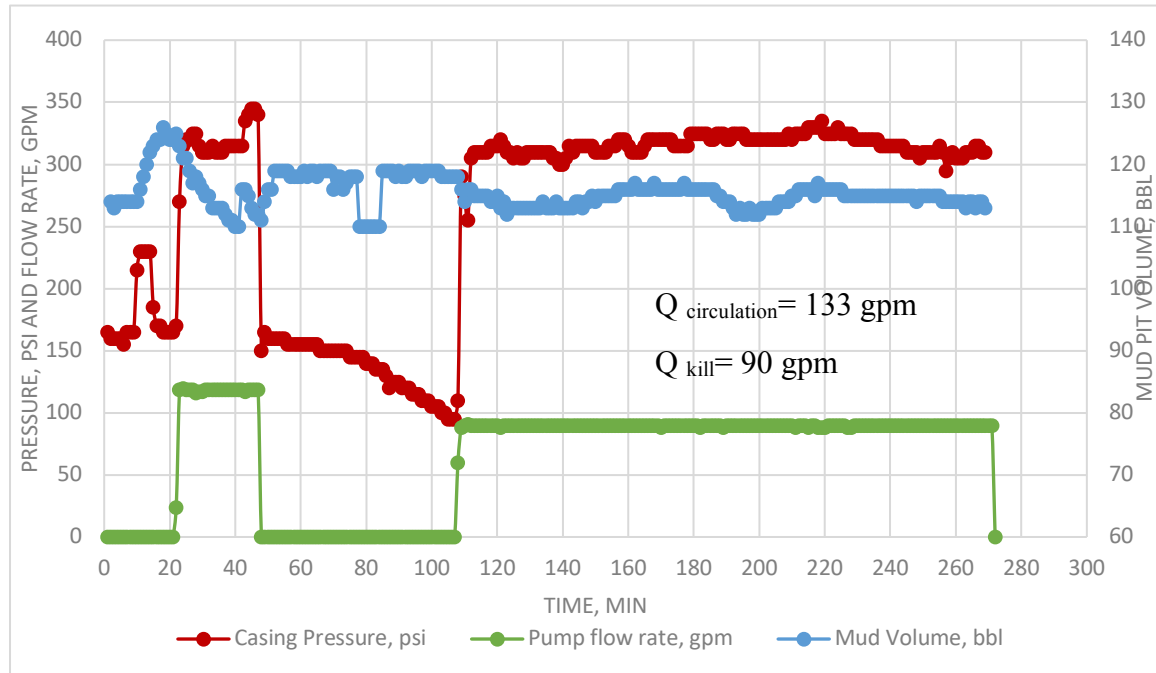


Figure 3. 2: Test 2-5 (OM10) data measurement and output.

3.4 Pipe Rotation Effect on Casing Pressure in OBM Using Dissolved Gas Model

Four different tests were analyzed for the effect of frictional pressure loss variations caused by pipe rotation on the casing pressure. The frictional pressure loss was calculated for both concentric and eccentric schematics in LSU #2. Both setups were calculated because the eccentricity of LSU #2 is not certain. The main outcome of all these test showed an increase in the casing pressure. The reason is that the frictional pressure loss actually decreases from the non-rotational case (eccentric and concentric) to the rotational case at 120 RPM. The frictional pressure loss when the pipe is not rotating has higher frictional pressure loss than when the pipe is rotating. Practically in the field, this rarely occurs but some experimental results do suggest

that the non-rotational case can have a higher frictional pressure loss as in the work of Erge and the correlation based on it (Erge et al. 2015).

Since OM6 and OM10 tests have the same mud properties and similar flow rates, the effect of pipe rotation has shown the same trend of an increase casing pressure. The maximum increase of casing pressure of the OM6 and OM10 tests was a value of 16 psi. This accounts for a 5 % increase of the average casing pressure of 300 psi and an increase of 4% of the average of 325 psi for Test 2-1 (OM6) and (Test 2-5) OM10 respectively as can be observed in Fig 3.3 and Fig 3.4. This is an increase that probably would not make a practical difference for a case similar to the LSU#2 data with low mud rheology and only 6000 ft depth.

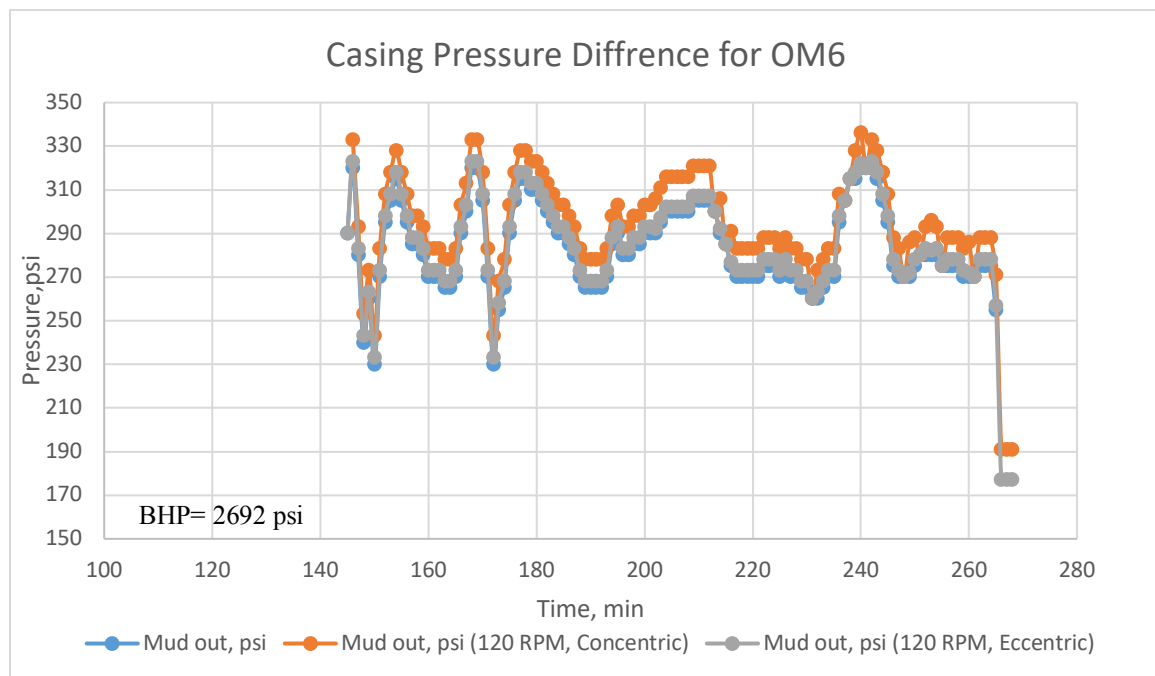


Figure 3. 3: Effect of pipe rotation using Erge's model for OM6

In Fig 3.5, a comparison between Erge and Ozbayoglu correlations was conducted. The Ozbayoglu correlation has the starting position before rotation set to be eccentric. The rotation for the set of data in DEA project mud properties and flow rates has no practical effect. With

only 1 psi decrease, this could be a correlation error. Ozbayoglu correlation was not run on the rest of the tests because of that small effect.

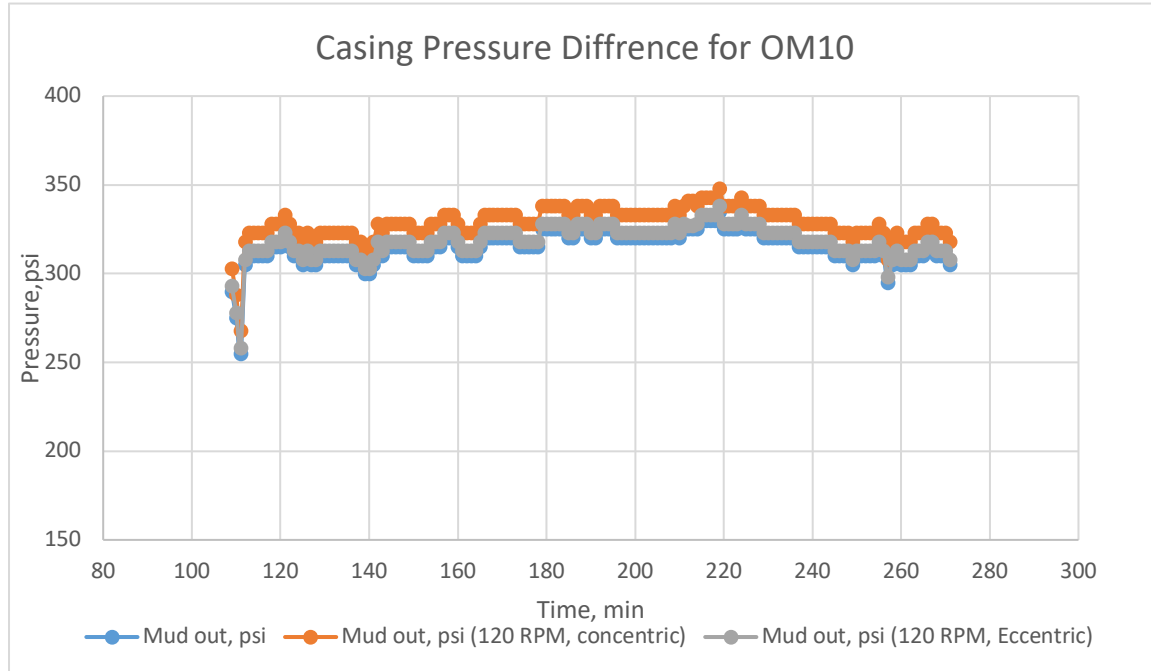


Figure 3.4: Effect of pipe rotation using Erge's mdoel for OM10

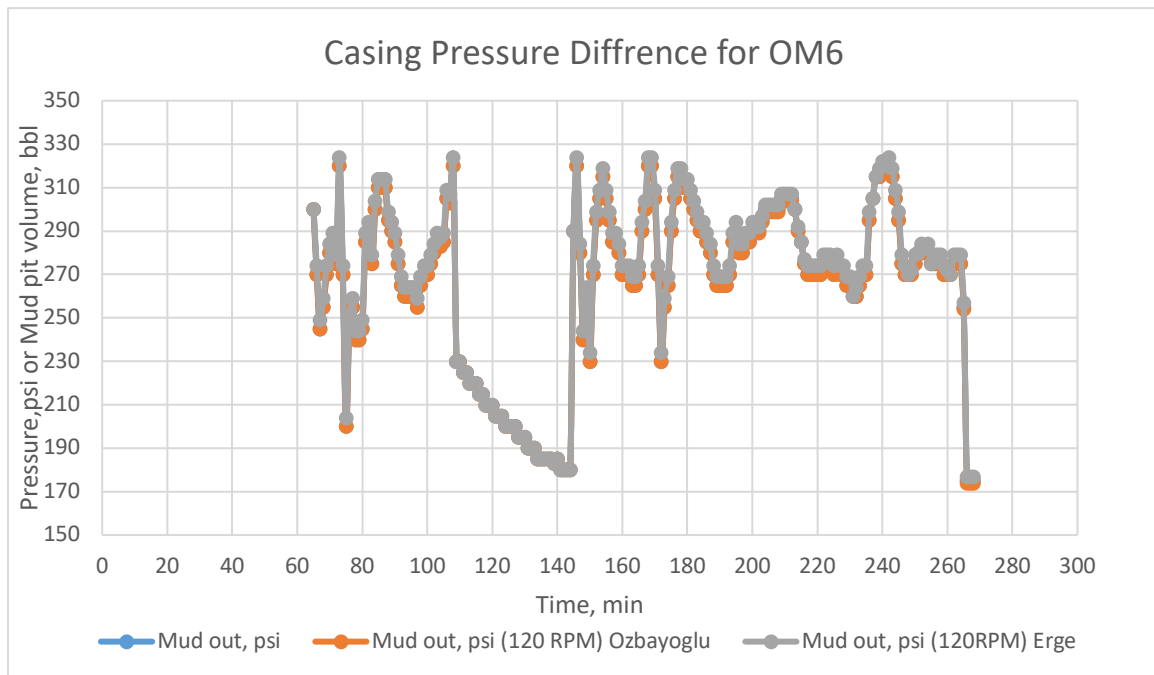


Figure 3. 5: Comparison between Erge and Ozbayoglu eccentric starting position

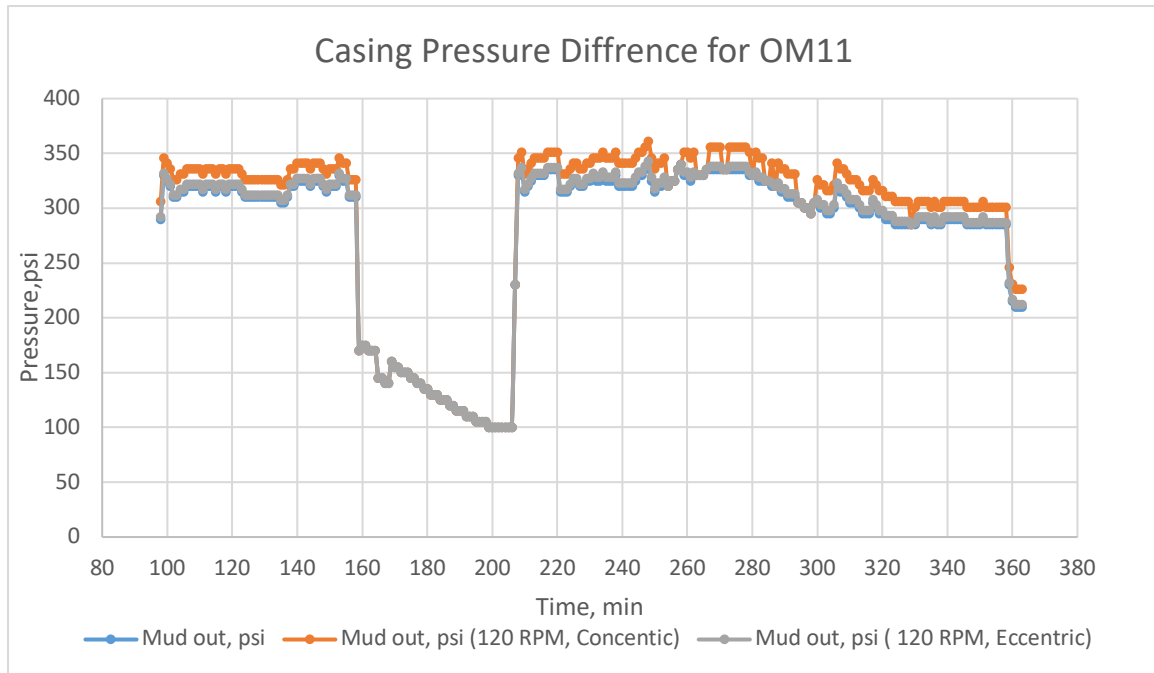


Figure 3. 6: Effect of pipe rotation using Erge's mdoel for OM11

As for Test 3-1 (OM11) as in Fig 3.6, the maximum change of the casing pressure is an increase of 21 psi for the case of the pipe rotation is 120 RPM assuming a starting concentric layout of the LSU#2 schematic. The 21 psi difference accounts for 6% increase of the casing pressure and these results are very similar to both OM6 and OM10 tests with an increase of the casing pressure instead of the expected decrease.

In Fig 3.7, Test 3-5 (OM 15) is shown. The effect of pipe rotation on OM15 has the same results as for OM11. The main difference between the two tests are in the circulation rate while the kick is being injected. In OM11, the gas is injected with no mud circulation where OM15 had a circulation rate of 90 gpm while the gas kick was being injected. The overall casing pressure of OM 15 was higher than OM 11. The overall pipe rotation effect was a maximum increase of 21 psi which is 6% increase in casing pressure.

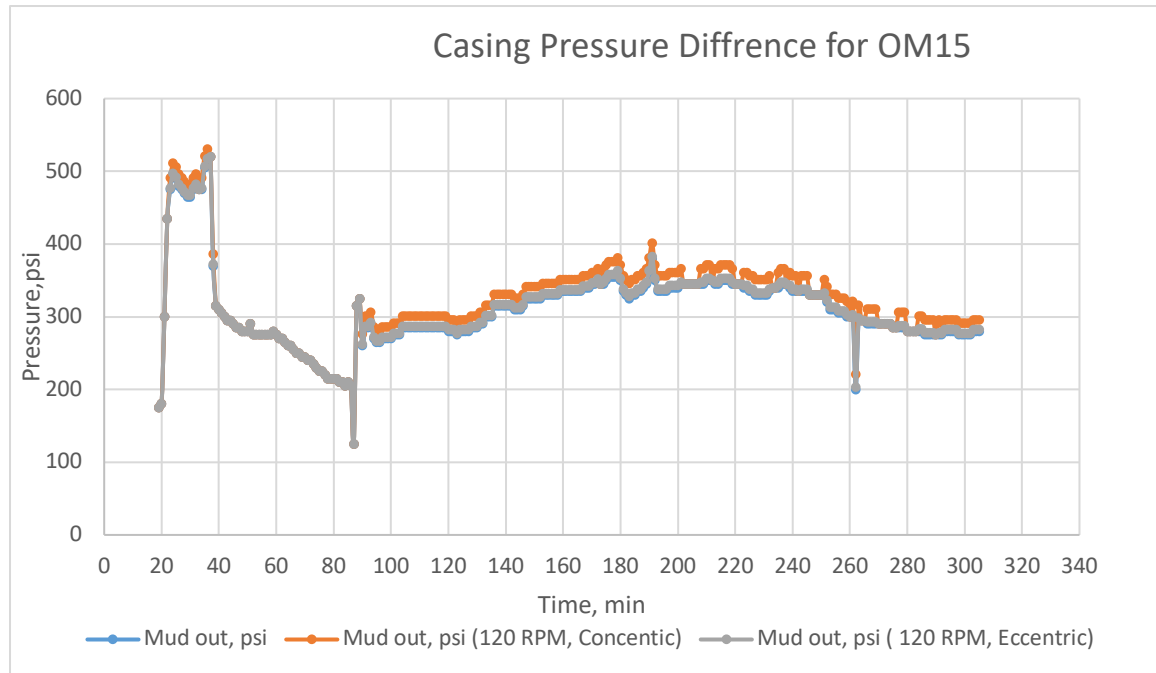


Figure 3.7: Effect of pipe rotation using Erge's mdoel for OM15

3.4.1 RCD rating

The selection of RDC rating is decided based on the maximum anticipated casing pressure. The above four tests were analyzed to see if any changes of the casing pressure would have a practical significance on the rating selection of RDC. For all these tests, the changes of the casing pressure ranged from 4% to 6%. These changes are not significant to recommend a rating change in the RDC of choice. However, MPD engineers are encouraged to make case specific calculations of each well to accurately decide the changes on the annular frictional pressure caused by the pipe rotation because in an environment with such narrow pore pressure and fracture pressure limits, any change in the frictional pressure loss can help the precision on the downhole pressure profile.

3.5 Validity of the Dissolved Gas Model in OBM

The OBM model in this chapter assumes that the gas is completely dissolved in the wellbore at all depths. This assumption needs further investigation for the considered tests because gas could come out of solution at shallower depth and lower pressures. Real scale data for mud flow rate out of the well shows some variations compared to mud pump flow rate. Each test was briefly analyzed for this behavior.

Early conclusions made by the team that ran the real scale OBM experiments suggests that the gas does not come out of solution until after it has passed the choke coming out of the well (“DEA Project 7” 1986). However, the four tests, except for some poorly recorded data in Test 2-5, showed an increase in the mud flow rate coming out of the well compared to the pump flow rate. This increase could correspond to the gas coming out of solution closer to surface. Test 2-1 showed only a brief increase for few minutes. While Test 3-1 (OM 11) and Test 3-5(OM15) exhibited an increase for a longer period of time. Fig 3.8 shows test 3-1. The flow rate out of the casing was at an average of 220 gpm where the pump rate was at 90 gpm, that increase continued for over 100 minutes. The increase of flow rate out of the well indicates some gas coming out of solution. However, the mass micromotion measurements are not reliable. The micromotion does not accurately measure the flow rate and the value could be exaggerated. The velocity estimation of gas dissolved in oil based mud further explained in chapter 4 (section 4.2.1) shows that the depth location is shallow when gas comes out of solution (270 ft for some cases) and that the change in frictional pressure caused by it is negligible.

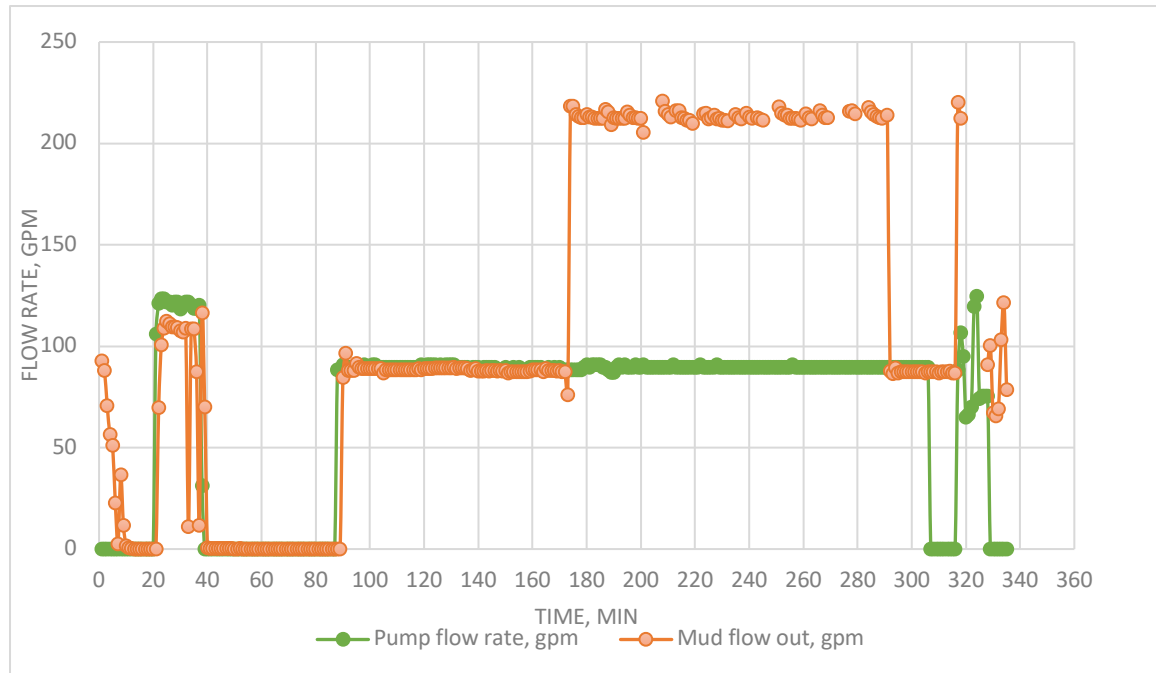


Figure 3. 8: Test 3-5 (OM15) pump flow rate compared to mud flow rate out of well

3.6 Summary of the Results and Conclusion of Dissolved Gas Model for OBM

Analyzing the results from test group of the mud properties of OBM has shown that, the casing pressure increases with 120 RPM of pipe rotation with a range of 4- 6% increase. Summary of the results is in Table 3.1. This is primarily caused by the decrease in frictional pressure loss when pipe rotation is carried. Usually, and based on field data, the frictional pressure loss increases when the pipe rotates, however, in some experimental data that Erge based his correlation on, the frictional pressure loss for non-rotational case is actually higher than the rotational case (Erge et al. 2015). The four tests analyzed in this chapter fall in the range that exhibits a decrease in frictional pressure loss with rotation.

Table 3.1: Summary of results for OBM test data

Test #	μ_p , eq cp/ Pa.s	τ_y , Pa/ lbf/100 ft ²	MW, ppg	120 RPM effect on casing pressure	RCD rating
2-1 (OM6)	.02/20	2.3/6	8	5% increase	No change
2-5 (OM10)	.02/20	2.3/6	8	4 % increase	No change
3-1 (OM11)	.031/33	3.1/10	13	6 % increase	No change
3-5 (OM15)	.031/10	3.1/10	13	6 % increase	No change

For practical considerations, the change in casing pressure is insignificant to select a different RCD rating. Furthermore, for mud rheology and flow rates similar to the real scale tests, it is not recommended to apply pipe rotation because the rotation increases the planned casing pressure based on applying the dissolved bubble model as in this chapter. However, precisely controlling the annular pressure profile and accounting for the rotational frictional pressure changes, is going to ascertain the downhole pressure limits with narrow pore-fracture pressure operational window. Further analysis of the flow rate data shows that gas comes out of solution closer to the surface caused by the decrease in hydrostatic pressure.

CHAPTER 4: ANALYSIS OF FRICTIONAL PRESSURE CHANGES ON CASING PRESSURE CAUSED BY PIPE ROTATION IN WATER BASED MUDS USING SINGLE BUBBLE MODEL

4.1 Overview

The aim of this study is to calculate the changes in casing pressure caused by the pipe rotation in WBM while a kick is circulated out of the well. As it has been mentioned earlier, the setup of MPD systems allow for gas kicks to be circulated out while continuing drilling or other related operations that involve pipe rotation. The main factor that alters the casing pressure, considered for this section, is the change in annular frictional pressure loss when the pipe is being rotated. This is accomplished by the analysis of the WBM real scale experiments. These experiments were then coupled with the pipe rotation correlations (sec 2.4) to calculate the frictional pressure loss of each test.

Three different tests were analyzed for the effect of pipe rotation on WBM casing pressure operations when displacing the gas to surface. Each test had a distinct set of operational variations, mud rheology, and mud weight. The data for the casing pressure profile, mud flow rates, is collected throughout the procedure. Then, the effect of frictional pressure changes is applied. That change in casing pressure is analyzed to understand if it has any practical effect for the RCD rating selection.

The single bubble model in WBM used in this chapter is a simplified model. It assumes that the gas kick is going to migrate keeping one single body of gas throughout the circulation process. The volume of the gas bubble changes as it raises up the wellbore with the change in hydrostatic pressure is considered using ideal gas law. The closest pattern to this model in two phase flow is what is known as slug flow (section 1.4.2). The location of the gas at each time step is estimated

from correlations from the real scale data being used. The single bubble model, although very common in the industry, is inaccurate. The gas bubble rarely stays in one single body. A discussion of the single bubble model validity is included in chapter 5.

4.2 Single Bubble Model for Water Based Muds

Dealing with WBM represents a different engineering question than OBM. The gas kick that comes from the wellbore no longer dissolves into the mud. The natural gas hydrocarbon stays in its gaseous phase. This poses further implication about the estimation of frictional pressure loss caused by pipe rotation. The proposed simple model assumes the kick to be one single bubble of a gaseous phase. The bubble enters the well and moves up and stays intact as one body of gaseous fluid. Therefore, the well is divided into three different sections at each time step. 1) Liquid phase: the section of drilling mud that lies below the gas bubble with the same flow rate as the pump (i.e. kill rate). 2) Gas phase: the gas bubble itself whose volume is calculated using the ideal gas law. 3) Liquid phase of higher flow rate: the section of the mud that lies above the gas bubble and its flow rate is affected by the expandability of the gas below it, resulting in a higher flow rate than the kill rate. Fig 4.1 shows schematic of the model at one-time step. This simplification rules out dealing with complex multiphase flow within the well and starts with the simplest approach.

4.2.1 Location and velocity of gas

For the single bubble approximation, the method used to estimate the velocity and location of the gas in the well at each time step uses the results from the DEA project 7 correlations. The correlations includes the rheology and density of mud to normalize the value of velocity as in Eq

4.1. It also depends on the average void fraction of gas (β); gas void fraction is defined as the fraction of the cross sectional area of the

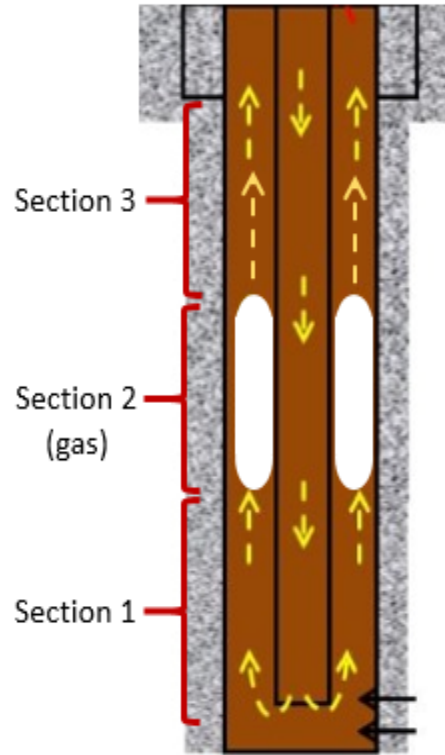


Figure 4. 1: Single bubble model approximation schmatic at one time step

wellbore occupied by the gas when gas is at a certain point. The average value was taken for gas void fraction from gradiometer measurements in LSU#2. A correlation that was found by the DEA project results to estimate the increase in gas velocity compared to liquid velocity is in Eq.4.1. The extra gas velocity (v_e) is defined as the difference between the gas velocity and the peak velocity of liquid that occurs in the center of the flow between the two annulus walls. The peak velocity of liquid is estimated from the OBM tests with the gas dissolved in it taken from Fig. 4.2 which is a reproduced graph from DEA data analysis. The average velocity is the pump-induced velocity of mud. The additional gas velocity is then added to that peak velocity to find the middle location of gas in the well.

$$v_e = \left(\frac{\tau_y}{K^3}\right)^{.12} \left(\frac{\rho_m - \rho_g}{\rho_m}\right)^{.25} (4.92\beta + 1.25) \quad \text{Eq 4. 1}$$

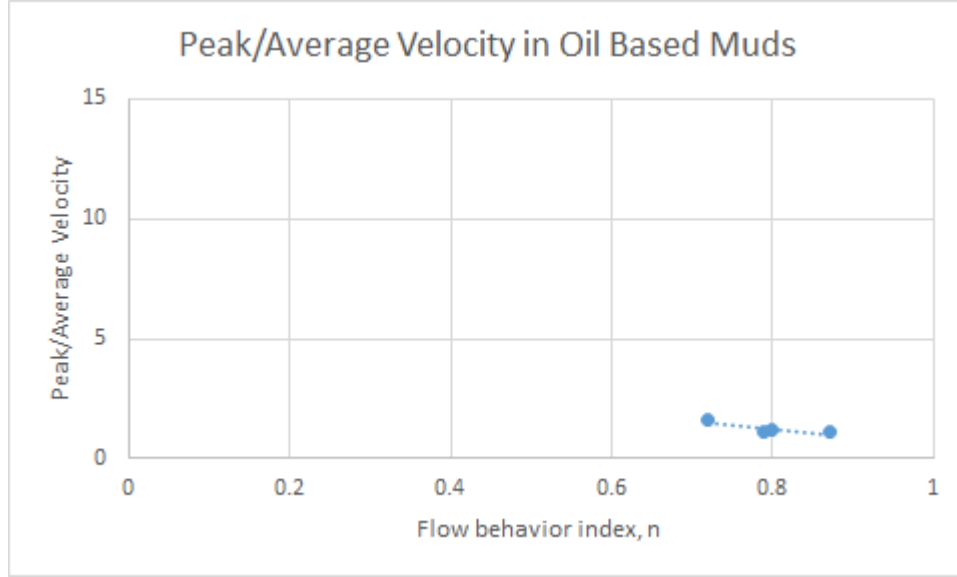


Figure 4. 2: Estimate of the peak velocity of mud from the OBM tests [reproduced graph from (“DEA Project 7” 1986)]

The ideal gas law was used to find the volume of the gas at a certain point as in Eq. 4.2 where the volume (V_b) of the kick at bottom hole pressure is known

$$BHP V_b = P_t V_t \quad \text{Eq 4. 2}$$

$$D_g = (t_0 - t) * (v_{peak} + v_e) + \frac{L_g}{2} \quad \text{Eq 4. 3}$$

D_g is the location of gas depth in (ft), BHP is the bottom hole pressure in (psi), V is the volume at bottom or at a certain point of time in bbl, t_0 is the time at which the gas has reached the surface in (seconds), v is the velocity in (ft/s), and L_g is the length of the gas bubble in (ft)

The flow rate of section 3 was estimated using Eq.4.4, the mass flow provided from the data (taken by micromotion before the choke) divided by the density of the mud

$$Q_{gpm} = \frac{Q_{lb/min}}{MW} \quad \text{Eq 4. 4}$$

4.2.2 Estimation of Frictional Pressure Loss Caused by Pipe Rotation

At each time step, the difference in frictional pressure loss caused by the rotation of the pipe is applied for the three different sections depending of the length of each section at each time step as in Eq 4.5. It can also be explained as the weighted average of frictional pressure loss for the entire well.

$$FP = \frac{L_1}{TD} FP_1 + \frac{L_g}{TD} FP_g + \frac{L_3}{TD} FP_3 \quad \text{Eq 4. 5}$$

Where L_1 , L_g and L_3 are the lengths of section 1, section2 or gas bubble, and section 3, respectively in (ft) at one point of time as shown in Fig 4.1. TD is the total depth of the well in (ft). FP is the frictional pressure loss at each section in (psi), FP_g is negligible because the frictional pressure loss for the gas section is less than 10^{-3} psi

Then, that difference is subtracted from the static no rotation casing pressure collected from the real scale experiments (Eq.4.6)

$$CP_{RPM} = CP_{static} - FP \quad \text{Eq 4. 6}$$

CP is casing pressure in (psi) for rotating and non-rotating cases. FP is the annular frictional pressure in (psi) from the correlations as in section 2.4

4.3 Example of Full Scale Data Output (WBM)

One example of the output of WBM test is shown in Fig 4.3. For this test, there is no circulation while the gas injection was taking place and 90 gpm is used as a kill rate (refer to driller's method). For instance, this test's flow rate for section 1 is 90 gpm. The increased flow rate Section 3 is 220 gpm. The point of time at which the gas reached the surface (t_0) is the point of increase in mud pit volume.

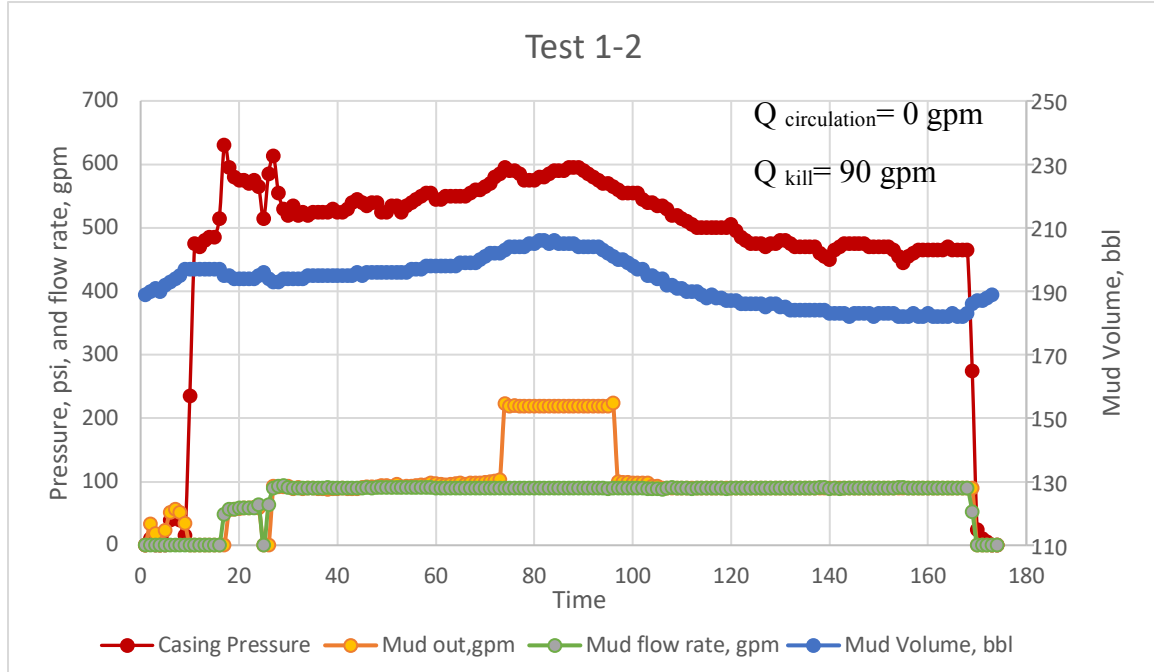


Figure 4. 3: WN2 (test 1-2) data output

4.4 Pipe Rotation Effect on Casing Pressure in WBM Using Single Bubble Model

The main effect on casing pressure while applying the single bubble model is the change in frictional pressure loss throughout the annulus. When the drill pipe rotates at 120 rpm speed, for example, the annulus frictional pressure loss is going to differ from a non-rotation case. This difference is the proposed change on the casing pressure. Since LSU #2 schematic is uncertain, both eccentric and concentric schematics are applied to find the frictional pressure loss of the non-rotational case.

Test 1-2: Fig 4.4 shows the results of applying the above-mentioned model to calculate the casing pressure with rotation. Both concentric and eccentric non-rotational cases use Erge's model on Test 1-2 (Table 4.1). The results showed primarily an increase in the casing pressure instead of the expected decrease. The overall frictional pressure loss actually was lower with rotation (120 RPM) than the non-rotation cases. For this case, the maximum increase happens

when the configuration was assumed to be concentric and the pipe rotation is 120 RPM. The value of the increase was 12 psi which accounts for 2% increase in the overall casing pressure.

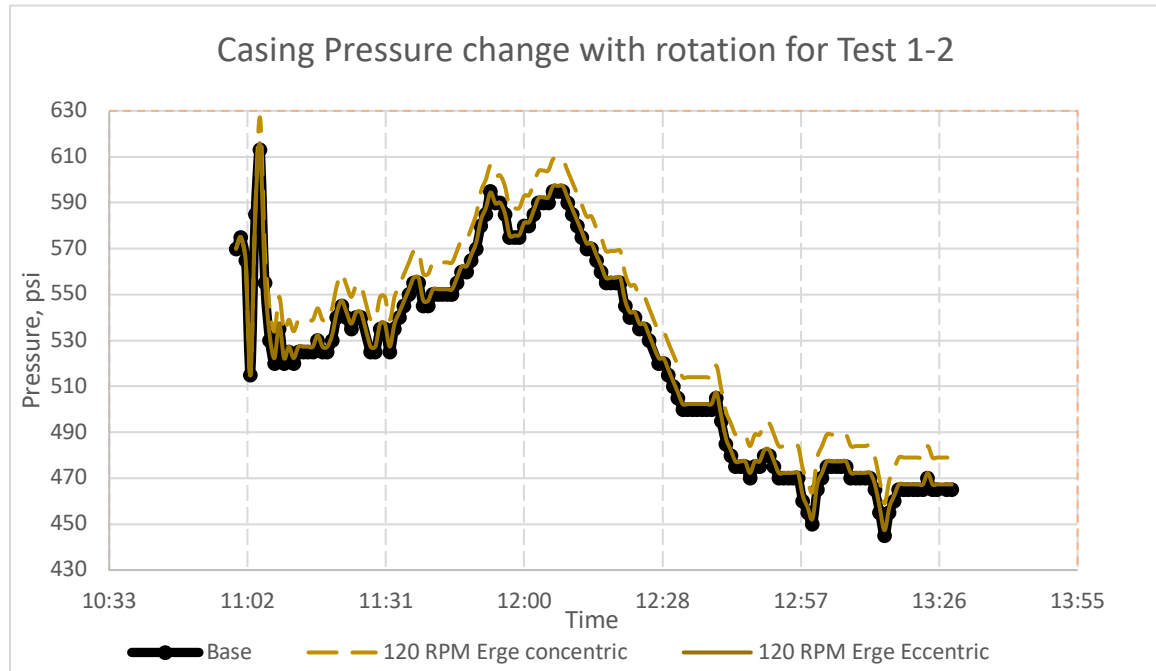


Figure 4. 4: Comparison between eccentric and concentric schematic assumptions (Erg's correlation)

The eccentric non-rotational cases have a lower frictional pressure loss in the annulus than the concentric case. The difference between eccentric non-rotational and 120 RPM rotation was negligible (< 2 psi) using Erge correlations as shown in Fig 4.4 and 4.5. Ozaboyglu correlation, on the other hand showed a decrease in the casing pressure with a maximum decrease of 16 psi which is around 3% of the overall casing pressure (Fig 4.5).

Test 1-5: frictional pressure loss was found using Erge's model by applying the single bubble model explained earlier. The mud circulation rate while the gas is being injected for this test is 133 gpm, compared to the previous analyzed test of zero circulation rate. The kill rate is 90 gpm

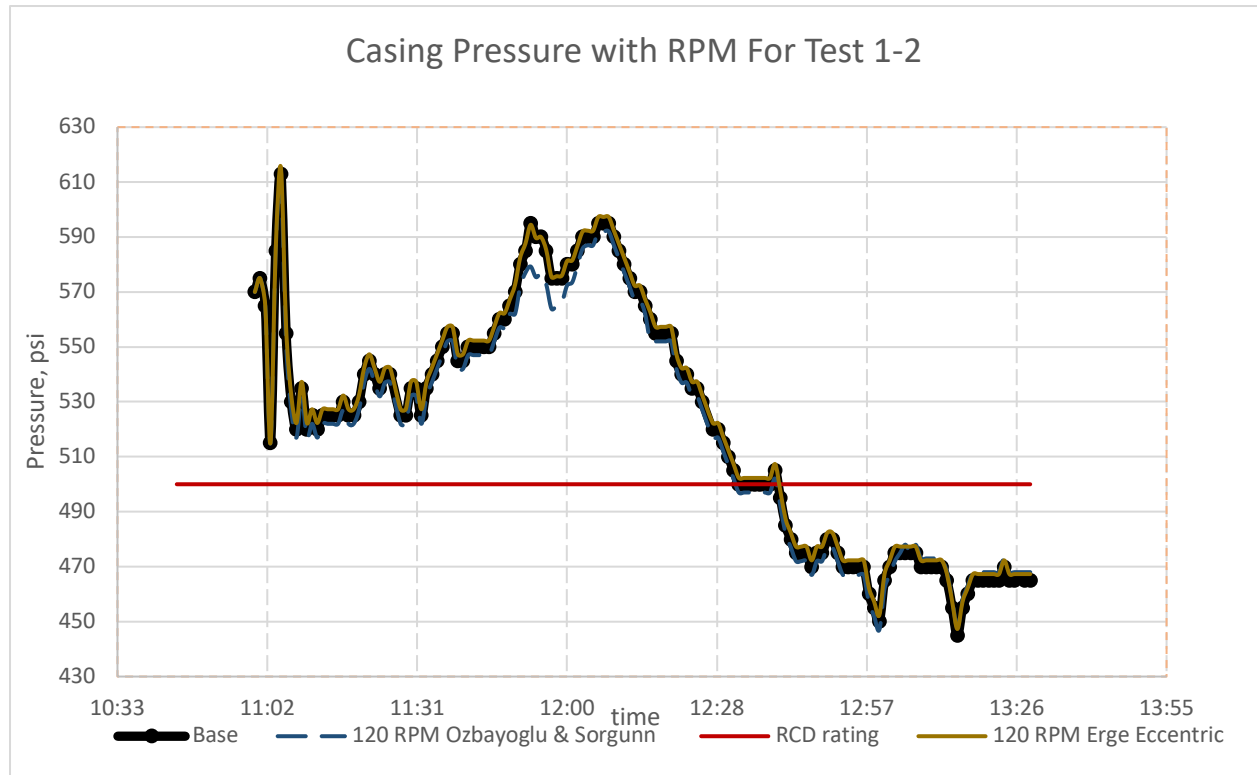


Figure 4. 5: Comparison between Ozabayoglu and Erge's eccentric schematic

Table 4. 1: Pressures loss for various flow rates and rotational speeds for WBM1

Model	Erge Concentric FP, psi			Erge Eccentric FP, psi			Ozabayoglu FP, psi		
Q, gpm → ω, RPM	90	133	340	90	133	340	90	133	340
0	29	32	12	18	19	29	2	3	13
120	15	17	9	15	17	39	5	11	69

(Section 1), similar to test 1-2. The flow rate out of the well was calculated to be around 340 gpm (Section 3). The frictional pressure loss for non -rotational cases (eccentric and concentric) was found as well as the frictional pressure loss at 120 RPM. As it can be seen in Table 4.1. at 340 gpm, the eccentric cases (applying both correlations) showed an increase, although

insignificant, in frictional pressure loss with pipe rotation. This corresponded to a decrease in casing pressure. However, frictional pressure loss for a 90 gpm static concentric case was higher than the 120 RPM rotational case. This corresponded to an increase in casing pressure. For that reason, concentric cases in Fig 4.6 mostly shows an increase for casing pressure. The maximum increase in the casing pressure is for concentric and 120 RPM with 15 psi that accounts for 3% increase. However, eccentric cases show a decrease in casing pressure as shown Fig 4.7. The maximum decrease happens when Section 3 (at 340 gpm) is longer than the other two sections. The frictional pressure loss when applying Ozbayoglu change is 6% of the maximum casing pressure with a value of 32 psi as in Fig 4.7.

Test 4-2: The analysis for higher rheology mud as in Test 4-2 (Table 1.1) has been done discretely accounting for only the maximum casing pressure instead of applying the whole pressure time profile with time. The frictional pressure changes were taken based on the highest change scenario (using the highest flow rate: 320 gpm) over the entire well. The maximum casing pressure for test 4-2 was 640 psi and the maximum frictional pressure effect was a decrease from concentric non rotational case to a 120 RPM speed of pipe with 34 psi which corresponded to 5 % increase in the casing pressure. The maximum change on the opposite direction happens using Ozbayoglu correlation which resulted in an increase in frictional pressure loss of 12 psi which corresponds to 2% decrease in casing pressure.

In all of the above mentioned cases, the change is not significant enough to cause a change in the RCD design. The next lower RCD dynamic rating is not reached with pressures changes for due to the frictional pressure loss caused by that rotation. However, the slightest change in the frictional pressure loss in the annulus and specially above the casing shoes is important as MPD

operations typically addresses narrow fracture-pore pressure window. Even minor changes in the frictional pressure loss can affect the wellbore stability.

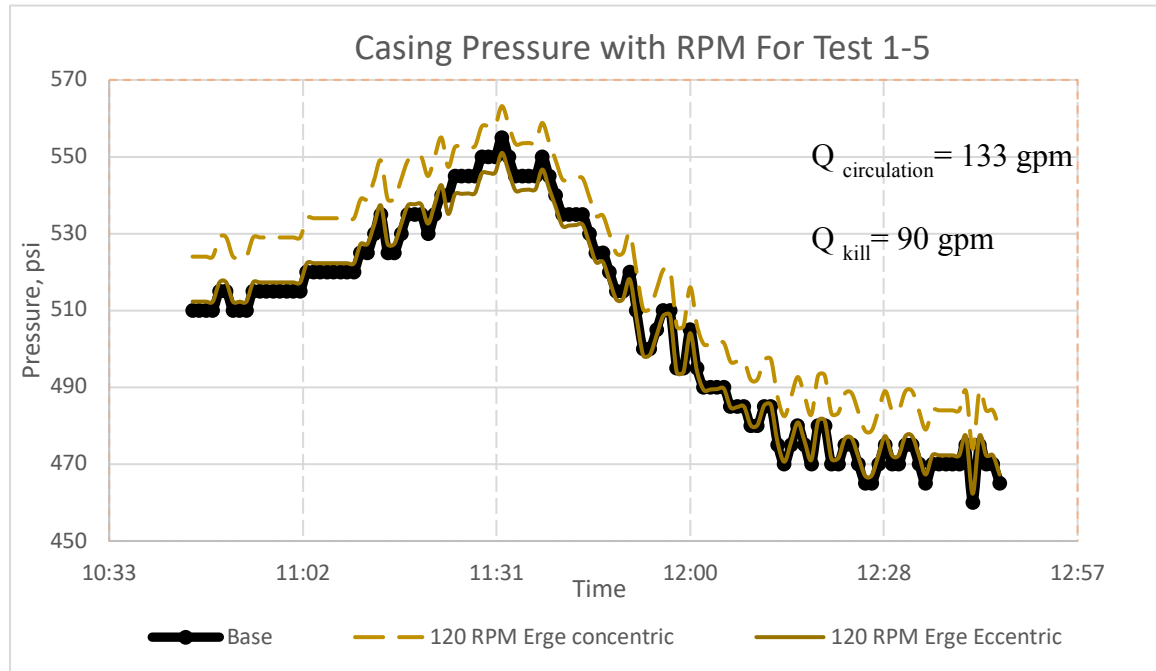


Figure 4. 6: Comparison between eccentric and concentric schematic with Erg's Model

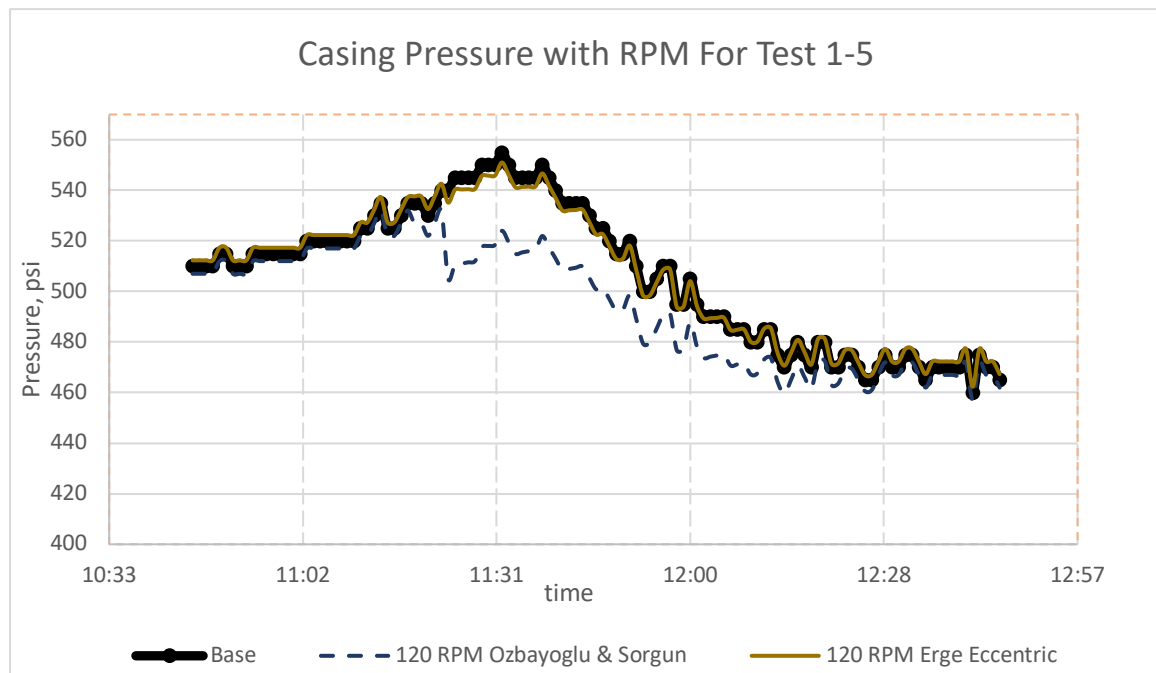


Figure 4. 7: Comparison between Ozbayoglu and Erge's eccentric Schematic

4.5 Summary of the Results and Conclusion of Single Bubble Model for WBM

Three full scale WBM tests measurements and data were analyzed for the effect of pipe rotation on the casing pressure, and specifically the effect of change in frictional pressure loss on the casing pressure. A summary of the analysis is shown in Table 4.2. The maximum increase of casing pressure using the single bubble model is observed when assuming a concentric schematic and applying 120 RPM rotation for drill pipe. The maximum decrease in casing pressure is observed when Ozaboyglu is applied for eccentric schematic and a rotational speed of 120 RPM. For geometries and mud rheology's similar to DEA project (Shallow wells and low mud rheology's), the effect of pipe rotation assuming a single bubble of gas is insignificant with a maximum of 6% percentage decrease in the casing pressure.

Table 4. 2:Summary of results for single bubble model

Test #	μ_p, eq cp	τ_y, lbf/100ft²	MW, ppg	ΔCP Eccentric & 120 RPM	ΔCP Concentric & 120 RPM	RCD rating
1-2((WN2)	8	2	8.5	3% decrease	2% increase	No change
1-5 (WN6)	7	3	8.5	6 % decrease	3 % increase	No change
4-2 (WN20)	33	10	13	2% decrease	5% increase	No change

The RCD dynamic rating selection is not changed based on the changes of the maximum casing pressure when using the single bubble models in rheology's and flow velocity similar to DEA project. Furthermore, pipe rotation for the cases discussed does not necessarily aid to the decrease in casing pressure. The decision to continue with operation that includes pipe rotation is

not significantly affected when accounting for only frictional pressure loss changes on casing pressure. However, in deep offshore cases with tight fracture-pore pressure limits, the effect of the change in frictional pressure loss is magnified. The accurate estimation of the change in frictional pressure loss with rotation can further the precision of the downhole pressure profile values and possibly increase the kick tolerance.

CHAPTER 5: VALIDITY OF SINGLE BUBBLE MODEL AND GAS DISTRIBUTION

5.1 Overview

The single bubble model, although used in most well control methods calculations, is believed to be inaccurate. The bubble is more likely to break into smaller bubbles and distribute throughout the well as it migrates upwards. The purpose of this chapter is to address the factors that aid or hinder gas distribution; this is divided into two sections. First, we analyze the gas distribution of the full scale tests with different operational variations and cross validating the results with the published literature. Second, we review the effect of pipe rotation on fluid flow through the discussion of a fluid flow phenomenon known as Taylor vortices. These vortices are speculated to increase the gas distribution and breaking the gas into smaller bubble.

The LSU #2 real scale experiments results and literature were cross validated with (Rommetveit and Olsen 1989; Spoerker, Gruber, and Brandstaetter 2012) in regards to factors affecting gas distribution. The gas distribution (i.e. higher gas breakage effect) has been shown to increase with the following factors: 1) less well inclination 2) lower mud rheology 3) lower kill rates

Furthermore, a phenomenon known as Taylor vortices which takes place above a certain critical speed of rotation was proposed to aid to the gas mixing and breakage of the bubble. The Taylor vortices occurrence has been established for the case of liquid flow in-between two pipes with the inner pipe rotating (Taylor 1923). Although the gas mixing has not been experimentally researched for a non-Newtonian fluid with cases similar to a gas kick in the wellbore, evidence from literature supports the hypothesis of Taylor vortices aiding the mixing of gas in the

wellbore and furthering the breakage of the gas (Spoerker, Gruber, and Brandstaetter 2012; Lockett, Richardson, and Worraker 1993).

It is vital to discuss the gas distribution because the distribution of gas and maximum casing pressure are closely related. Fig 5.1 shows the correlation between surface gas void fraction and maximum casing pressure from the DEA project data. The surface gas void fraction is defined as the fraction of the wellbore occupied by the gas when gas reaches the surface. Lower void fraction infers higher bubble breakage and higher gas distribution. As can be seen in the figure, the gas surface void fraction is highly correlated with maximum casing pressure. The void fraction is dependent on several factors including flow rate, mud properties and type.

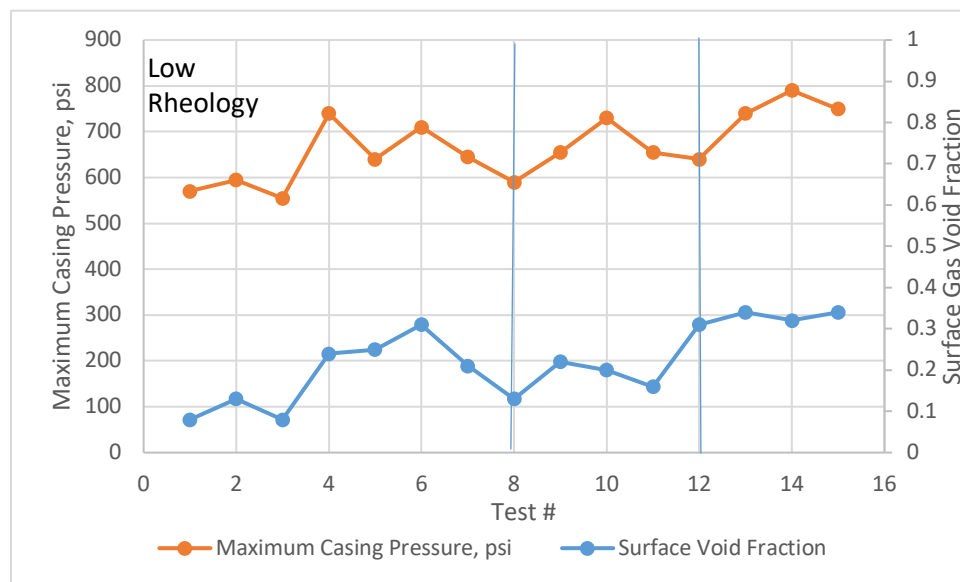


Figure 5.1: Correlation between surface gas void fraction and Maximum Casing Pressure

5.2 Gas Kick Distribution in Wellbore

5.2.1 Well inclination effect on gas distribution

A team of researchers from the university of Leoben, performed a simulation using the VOF (Volume of fluid) multiphase modeling method. The simulation only models 10 meters of the

well because the depth to annulus width is too high to graphically represent the behavior. Unlike most well control models of proposing a single bubble of gas moving upward, the vertical well model clearly illustrates that there is a streaking behavior of that gas and only a portion of gas stays as a single elongated bubble as in Fig 5.2 (Spoerker and Tuschl 2010). This streaking behavior is of an agreement with the results of the DEA tests because the results report a different gas void fraction at the bottom than at the top. When the inclination of the well was slightly altered, the behavior of the gas took a slightly different pattern. The inclination has induced a more consolidated bubble towards the upper facing side of the annulus (Fig 5.3). As the inclination increases, the gas has a tendency to stay in one bubble.

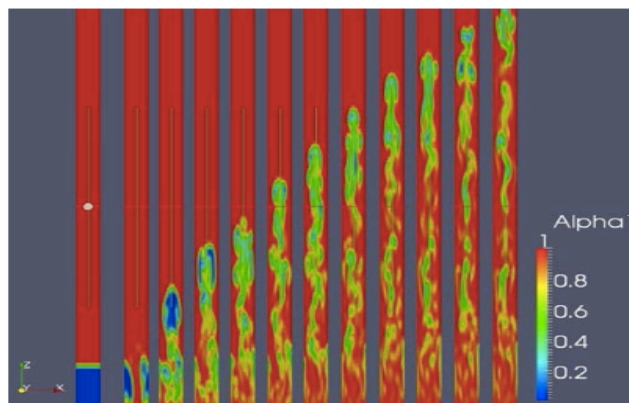


Figure 5.2: Gas bubble flow in mud in vertical open hole over 3 min(Spoerker and Tuschl 2010).

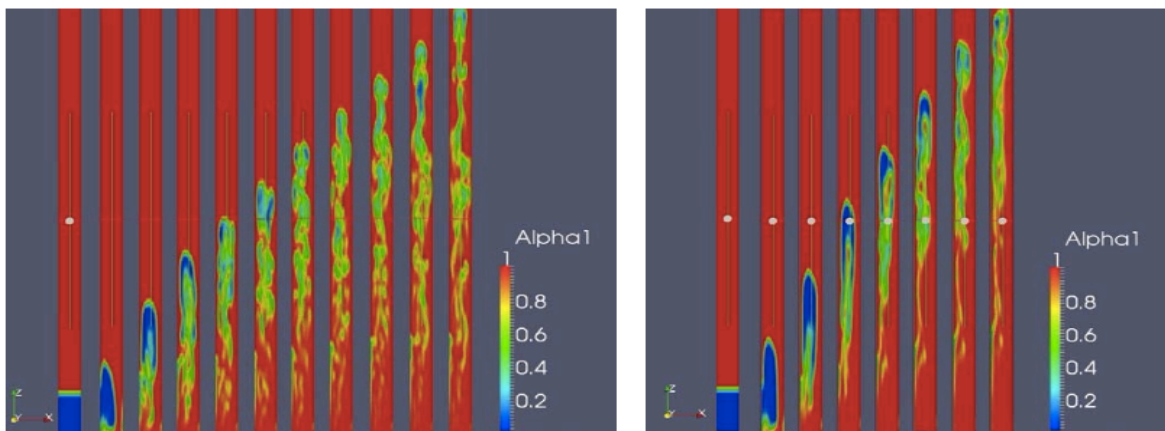


Figure 5. 3: Gas behavior with 1° inclination (left) and 10° inclination (Right) over 3 min (Spoerker and Tuschl 2010).

5.2.2 Mud flow rate effect on gas distribution

Experiments of gas distribution coming out of a full size well found in the literature indicate that the lower the rate of the kill operation for water based mud, the more dispersed the gas is (Rommetveit and Olsen 1989). Similarly, DEA project data analysis of the void fraction of gas at surface showed that the lower the kill rate, the more distributed the gas is in the wellbore. The data illustrates that gas distribution at surface increases as the kill flow rate increases as in Fig 5.4. For each set of tests, mud properties, kick size, and circulation rates are the same.

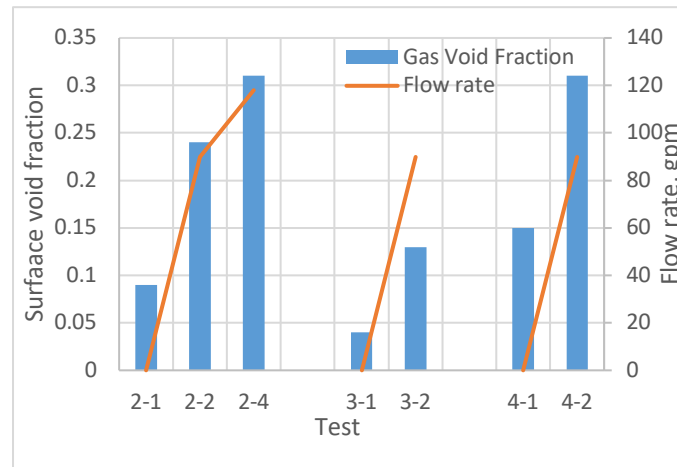


Figure 5.4: Effect of kill rate on gas distribution (“DEA Project 7” 1986).

5.2.3 Mud viscosity effect on gas distribution

Using the DEA project data, for the similar gas distributions at the bottom and same circulation rate, the increased mud viscosity induces a higher gas concentration at the surface. Fig 5.5 shows the difference of gas void fraction at surface with all other parameters kept the same except mud rheology. The higher the rheology, the higher the gas void fraction and, hence, the lower the distribution of gas. The low mud rheology in the figure refer to a range of plastic viscosity (μ_p)

of 7-19 eq cp and a yield stress (τ_y) of $2-4 \frac{\text{lbf}}{100\text{ft}^2}$, whereas the high mud rheology refer to a range of plastic viscosity (μ_p) of 25-33 eq cp and a yield stress (τ_y) of $12-9 \frac{\text{lbf}}{100\text{ft}^2}$.

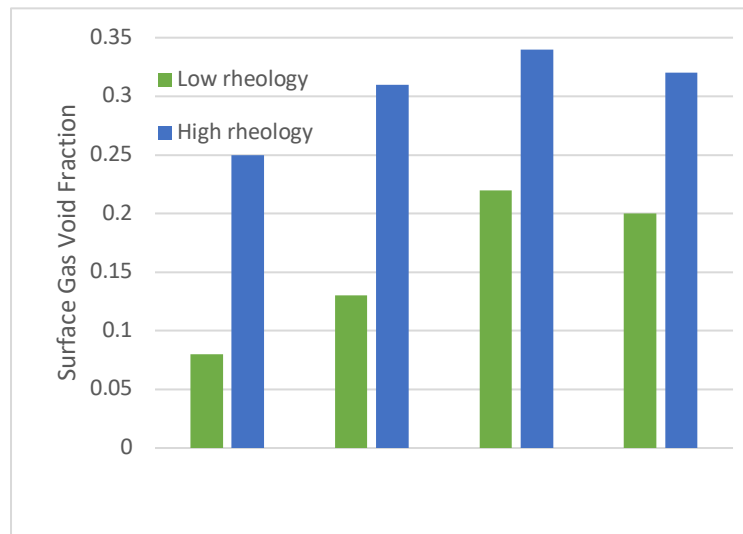


Figure 5.5: Mud rheology effect on gas distribution

Based on the above mentioned factors, optimum combination of the increased gas distribution and lower casing pressure therefore is low kill rate, low mud rheology and vertical well orientation. However, the only parameter that can be controlled at the time of the operation is the kill rate.

5.3 Pipe Rotation Effect on Gas Distribution

In this section, a fluid flow phenomenon known as Taylor vortices is proposed and is speculated to aid in the gas mixing. When these vortices occur, the gas bubble is suggested to break into smaller bubbles that is more likely to compromise the single bubble model.

5.3.1 Introduction to Taylor Vortices

In 1915, Taylor has concluded an interesting behavior for the fluid flow in between two concentric cylinders. He studied the effect of rotation for both the inner and outer cylinders. He found that behavior of fluid flow changes when the inner cylinder is in rotation. This is similar to the setup of inner drill pipe rotating inside a casing or open hole. Before Taylor's work, most flow was studied under a Couette flow, which entails that the fluid flow between two cylinders can be approximated by the azimuthal velocity parallel to the direction of pipe rotation. The highest velocity vector is at the inner pipe and lowest is at the outer pipe as in Fig 5.6. Taylor then found that this is only applicable within a certain range of fluid viscosity and angular velocity of the inner pipe.

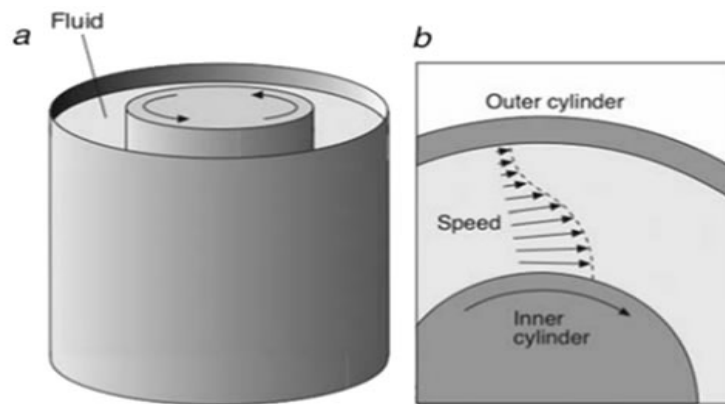


Figure 5. 6: Couette flow illustration (Ball 2009).

After a certain threshold, the fluid starts to take an interesting direction caused by the centrifugal forces coupled with the azimuthal velocity of the pipe. When the centrifugal forces overcome the viscous forces of the fluid, the flow takes a different direction. It produces what is known as Taylor vortices. These vortices are a circular flow perpendicular to the walls of the cylinder as illustrated in Fig 5.7.

The flow characteristics at which these vortices form depend on speed of rotation, liquid density, liquid viscosity and geometry. A dimensionless number known as Taylor number is defined as in Eq 5.1 for non-Newtonian fluids.

$$Ta = Ri(Ro - Ri)^3 \left(\frac{\rho\omega}{\mu_{app}} \right)^2 \quad \text{Eq 5. 1}$$

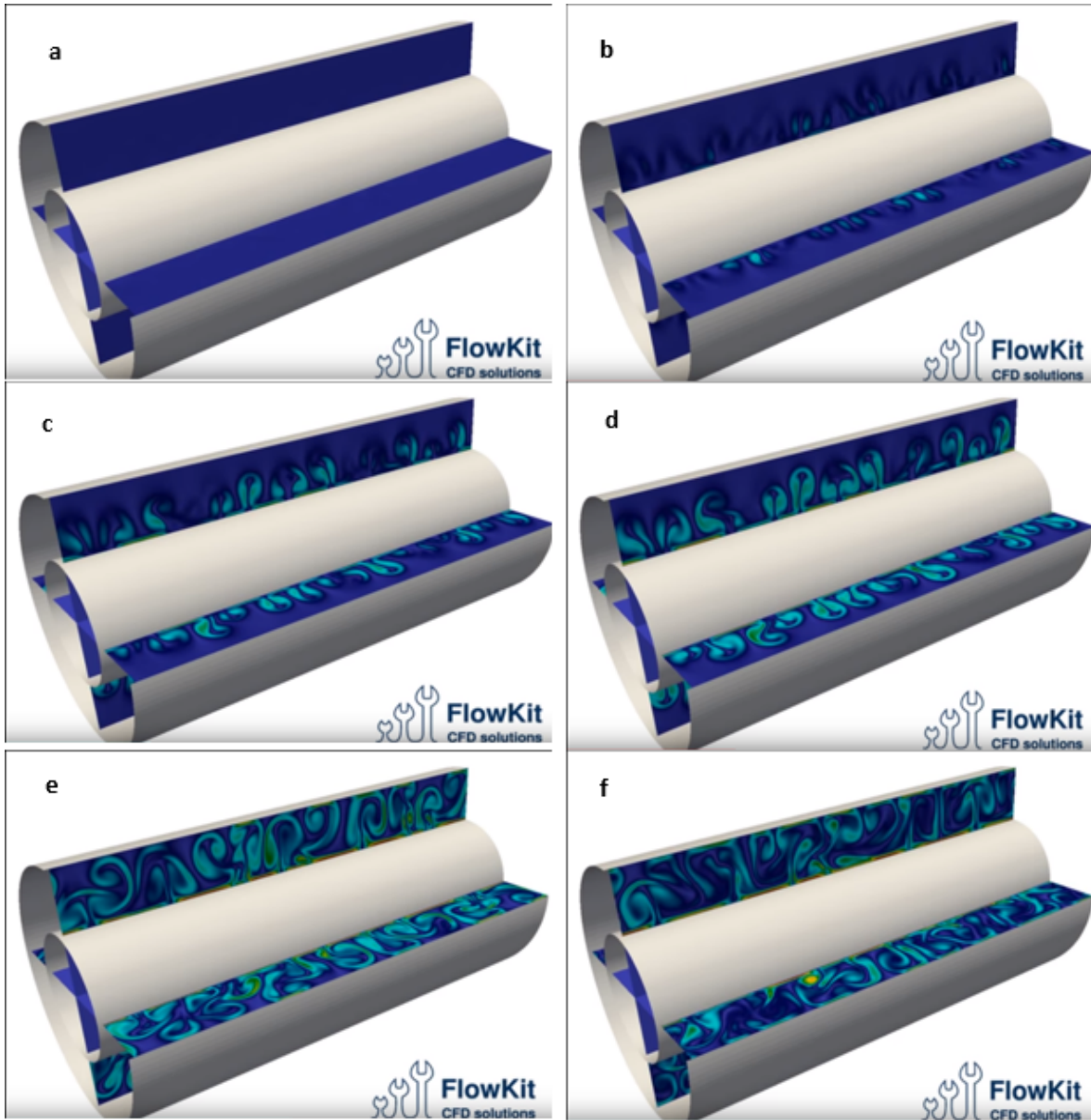


Figure 5. 7: Taylor Vortices Illustration. Snapshots a through f show the time-lapse of the formation of the Taylor vortices with the rotation of the inner Cylinder (FlowKit 2016).

The Taylor number (Ta) is a dimensionless number; any combination of unit's weather field or metric that yields a dimensionless value can be implemented. For the examples illustrated later of Taylor's number, the R_i and R_o are inner and outer radius in (m), ρ is density in (kg/m³), ω is radial speed of rotation in (rad/s), and μ_{app} is apparent viscosity in (Pa.s) found by Eq. 5.2

Since the fluid we are dealing with is non-Newtonian shear thinning, the apparent viscosity changes with increased axial and radial velocity (pipe rotation). Ahmed presented a method at which the apparent viscosity can be estimated (Ahmed and Miska 2008) as in Eq 5.2 to Eq 5.5.

$$\mu_{app} = \frac{\tau_y}{\gamma_{\theta-z}} + K \gamma_{\theta-z}^{m-1} \quad \text{Eq 5. 2}$$

$$\gamma_{\theta-z} = \sqrt{\dot{\gamma}_{\theta}^2 + \dot{\gamma}_z^2} \quad \text{Eq 5. 3}$$

$$\gamma_{\theta} = \frac{\omega R_i}{R_o - R_i} \quad \text{Eq 5. 4}$$

$$\gamma_z = \frac{1+2N}{3N} \frac{6v}{R_o - R_i} \quad \text{Eq 5. 5}$$

τ_y , K, and N are properties of the mud as explained in section 2.4, γ_{θ} , γ_z , and $\gamma_{\theta-z}$ are radial axial and combined shear rate in (s⁻¹), v is velocity of the mud in (m/s)

Critical Taylor number

The critical Taylor number is a number after which Taylor vortices appear. This number has been an area of study in itself. Taylor has defined the critical number to be 1708. Other studies such as Meksyn, Chandrasekhar, DiPrima, Duty, Watanabe, Harris, and Ried found a range of Critical Taylor number between 1075 to 2255 (Drazin and Reid 2004; Watanabe, Sumio, and Ogata 2006; Walowit 1966). Further studies accounting for fluid rheology model, Soundalgekar et al found the critical Taylor number for stationary outer cylinder in an isothermal system to be

3389.9 (Soundalgekar, Takhar, and Smith 1981). In this analysis, the Taylor critical number used is 3400.

Critical rotation example

An example of a high rheology mud referred to as Mud1 (Table 5.1), is plotted to find the Taylor number for each rotational speed. In Fig 5.8, the rotation speed is plotted against the Taylor number for a mud rheology presented in Erge's paper (Erge et al. 2015). The mud flow rate was set at 90 gpm. The point of intersection between critical Taylor number (3400) and the curve gives the highest rotation speed after which the vortices start to appear (Critical rotation). Since the speed of rotation appears twice in the above mentioned equations (Eq. 5.1 to 5.5), an iterative method is used to find the critical rotation speed. It is observed from Fig 5.8, the increase in Taylor number is not linear with the increase in pipe rotation. This is due to the shear thinning properties of the fluid. The rotation speed is inversely proportional to the apparent viscosity and proportional to the Taylor number. The geometry used for these graphs are LSU#2's.

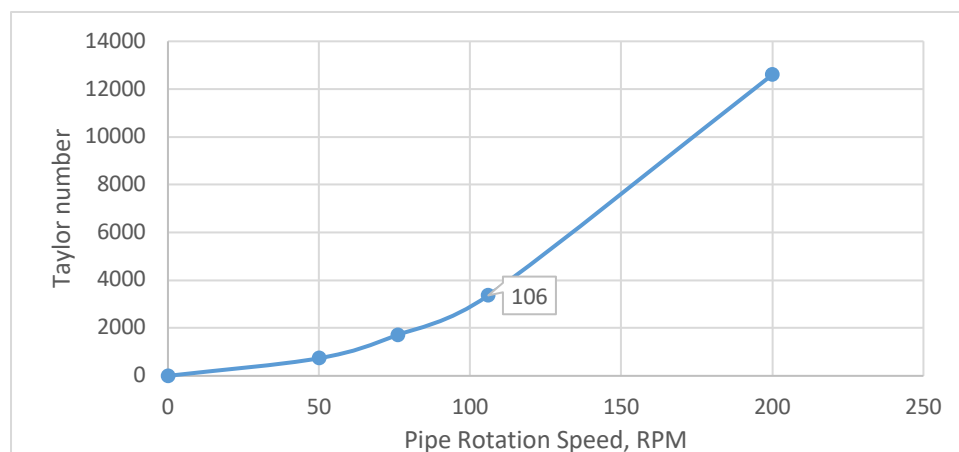


Figure 5. 8: Taylor number increase with increased rotation speed for mud1 at 90 gpm

The process was done for two more mud properties (Table 5.1). Fig 5.9 shows the critical speed of rotation for each mud rheology with the increase in flow rate. The observation from Fig 5.9 shows a decrease in the value of the critical rotation speed with the increase in flow rate because the apparent viscosity decreases. This is caused by the shear thinning properties of the mud.

Table 5.1: Mud rheology models.

Mud	τ_y, Pa	$K, Pa.sm$	n	Critical speed of rotation at 90 gpm, RPM
WN6 (Test 1-2 & 1-5)	1.2	.01	1	4
WN20 (Test 4-2)	2.85	.2	0.74	27
Mud1 (literature)	9.65	3.33	0.31	106
Mud2 (literature)	7.1	1.09	0.4	60

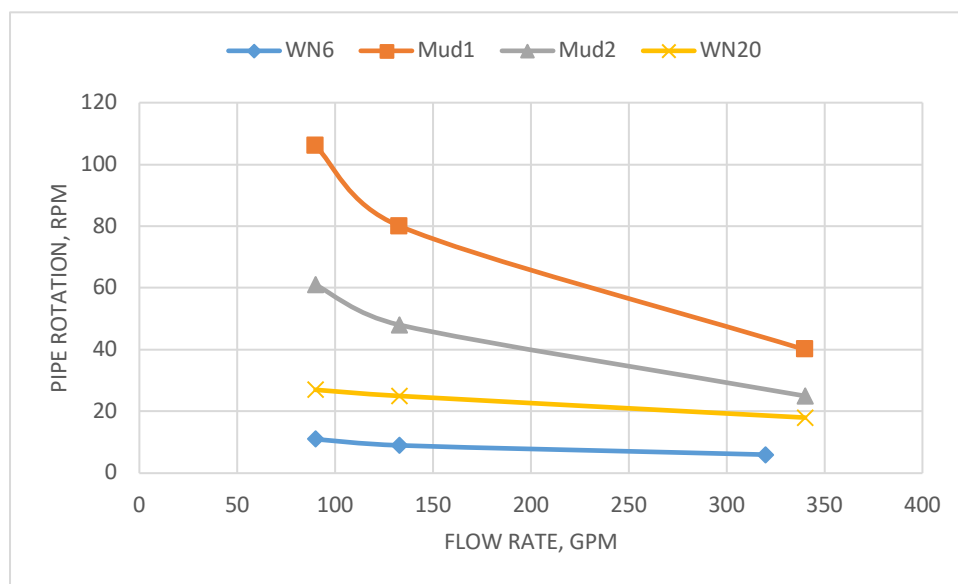


Figure 5. 9: Critical rotation speed

5.3.2 Effectiveness of Taylor vortices in breaking the gas bubble

Although the Taylor vortices criteria is speculated to break the bubble into smaller gas droplets, and consequently compromise the single bubble model, the vortices implications on drilling application were further discussed in the literature. These vortices were studied in reference to hole cleaning, influence on frictional pressure with pipe rotation, experimental two phase flow with rotating cylinder in Newtonian fluids, and numerical simulation of two phase flow with non-Newtonian fluid for kick purposes (Lockett, Richardson, and Worraaker 1993; Ahmed and Miska 2008; Shiomi et al. 1992; Spoerker, Gruber, and Brandstaetter 2012). Details on Taylor vortices discussion in regards to hole cleaning and numerical kick simulation with rotation are presented.

Lockett has conducted numerical simulations to understand the path that the particle takes with both pipe rotation and axial flow in a vertical well. The two phase (solid and liquid) investigation of Lockett may aid in the understanding of gas path with the introduction of pipe rotation. He found that depending on the density ration between the fluid and the solid particles, the path of the particle is decided. The simulation results show that as long as the solid density to liquid density ratio is 2.4 or lower, the Taylor vortices produced by the rotation is able to suspend the particles at place. It is concluded that after the Taylor vortices are formed, the fluid has the ability to capture the particle and rotate it along the axis of the vortex (Lockett, Richardson, and Worraaker 1993).

A computational fluid dynamics simulation using the volume of fluid method to understand the two phase flow of non-Newtonian fluid and gas kick interaction in a wellbore, specifically at the bottom of the well. Fig 5.10 shows the volume fraction of gas (red) to mud (blue). The figures are numbered representing their positions from the bottom of the well. It can be observed that as

the gas bubble moves upward, the phase mixing (bubble breakage) is more evident, potentially caused by pipe rotation (120 RPM in the simulations) (Spoerker, Gruber, and Brandstaetter 2012). The pattern in (Fig 5.10 (2)), visibly illustrates the Tylor vortices phenomena.

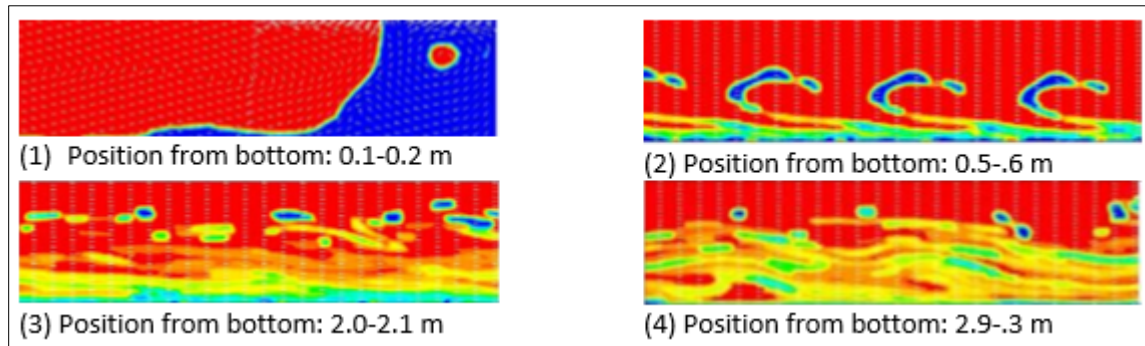


Figure 5.10: A simulated gas distribution as kick moves upward in non-Newtonian mud (Spoerker, Gruber, and Brandstaetter 2012).

The work of (Spoerker, Gruber, and Brandstaetter 2012; Lockett, Richardson, and Worraker 1993) discusses a two phase observation with pipe rotation. It is proposed with the presence of Taylor vortices, their trajectory is able to aid to the gas mixing as they help in solid- mud interaction and gas-mud interaction as shown by the above mentioned simulations. The axial flow is forcing the gas and mud to move upwards, while Taylor vortices move fluid from inner pipe to outer pipe in a circular motion.

The speculated effect of Taylor vortices on the gas distribution may compromise the accuracy of the single bubble model. For that reason, it is important to note that for the tests discussed in chapter 4, the critical speed of rotation is at 4 RPM for lower mud rheology and 27 RPM to the higher mud rheology (Table 5.1 and Fig 5.9).

An example of the suggested criteria is shown in Fig 5.11. The above mentioned process to find the critical number with mud flow rate needs to be implemented and planned before the

operation. For instance, in Fig 5.11, if the operation flow rate, mud properties and rotational speed falls inside the envelope, the single bubble model can probably have adequate accuracy.

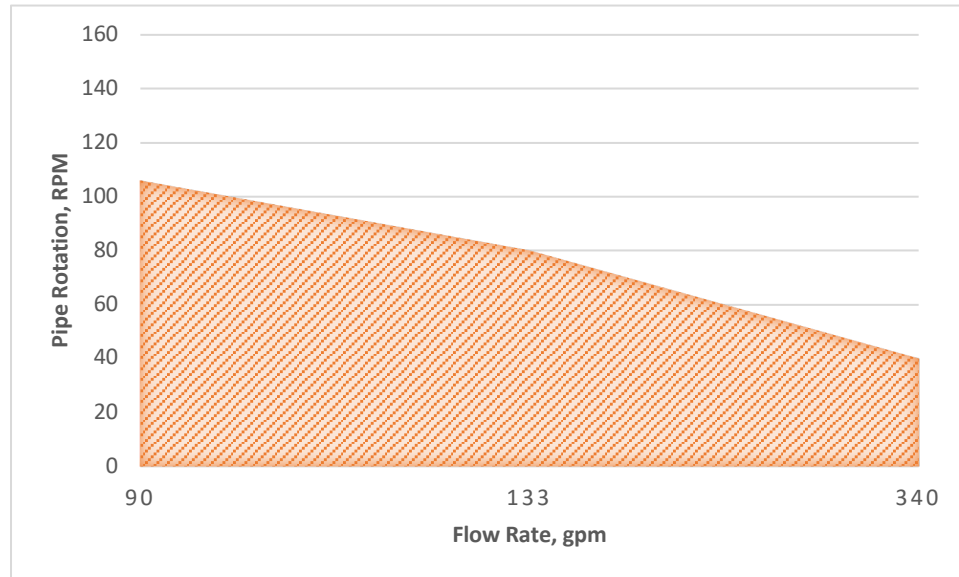


Figure 5. 11: Example envelope at which the single bubble model is proposed to be effective for mud1.

5.4 Conclusion on Validity of the Single Bubble Model

Evidence from the analysis of the real scale experiments casing pressure and the gas void fraction shows a clear relation between gas dispersion and reducing the surface pressure. If gas stays in one single bubble, the casing pressure is maximized which is an undesirable outcome as it puts the surface equipment and downhole formations near the casing shoe in jeopardy and increases the risk on the crew. Coupling the real scale data analysis with literature has presented that, in many cases, the single bubble model is invalid for a kick situation with non-Newtonian mud. Low kill rate, low mud rheology and vertical well inclination are all among the factors that can aid to the breakage of gas into smaller gas bubbles dispersed in the mud. Furthermore, a fluid flow phenomenon known as Taylor vortices that is known to occur above a critical speed of drill pipe rotation is reviewed. This critical speed of rotation depends on mud density, mud apparent

viscosity, and geometry. Further literature investigation on Taylor vortices (hole cleaning and kick situation simulations) showed that these vortices might be a factor into aiding to gas mixing and breaking the single bubble. Therefore, all these results suggest that optimum combination for breaking the gas bubble are a vertical well inclination, low mud rheology, low kill rate and a drill pipe rotation above the critical speed. However, the only operational parameters that can be controlled after taking a kick is the kill rate and pipe rotation speed.

CHAPTER 6: ANALYSIS OF CASING PRESSURE CHANGES CAUSED BY GAS BUBBLE BREAKAGE USING DISPERSED BUBBLE MODEL

6.1 Overview

As it has been shown in Chapter 5, the gas distribution is highly affected by different operation variations, mud rheology, well inclination and pipe rotation. In this chapter, the effect of breaking the bubble of a gas kick on casing pressure is studied. This is done by the application of a dispersed bubble model which is an extreme opposite to the single bubble model. The model assumes that all the above mentioned factors and specially pipe rotation had broken down the kick into very small bubbles. These bubbles are small enough so that gas and liquid have the same flow rate with no slip velocity (refer sect 1.4.2). More than twenty real scale tests were analyzed for the gas bubble breakage effect on casing pressure. The first case studied considers only gas bubble breakage and the second case combines the breakage effect and frictional pressure loss on casing pressure.

6.2 Dispersed Bubble Model for WBM

6.2.1 Conditions and Assumptions

The gas distribution study presented in Chapter 5 concludes that the single bubble model is likely not to be valid especially with the presence of rotation. The dispersed gas model for kick migration is proposed as an alternative. The first assumption for this model is that the kick has broken down into very small bubbles in contrast to the single bubble model. The second assumption is that the void fraction of mud is constant throughout the well. These assumptions are, to a certain extent, idealistic as some of the gas will not be broken down.

The key step in this model is to compare the Hydrostatic Pressure (HP) using single bubble model versus the dispersed bubble model when the gas reaches the surface. The HP is exerted by both gas and liquid on the bottom of the well. Fig 6.1 illustrates how for the dispersed bubble model (b), the gas bubbles could be distributed over a longer interval than the single bubble model. This is because the single bubble assumption has gas occupying the entire cross sectional area of the annulus. However, the dispersed bubbles occupy only a fraction of the cross sectional area in the region of gas-mud mixture. The HP for both cases are calculated. Since BHP is kept constant for these tests and well control operations, the difference in HP between the two cases (dispersed and single bubble) is the difference in the expected casing surface pressure. The HP for the dispersed bubble model is higher than that of the single bubble model. This corresponds to a reduction in the casing pressure with gas dispersion.

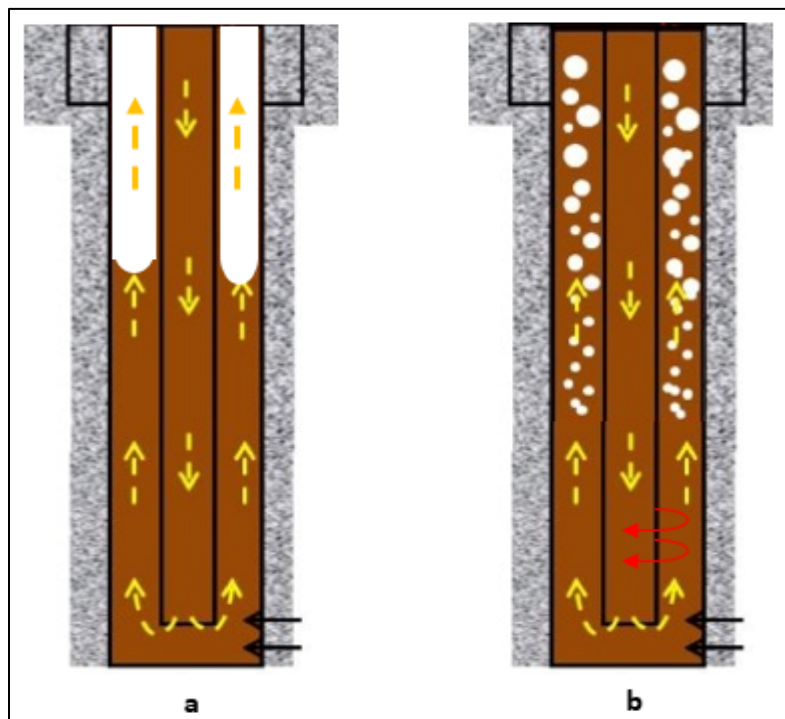


Figure 6. 1 :a)Single Bubble Model Illustration b) Dispersed Bubble Model

6.2.2 Equations to Approximate the Reduction in Casing Pressure with Gas Dispersion

Equation 6.1 shows the estimated casing pressure for each case (single bubble and dispersed bubble)

$$CP = BHP - HP \quad \text{Eq 6. 1}$$

Where CP, BHP and HP are casing, bottom hole and hydrostatic pressure respectively all in (psi) and neglecting the changes in frictional pressure loss.

The dispersed gas bubbles is assumed to have no slippage, and the void fraction of mud to the overall volume is taken from Eq 6.2 (Shoham 2005).

$$\lambda_{mud} = \frac{Q_m}{Q_m + Q_g} \quad \text{Eq 6. 2}$$

Where λ_{mud} is the void fraction of mud and Q is the flow rate of gas and mud in (gpm) at the bottom of the well. λ_{mud} is assumed to stay constant throughout the time of circulation until gas exits the well. Then, Eq 6.3 shows the density of the mixture.

$$\rho_{mix} = \lambda_{mud} \rho_{mud} + (1 - \lambda_{mud}) \rho_g \quad \text{Eq 6. 3}$$

Where ρ_{mud} , ρ_g , and ρ_{mix} are the densities of the mud, gas and the mixture region respectively.

The hydrostatic pressure of the dispersed gas bubble is estimated using the two phase mixture density and the length of that zone. The mud zone hydrostatic pressure is summed with the mixture zone hydrostatic pressure to find the overall hydrostatic pressure as in Eq.4.10

$$HP(\text{Dispersed Bubble}) = .052 \rho_{mud} (TD - L_{Mix}) + .052 \rho_{mix} L_{Mix} \quad \text{Eq 6. 4}$$

Where ρ is the density for mud and the mixture in (ppg), TD and L_{Mix} are the total depth of the well and the length of the mixture in (ft).

Since bottom hole pressure needs to stay constant for either models (single bubble or dispersed bubbles) Eq 6.5 was applied. The difference in the hydrostatic between single bubble data and dispersed bubble model is the same as the difference between the casing pressures for both cases (Eq 6.5).

$$\Delta CP = HP (\text{Dispersed Bubbles}) - HP (\text{Single Bubble}) \quad \text{Eq 6. 5}$$

For the dispersed gas model, the density of the gas component is dependent on the pressure.

Using the ideal gas law density of gas can be estimated using Eq 6.6.

$$\rho_g = \frac{SG \times MM \times P_d}{RT} \quad \text{Eq 6. 6}$$

MM is molecular weight in (lbmole), SG is specific gravity of gas, P_d is the pressure at the gas depth in (psi), R is the gas constant in (psi-ft³/lb mole-°R) and T is the temperature in(°R)

Since the BHP and kick size (at bottom) are known for all tests, the density is calculated and the mass of the gas is found using Eq.6.7

$$M_g = \rho_g \times V_b \quad \text{Eq 6. 7}$$

Where M_g is the mass of gas in (lbm), ρ_g is the density of gas in (ppg), and V_b is the volume of gas at bottom in (gal). Mass balance is used to find the volume of the gas at the new location of gas and dividing the volume by the area of the annulus occupied by the gas gives the length of the dispersed gas mixture as in Eq. 6.8

$$L_{\text{Mix}} = \frac{M_g / \rho_g}{A_{\text{ann}} * (1 - \lambda_{\text{mud}}) * 7.48} \quad \text{Eq 6. 8}$$

Where A_{ann} is in (ft²) and L_{Mix} in ft .

To find the volume of gas at that location, pressure is needed to calculate the difference in hydrostatic pressure between BHP and the current gas depth in the well. The pressure was taken at the bottom of the gas-mud mixture.

$$P_d = BHP - .052 * \rho_{mud} * (TD - L_{Mix}) \quad \text{Eq 6. 9}$$

As it can be seen, Eq 6.6 is dependent of Eq 6.9. Therefore, an iterative method or a solving the quadratic equation (Eq. 6.10) by the standard solution (Eq. 6.11) is implemented to find P_d and then calculating length of mixture.

$$a P_d^2 + b P_d + c = 0 \quad \text{Eq 6. 10}$$

$$p_d = \frac{-b \pm \sqrt{b^2 - 4ac}}{2a} \quad \text{Eq 6. 11}$$

Where $a = 1$, $b = \rho_{mud} \times TD - BHP$, and $c = -\frac{\rho_{mud} \times M_g \times RT}{A_{Ann} \times (1 - \lambda_{mud}) \times SG \times MM}$

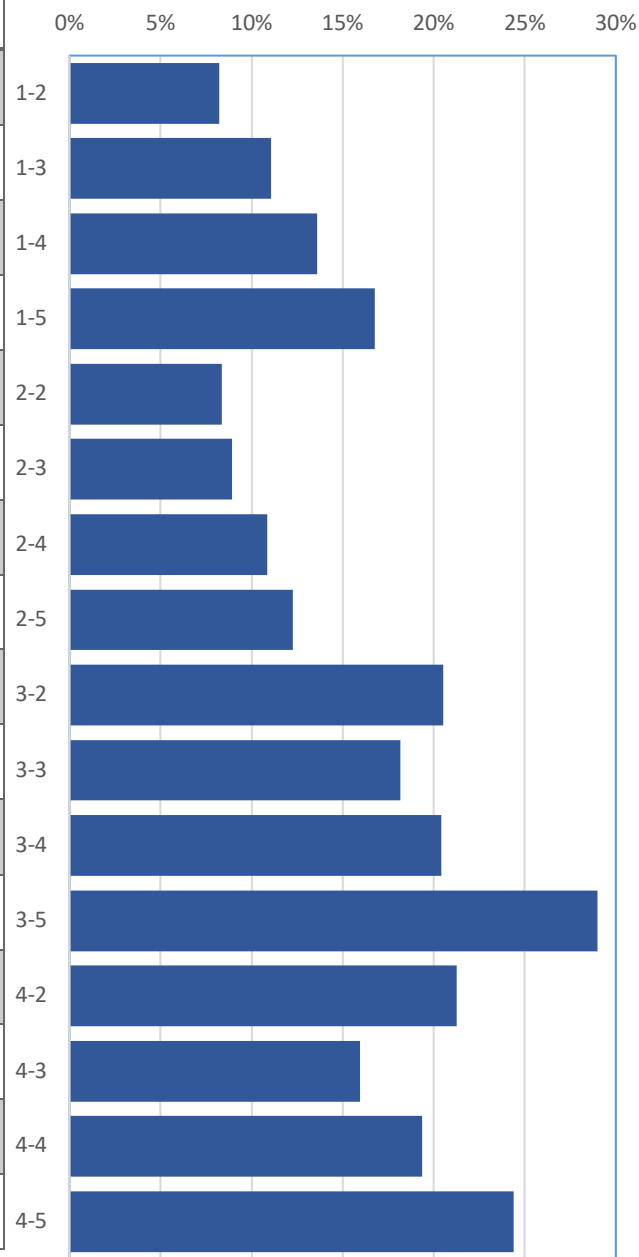
6.2.3 Dispersion of Gas Effect on Casing Pressure

The equations presented in the earlier sections were implemented in the real scale data. The single bubble model was compared to the dispersed bubble model in terms of HP and the effect of that on surface casing pressure for both cases.

Table 6.1 and Fig 6.2 show the result of the analysis. The decrease in the casing pressure is significant; as high as 29%. The major change in casing pressure happens for tests with heavier mud weights because the initial BHP is higher than the lower mud weights and this causes further expansion of the gas and higher difference between single bubble and dispersed bubble model. The greatest change happens when the kick flow rate is low. This is because the void fraction of gas is going to be lower and hence the length of the mixture is higher and the overall changes in hydrostatic pressure is higher.

Table 6. 1: Effect of dispersion in reducing casing pressure

Test	MW, ppg	Original CP, psi	Δ CP, psi	New CP, psi	Decrease percentage
1-2	8.55	595	49	546	8%
1-3	8.55	570	63	507	11%
1-4	8.55	595	81	514	14%
1-5	8.55	555	93	462	17%
2-2	8.7	740	62	678	8%
2-3	8.7	640	57	583	9%
2-4	8.7	710	77	633	11%
2-5	8.7	645	79	566	12%
3-2	12.5	590	121	469	21%
3-3	12.3	655	119	536	18%
3-4	12.4	730	149	581	20%
3-5	12.4	655	190	465	29%
4-2	12.4	640	136	504	21%
4-3	12.4	740	118	622	16%
4-4	12.4	790	153	637	19%
4-5	12.4	750	183	567	24%



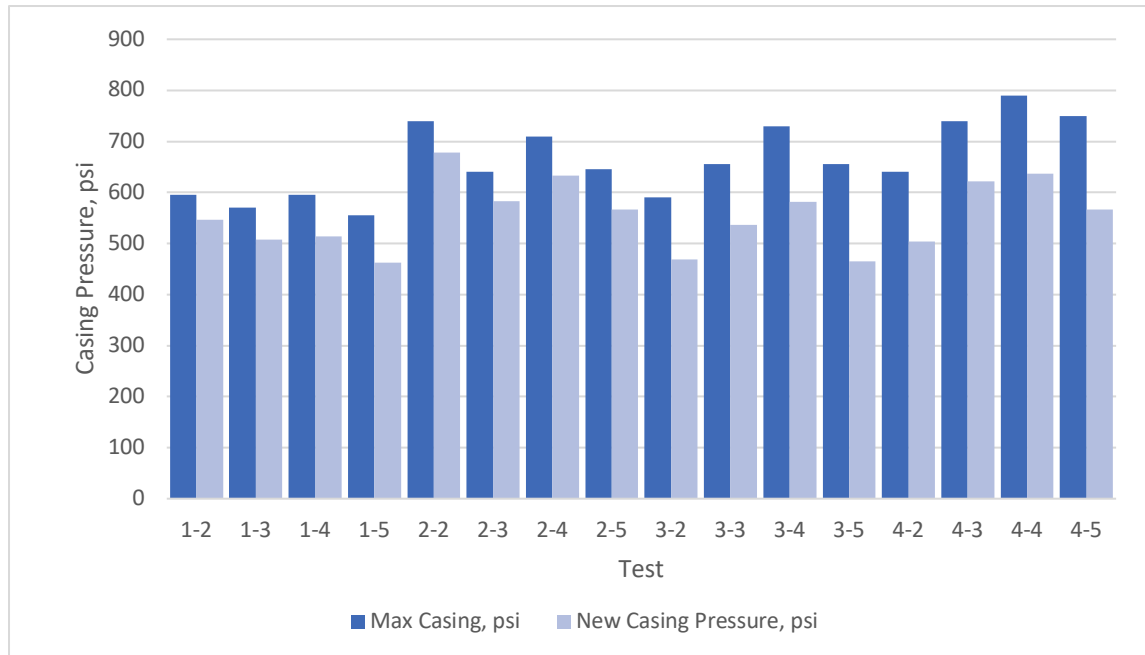


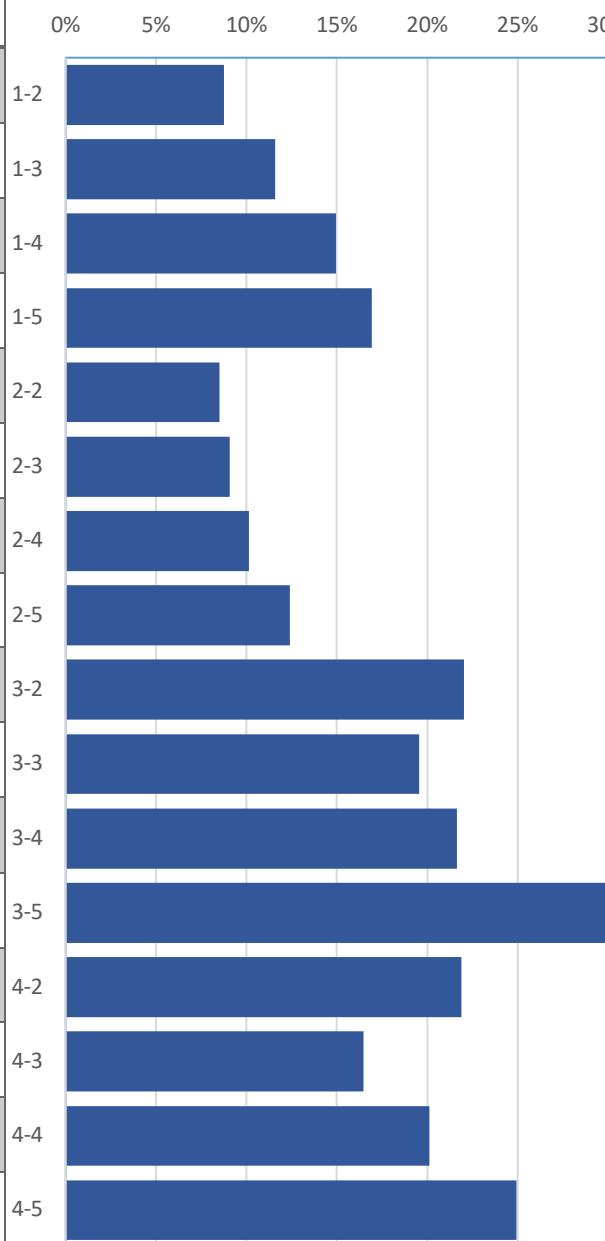
Figure 6. 2: Casing pressure changes when applying the dispersed bubble model

Frictional Pressure loss and dispersed bubble model

The estimated frictional pressure loss was added to the calculated reduction of casing pressure to find the combined effect. The frictional pressure loss caused by the introduction of rotation is added using Ozaboyglu and Sorgun correlations. The analysis for friction assumes only liquid in the well since the gas bubbles was assumed to be small enough to not have any slip velocity. Also, the wall shear rate on both casing and drill pipe is responsible for frictional pressure loss which is going to be occupied by the liquid mostly. Table 6.2 shows the results. Accounting for the frictional pressure loss intensifies the decrease in the casing pressure to a maximum of 30% and a minimum of 9%

Table 6. 2: Effect of dispersion in reducing casing pressure with friction

Test	MW, ppg	Original CP, psi	Δ CP, psi	New CP, psi	Decrease percentage
1-2	8.55	595	52	546	9%
1-3	8.55	570	66	507	12%
1-4	8.55	595	89	514	15%
1-5	8.55	555	94	462	17%
2-2	8.7	740	63	678	9%
2-3	8.7	640	58	583	9%
2-4	8.7	710	72	633	10%
2-5	8.7	645	80	566	12%
3-2	12.5	590	130	469	22%
3-3	12.3	655	128	536	20%
3-4	12.4	730	158	581	22%
3-5	12.4	655	199	465	30%
4-2	12.4	640	140	504	22%
4-3	12.4	740	122	622	16%
4-4	12.4	790	159	637	20%
4-5	12.4	750	187	567	25%



6.3 Conclusion of Dispersed Bubble Model

In conclusion, the results of the previous chapter suggest that the gas bubble is unlikely to stay as a single body of gas when it migrates upward. Various factors, including pipe rotation may aid to

breakage of gas into smaller bubbles. A model that assumes the complete dispersion of gas using a constant gas/mud void fraction compared to a single bubble model was investigated. The main comparison was in the difference in hydrostatic pressure for the two cases and its reflection on surface casing pressure. The reduction in casing pressure caused by the dispersion is significant and more prominent than the effect of change in frictional pressure loss. The decrease in CP had an average of 17% and reaches up to 30% for test of higher mud weights. The highest decrease in casing pressure for dispersed bubble model occurs for higher mud weights because the more expansion of the gas bubble.

CHAPTER 7: SUMMARY, APPLICATIONS, AND RECOMMENDATIONS FOR FUTURE RESEARCH

7.1 Summary

Well control is one of the most important aspects of drilling engineering as it involves the protection of human lives. New technologies such as MPD have opened doors to untouched territories for drilling that were not possible otherwise; this includes narrow operational window and deep offshore drilling. The MPD system holds special well control capabilities when circulating a gas kick. The MPD equipment allows for the operation including drilling and pipe rotation to continue while the gas kick is being circulated out. This capability has raised the question of this thesis: how does the pipe rotation affect the kick circulation operation in terms of the change in the expected casing pressure and how would the gas behave with the presence of pipe rotation?

These questions have been partially addressed by analyzing real scale experimental data of gas kick circulation ran in LSU PERTT lab for both OBM and WBM. The records of the experiments included operational data such as casing pressure, mud flow rates, mud properties and gas void fraction throughout the operation. However, pipe rotation was not possible for the set up in the well. Therefore, a set of correlations were used to account for frictional pressure losses changes caused by pipe rotation. These changes in the annular pressure affect the surface casing pressure directly because of the constant BHP. Furthermore, the effect of bubble breakage due to operational variations such as kill rate, mud properties and pipe rotation has been studied through the analysis of these real scale experiments coupled with an extensive review of the literature of a physical observation known as Taylor vortices caused by pipe rotation.

The thesis included the study of three different models each with a distinct set of assumptions. First, OBM tests were analyzed for frictional pressure changes caused by pipe rotation. This model assumes that the gas is completely dissolved in the oil based mud. It assumes only liquid in the wellbore during the circulation process. Second, WBM tests were also analyzed for frictional pressure changes caused by pipe rotation. However, the gas kick was assumed to follow a single bubble model. This assumption entails that the gas stays in one body of gas throughout the circulation process. Third, WBM tests were analyzed for the effect of bubble breakages due to different operational variations and the proposed effect of pipe rotation.

The dissolved gas model for OBM was applied using the pipe rotation frictional pressure correlations. Since these tests were done on a constant bottom hole setting, the frictional pressure difference between the non-rotational case and the rotational case was the difference in the casing pressure. These correlations were applied for both concentric and eccentric non-rotational schematics. The results of the analysis of OBM tests showed that the change was insignificant with a maximum of 6% increase in the casing pressure. This does not have any practical impact of the choice of applying pipe rotation. Also, the RCD rating selection is unchanged because of the trivial change of casing pressure. This small change could be attributed to low mud rheology of the tests as well as low mud flow rates in a shallow well. However, precisely controlling the annular pressure profile and accounting for the rotational frictional pressure changes, is going to ascertain the downhole pressure limits with narrow pore-fracture pressure operational window.

The single bubble model for WBM were also applied using the pipe rotation correlations. The well was divided into three sections: (1) liquid section with pump mud flow rate below the gas bubble. (2) gas section with the gas expanding as it moves upward (ideal gas law used). (3)

liquid section above the gas with a flow rate higher than the pump follow rate caused by gas expansion. The length of these sections were changed for each time step. The frictional pressure loss for the entire well was taken as a weighted average of each section. The results of the analysis using the single bubble model showed also an insignificant 6% change on the casing pressure. This does not impact the choice of applying pipe rotation and the RCD rating selection of the operation. However, in deep offshore cases with tight fracture-pore pressure limits, the effect of the change in frictional pressure loss is magnified. The accurate estimation of the change in frictional pressure loss with rotation can further the precision of the downhole pressure profile values and possibly increase the kick tolerance.

Although widely used for well control operations, the single bubble model is considered inaccurate for many cases. Operational changes such as kill rate, well inclination, type and properties of the mud affect the gas distribution. The results of the DEA gas surface distribution showed that surface casing pressure is highly affected by the gas distribution throughout the well. Furthermore, discussion on the gas bubble breakage due to pipe rotation from the literature supports the hypothesis of pipe rotation aiding to the gas distribution. A physical fluid flow phenomenon known as Taylor vortices which occurs between two pipes with inner pipe rotating is speculated to help break the gas bubble. These vortices only appear after a critical rotational speed depending on mud viscosity, density and flow rate. Based on the study, the maximum distribution of gas and, hence, the lowest casing pressure occurs with low mud rheology, vertical well inclination, low kill rate and, hypothetically, high speed of rotation.

The gas bubble breakage effect on casing pressure for gas kick situations has been studied using the dispersed bubble model. As mentioned, many factors may compromise the single bubble

model. The dispersed model assumes that the gas bubble due these factors breaks down into many very small bubbles. The size of the bubbles follows a no slip velocity model. The change in casing pressure, keeping BHP constant, was done by comparing the anticipated casing pressure for dispersed bubble model versus the single bubble model. The difference in hydrostatic pressure between the two models, for each test, was used as the difference in surface casing pressure. The results of the analysis of this model showed a significant decrease in the casing pressure due to the gas bubble breakage. For the tests analyzed, the casing pressure decreased down to 30% of the original pressure value when accounting for frictional pressure loss as well.

The analysis of the three models, for mud properties and flow rates similar to the real scale data, showed that the major effect on the casing pressure when applying pipe rotation happens due to the breakage of the bubble rather than frictional pressure changes. The decision of rotation should be based on the ability to break the gas bubble whether by applying the speed of rotation higher than the critical speed of Taylor vortices appearance or considering other bottom hole assembly mechanisms aiding to the breakage of the gas.

7.2 Application

The flow chart (Fig 7.1) summarizes the recommended application. The decision is divided into two sections based on the type of mud. If the operation was carried with OBM, a check on the gas dissolving in the mud is needed. This can be done by checking the increase in mud volume of pits and PWD measurements, if the mud properties and flow rates were similar to those in the real scale experiments in this thesis, the recommendation is not to rotate the pipe. The casing pressure has an insignificant change with the introduction of pipe rotation.

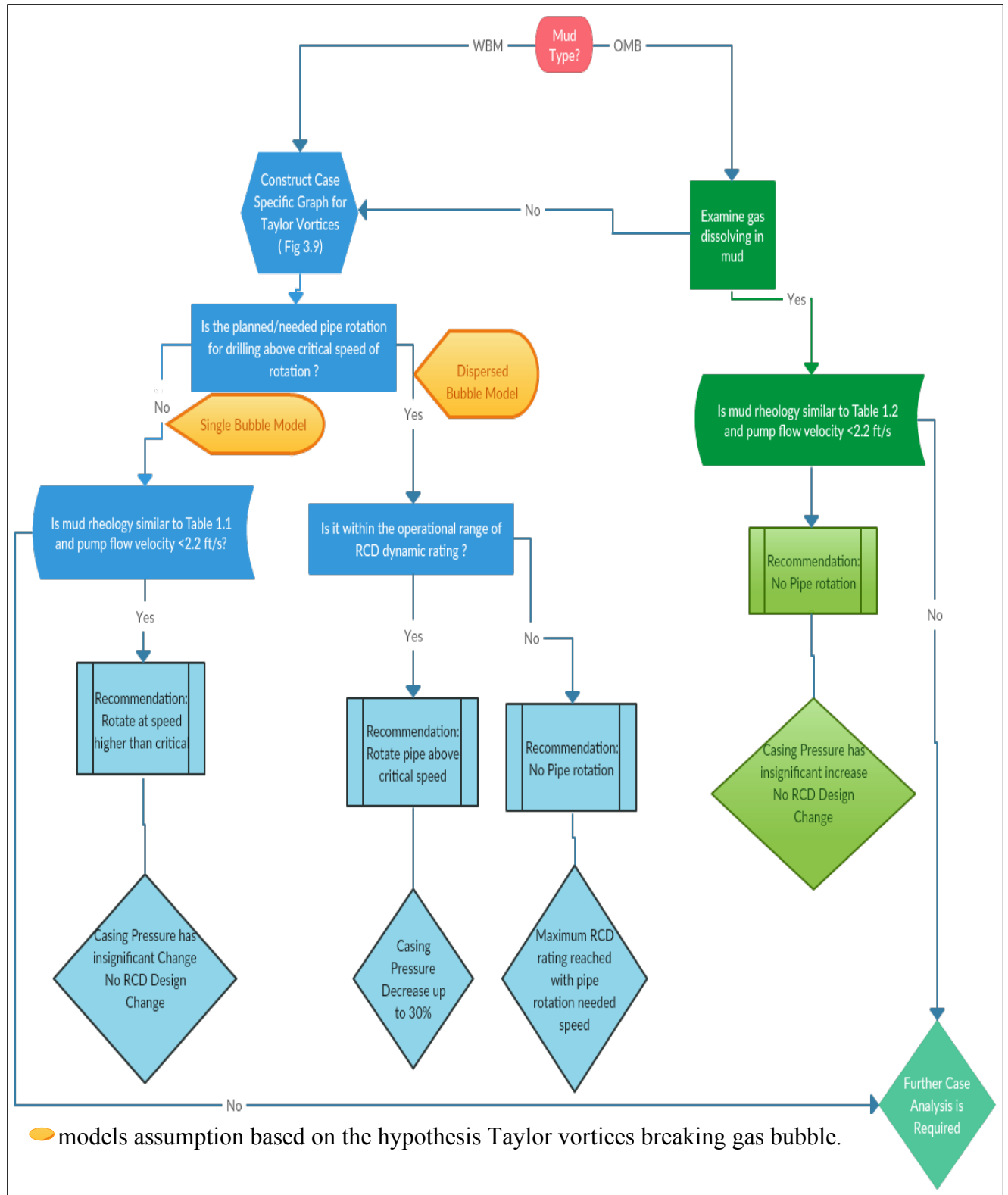


Figure 7. 1: Flow chart pipe rotation decision

If the operation was carried with WBM or the gas did not dissolve in OBM, Taylor vortices envelope of presence as in Fig 7.2 needs to be generated during the planning stage, for mud properties and flow rates in the well. If the Taylor vortices were present, the recommendation, based on the hypothesis, is to follow the dispersed bubble model. Then, engineers need to examine the RCD dynamic rating. The RCD rating is affected by the speed of rotation in the operation. Fig 7.3 shows an example of the RCD rating change as the speed of rotation changes. Deciding if pipe rotation is safe to be carried and drilling to be continued is a balance between the operational envelope of the RCD and the presence of the Taylor vortices for the mud properties of the operation as the example in Fig 7.2. The engineer is encouraged, therefore, to account for both factors when making the decision, the flow chart (Fig 7.1) shows the main recommendations for both models.

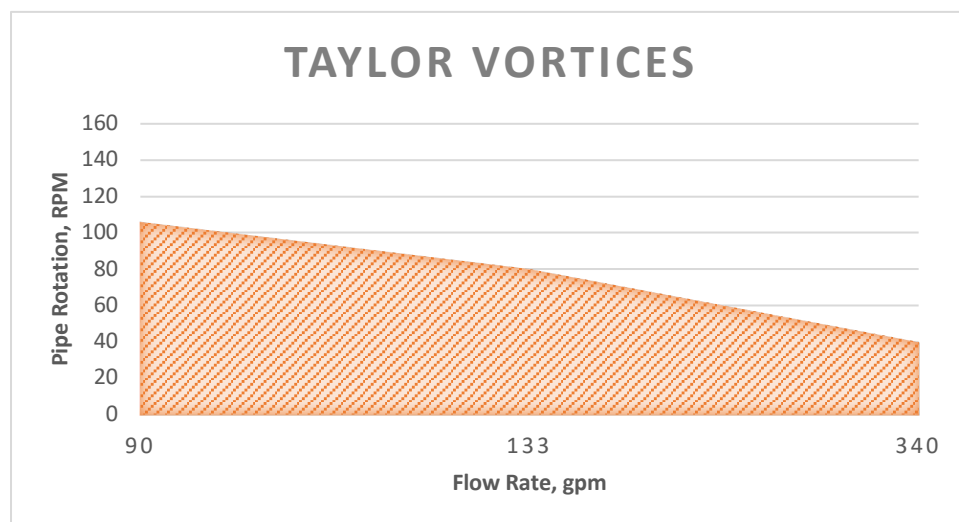


Figure 7.2: Taylor vortices appearance mud example

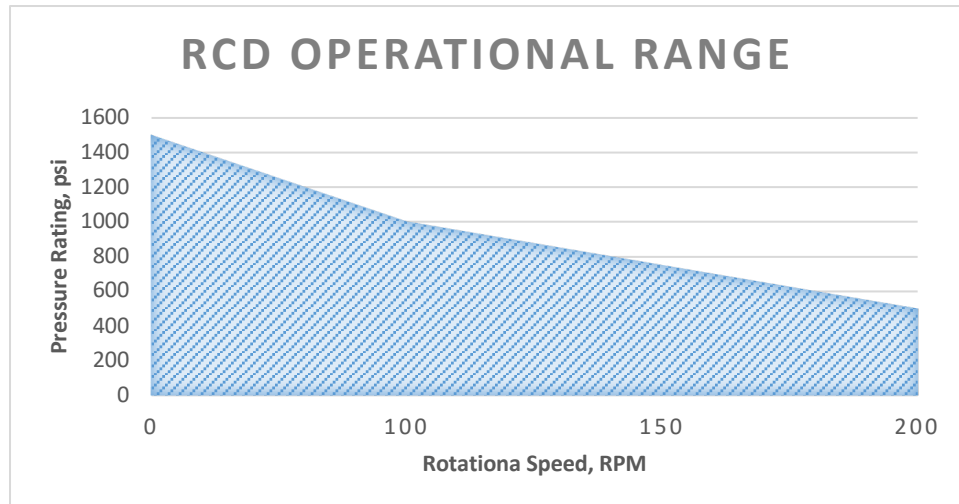


Figure 7.3: RCD operational envelope

7.3 Recommendations for Future Research

- Research to complement this work would be validating the hypothesis of Taylor vortices breaking down the gas bubble when the pipe is rotated at higher speeds. Experimental study, preferably on a full scale schematic, is recommended for multiphase gas bubble in an annulus with Non-Newtonian fluid including pipe rotation to see the effect on gas dissipation with rotation. The experiment apparatus should include pressure sensors to find the difference in frictional pressure differential when pipe rotation is applied.
- A numerical simulation of the effect of rotation on gas with axial flow is needed to simulate the details of the gas path in the wellbore with rotation. Input parameters should include a wide range of flow rates, well geometries, mud properties and speed of rotation to include all possible outcome when it comes to behavior of gas distribution.
- The effect of inclination needs to be further studied on the gas behavior and pressure variations when taking a kick while applying pipe rotation.

- Analysis of various well geometries other than LSU#2 is needed to measure the effect of geometry on the gas behavior within the wellbore.
- The dispersed bubble model needs additional investigation to see the effect of more complex models such as including the drift velocity of gas bubbles after the Taylor vortices appeared and finding a method to estimate the size of the bubble caused by these vortices.
- Research concerning the pipe rotation effect on the dissolution of gas into OBM needs to be done. The possibilities of gas coming out of solution caused by the difference velocity vectors and differential pressure changes of the fluid flow would be beneficial.

BIBLIOGRAPHY

- Ahmed, Ramadan, and Stefan Miska. 2008. "Experimental Study and Modeling of Yield Power-Law Fluid Flow in Annuli with Drillpipe Rotation." In *IADC/SPE Drilling Conference and Exhibition*, 13. Orlando: Society of Petroleum Engineers.
- Ball, Philip. 2009. *Flow*. Oxford: University Press.
- Chirinos, Jose Eduardo. 2010. "A Simulation Study of Factors That Affect Pressure Control During Kick Circulation in Managed Pressure Drilling Operations." Master's thesis, Louisiana State University.
- Chirinos, Jose, John Roger Smith, and Darryl Bourgoyne. 2011. "Alternative Shut-In and Pump Start-Up Procedures for Kicks Taken During MPD Operations." In *IADC/SPE Managed Pressure Drilling and Underbalanced Operations Conference & Exhibition*, 10. Denver: Society of Petroleum Engineers. doi:10.2118/143094-MS.
- Das, Asis Kumar. 2007. "Simulation Study Evaluating Alternative Initial Responses to Formation Fluid Influx during Managed Pressure Drilling." Master's thesis, Louisiana State University.
- Davoudi, Majid. 2009. "A Simulation-Based Evaluation Of Alternative Initial Responses To Gas Kicks During Managed Pressure Drilling Operations." Master's thesis, Louisiana State University.
- Drazin, P.G., and W. H. Reid. 2004. *Hydrodynamic Stability*. Cambridge University Press.
- Elmore, Robert J, George H Medley, and Robert C Goodwin. 2014. "MPD Techniques Optimize HPHT Well Control." In *SPE Annual Technical Conference and Exhibition*, 13. Amsterdam: Society of Petroleum Engineers.
- Erge, Oney, Evren M Ozbayoglu, Stefan Z Miska, Mengjiao Yu, Nicholas Takach, Arild Saasen, and Roland May. 2014. "The Effects of Drillstring Eccentricity, Rotation and Buckling Configurations on Annular Frictional Pressure Losses While Circulating Yield Power Law Fluids." In *IADC/SPE Drilling Conference and Exhibition*, 16. Fort Worth: Society of Petroleum Engineers.
- Erge, Oney, Evren M Ozbayoglu, Stefan Z Miska, Mengjiao Yu, Nicholas Takach, Arild Saasen, and Roland May. 2015. "The Effects of Drillstring-Eccentricity, -Rotation, and -Buckling Configurations on Annular Frictional Pressure Losses While Circulating Yield-Power-Law Fluids." *SPE Drilling & Completion* 30 (3): 257. doi:10.2118/167950-PA.
- FlowKit. 2016. "FlowKit Ltd.: Taylor-Couette Flow - Vorticity Field." *Youtube*. <https://www.youtube.com/watch?v=uCutXG9WK70>.
- Grace, Robert, Bob Cudd, Richard Carden, and Jerald Shursen. 1960. "Classic Pressure Control Procedures." In *Blowout and Well Control Handbook*, 1st ed., 40–81. Houston: Gulf Professional Publishing.

- Guner, Hakan. 2009. "Simulation Study of Emerging Well Control Methods for Influxes Caused by Bottomhole Pressure Fluctuations During Managed Pressure Drilling." Master's thesis, Louisiana State University.
- Hannegan, D, and K Fisher. 2005. "Managed Pressure Drilling in Marine Environment." In *International Petroleum Technology Conference*, 8. Doha. doi:10.2523/10173-MS.
- Ian, C Coker. 2004. "Managed Pressure Drilling Applications Index." In *Offshore Technology Conference*, 7. Houston. <http://www.onepetro.org/mslib/servlet/onepetropreview?id=OTC-16621-MS&soc=OTC&speAppNameCookie=ONEPETRO>.
- Jacobs, Steve, and John Donnelly. 2011. "Crossing the Technology Chasm: Managed Pressure Drilling." *Journal of Petroleum Technology* 63 (7): 30–35.
- Lockett, T J, S.M. Richardson, and W.J. Worraker. 1993. "The Importance of Rotation Effects for Efficient Cuttings Removal During Drilling." In *SPE/IADC Drilling Conference*, 861–69. Amsterdam: Society of Petroleum Engineers.
- Ozbayoglu, E. M., and M. Sorgun. 2010. "Frictional Pressure Loss Estimation of Non-Newtonian Fluids in Realistic Annulus with Pipe Rotation." *Journal of Canadian Petroleum Technology* 49 (2): 57–64. doi:10.2118/141518-PA.
- Piccolo, Brian. 2013. "The Diagnosis Of Well Control Complications During Managed Pressure Drilling." Master's thesis, Louisiana State University.
- Rajabi, Mehdi Mir, Don Hannegan, and Dennis Moore. 2014. "The MPD Well Control Matrix: What Is Actually Happening." In *SPE Annual Technical Conference and Exhibition*, 16. Amsterdam: Society of Petroleum Engineers.
- Rehm, Bill, Jerome Schubert, Arash Haghshenas, Amir Paknejad, and Jim Hughes. 2008. *Managed Pressure Drilling*. Houston: Gulf Professional Publishing. <http://www.sciencedirect.com/science/book/9781933762241>.
- Rommetveit, R, and T.L. Olsen. 1989. "Gas Kick Experiments in Oil-Based Drilling Muds in a Full-Scale, Inclined Research Well." In *SPE Annual Technical Conference and Exhibition*, 14. San Antonio: Society of Petroleum Engineers.
- Santos, Helio, Erdem Catak, Joe Kinder, and Paul Sonnemann. 2007. "Kick Detection and Control in Oil-Based Mud : Real Well - Test Results Using Micro F Lux Control Equipment." In *SPE/IADC Drilling Conference*, 10. Amsterdam: Society of Petroleum Engineers.
- Shiomi, Yoichi, Hiroaki Kutsuna, Koji Akagawa, and Mamoru Ozawa. 1992. "Two-Phase Flow in an Annulus with a Rotating Inner Cylinder (Flow Pattern in Bubbly Flow Region)." *Nuclear Engineering and Design* 141: 27–34.

- Shoham, Ovadia. 2005. *Mechanistic Modeling of Gas-Liquid Two-Phase Flow in Pipes*. Richardson: Society of Petroleum Engineers.
- Soundalgekar, V M, H S Takhar, and T J Smith. “Effects of Radial Temperature Gradient on the Stability of Viscous Flow in an Annulus with a Rotating Inner Cylinder.” *Warme- Und Stoffübertragung* 15 (1981): 233–38.
- Spoerker, H F, and T Tuschl. 2010. “Behavior and Shape of Gas Kicks in Well Bores.” In *IADC/SPE Drilling Conference and Exhibition*, 7. New Orleans: Society of Petroleum Engineers.
- Spoerker, H.F., C Gruber, and W. Brandstaetter. 2012. “Dynamic Modelling of Gas Distribution in the Wellbore During Kick Situations.” In *ADC/SPE Drilling Conference and Exhibition*, 9. San Diego: Society of Petroleum Engineers.
- Taylor, G. I. 1923. “Stability of a Viscous Liquid Contained between Two Rotating Cylinders.” *Philosophical Transactions of the Royal Society of London* 223 (A): 289–343.
doi:10.1098/rsta.1923.0008.
- Walowit, J A. 1966. “The Stability of Couette Flow Between Rotating Cylinders in the Presence of a Radial Temperature Gradient.” *A.I. Ch.E Journal* 12 (1): 104–9.
- Watanabe, Keizo, Shu Sumio, and Satoshi Ogata. 2006. “Formation of Taylor Vortex Flow of Polymer Solutions.” *Journal of Fluids Engineering* 128 (1): 95–100.
doi:10.1115/1.2137350.
- “DEA Project 7.” 1986. Baton Rouge.
- “Introduction to Managed Pressure Drilling with MicroFlux™ Control.” 2012. Weatherford.
- “PERTT Well Schematics.” 2016. Baton Rouge: Louisiana State University.
<https://drive.google.com/drive/folders/0Bz97qNAafgt9NFU2QTM1ZjVuWms>.

APPENDIX A: REAL SCALE EXPERIMENTS DATA OUTPUT

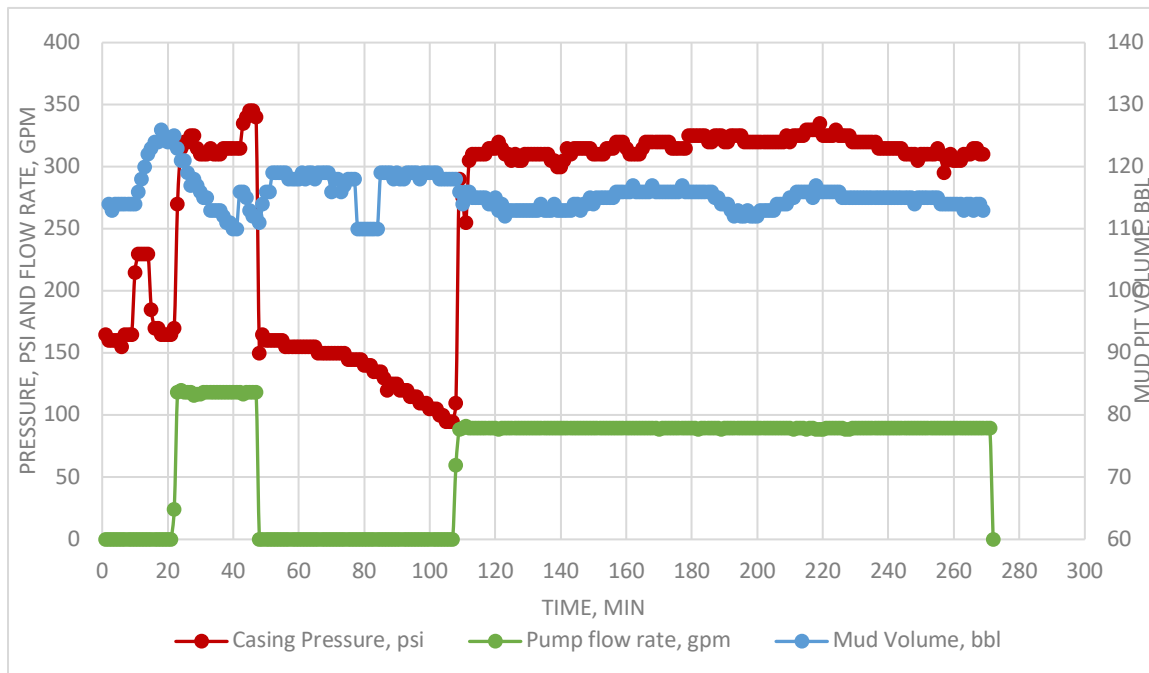


Figure A1: OM10 Data output

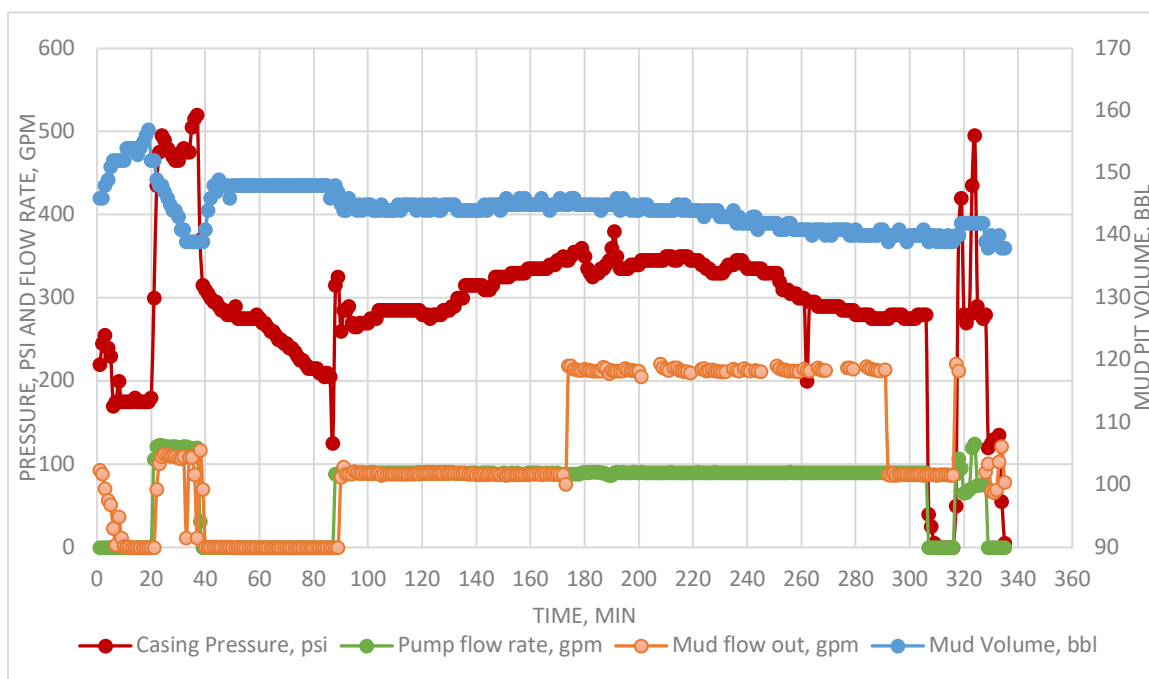


Figure A2: Test 3-5 (OM15) Data output

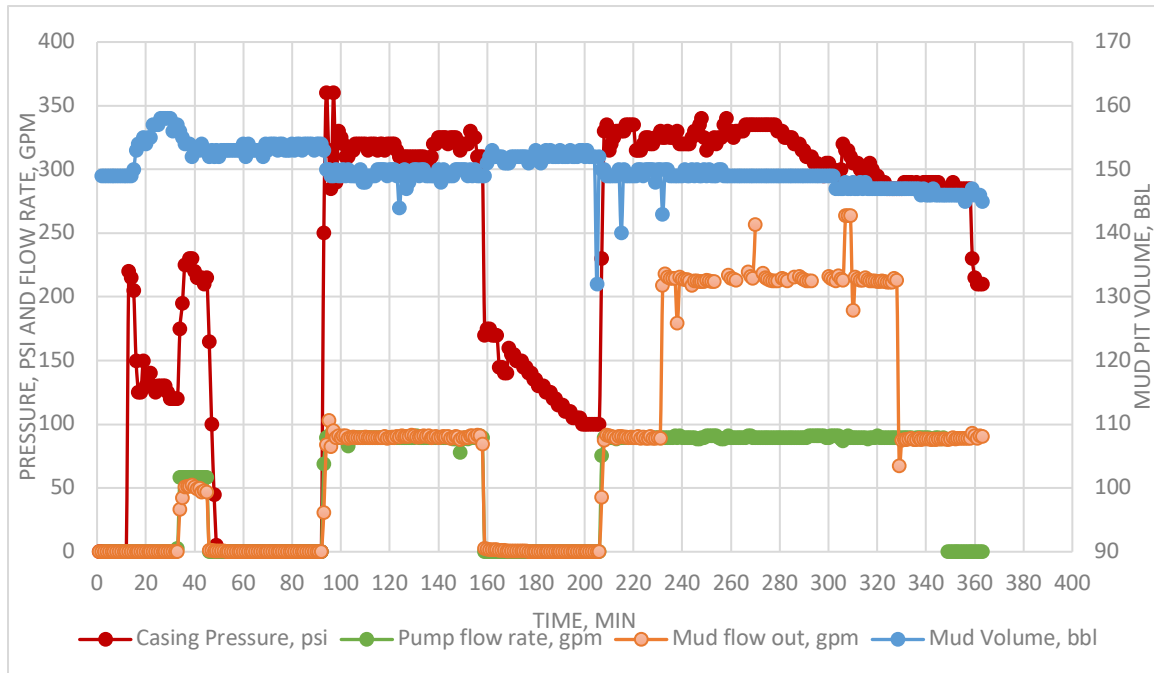


Figure A3: (Test 3-1)OM11 Datat Output

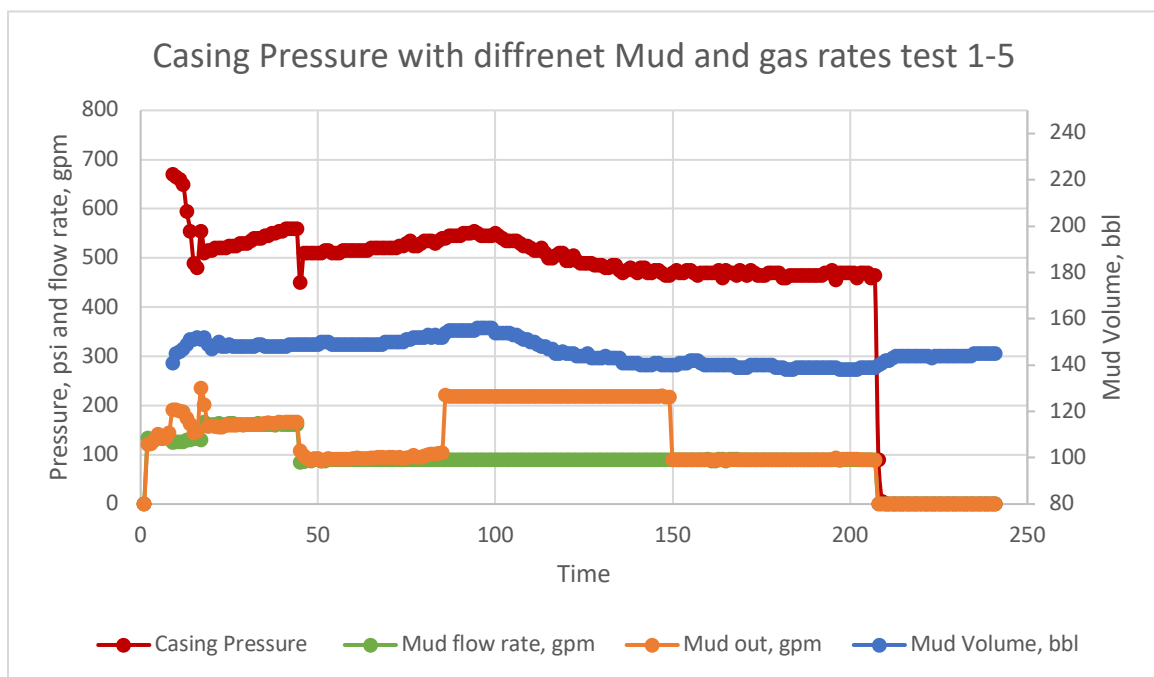


Figure A4: WN6 (test 1-5) Output data

APPENDIX B: COPYRIGHT MATERIAL



Thank you for your order!

Dear Zahrah Al Marhoon,

Thank you for placing your order through Copyright Clearance Center's RightsLink® service.

Order Summary

Licensee: Louisiana state
Order Date: Nov 21, 2017
Order Number: 4233960180865
Publication: Journal of Petroleum Technology
Title: Crossing the Technology Chasm: Managed Pressure Drilling
Type of Use: Thesis/Dissertation
Order Total: 8.00 USD

View or print complete [details](#) of your order and the publisher's terms and conditions.

Sincerely,

Copyright Clearance Center

How was your experience? Fill out this [survey](#) to let us know.

Tel: +1-855-239-3415 / +1-978-646-2777
customercare@copyright.com
<https://myaccount.copyright.com>



RightsLink®

APPENDIX C: FRICTIONAL PRESSURE CALCULATION EXAMPLE

These calculations show an example of single time step applying the dissolved gas model (Only liquid in the well) using both Erge and Ozbayoglu correlations [Test 2-1 (OM6)]:

Properties of mud: $K = .03 \text{ Pa.s}^m$, $\tau_y = 3.09 \text{ Pa}$, $m = 1$, and $MW = 8 \text{ ppg}$

Test measurements and output: $Q_m = 90 \text{ gpm}$, $TD = 5822 \text{ ft}$, $CP_{\text{static}} = 300 \text{ psi}$

1) Assuming concentric schematic (Ergle):

- Find frictional pressure loss of concentric ($e=0$) non rotational ($\omega=0$) case using Ergle correlation refer to (Ergle, et al., 2015) using the above mentioned mud properties, note that the $F_d=0$

$$\frac{dP}{dl} = 135 \text{ Pa/m}$$

converting to field unites and multiplying by well depth (5822 ft)

$FP_{\text{static}} = 35 \text{ psi}$ (annular pressure loss for real scale experiments)

- Find frictional pressure loss for 120 RPM rotational case using the same correlation: $\frac{dP}{dl} = 67 \text{ Pa/m}$,

converting to field unites and multiplying by well depth (5822 ft)

$FP_{120 \text{ RPM}} = 17 \text{ psi}$ (annular pressure loss while applying pipe rotation)

- Find the difference in frictional pressure loss between the rotational and non-rotational case: $\Delta FP = -18 \text{ psi}$

- Since the real scale experiment were done on a non-rotational drill pipe in a constant bottom hole pressure condition, the change in frictional pressure loss in the annulus is going to translate into a change in the casing pressure

$$CP_{RPM} = CP_{static} - \Delta FP = 300 \text{ psi} - (-18) \text{ psi} = 318 \text{ psi}$$

This example showed a 18 psi increase in the casing pressure with 120 RPM rotation.

2) Assuming eccentric schematic (Ozbayoglu):

- Find frictional pressure loss of eccentric non rotational($\omega=0$) case using Ozbayoglu correlation refer to (Ozbayoglu & Sorgun, 2010) using the above mentioned mud properties,

$$\frac{dP}{dl} = .0032 \text{ psi/f}$$

multiplying by well depth (5822 ft)

$$FP_{static} = 18.5 \text{ psi (annular pressure loss for real scale experiments)}$$

- Find frictional pressure loss for 120 RPM rotational case using the same

$$\text{correlation: } \frac{dP}{dl} = .0034 \text{ Pa/m,}$$

multiplying by well depth (5822 ft)

$$FP_{120 \text{ RPM}} = 19.7 \text{ psi (annular pressure loss while applying pipe rotation)}$$

- Find the difference in frictional pressure loss between the rotational and non-rotational case: $\Delta FP = +1 \text{ psi}$
- Since the real scale experiment were done on a non-rotational drill pipe in a constant bottom hole pressure condition, the change in frictional pressure loss in the annulus is going to translate into a change in the casing pressure

$$CP_{RPM} = CP_{static} - \Delta FP = 300 \text{ psi} - (1) \text{ psi} = 301 \text{ psi}$$

This example showed a 1 psi decrease in the casing pressure with 120 RPM rotation which was presumed as a correlation error.

Table C.1: Conversion factors used for calculations

Parameter	SI unit	Field unit
Pressure	Pa	0.000415 psi
Density	Kg/m ³	.00834 ppg
Dimensions	m	3.28 ft
Q (flow rate)	m ³ /s	15850 gpm
Velocity	m/s	3.28 ft/s
Viscosity	Pa.s	1000 cp
Shear stress	Pa	2.1 lbf/100ft ²
K(fluid consistency index)	Pa. s ^m	2.1 lbf/100ft ² .s ^m
Mass	Kg	2.2 lb

VITA

Zahrah Al Marhoon was born and raised in the Eastern Province of Saudi Arabia. She acquired her Bachelor of Science degree in Petroleum Engineering from Texas A&M University with Magna cum laude in 2012. Her professional experience included multiple positions in Saudi Aramco for three years. She worked as a drilling fluid researcher, a drilling engineer and a reservoir engineer. She started her graduate education in Fall of 2015. She anticipates to graduate with her Master's Degree from Louisiana State University in May 2018.

Zahrah is married to another Petroleum Engineer and she had her first child while pursuing her graduate degree. She was blessed with a baby girl named Rihana.